A Part of Transport

Testing sediment transport models under partial transport conditions

August 13, 2010

Author: Stephan R. Janssen
Water Engineering and Management
University of Twente
Enschede, The Netherlands

Supervisors: Dr.ir.J.S. Ribberink (Chairman)
Dr. A.P. Tuijnder
Dr.ir. P.C. Roos
Water Engineering and Management
University of Twente
Enschede, The Netherlands

Abstract

River managers rely on sediment transport models, for example when predicting morphological behavior. In rivers, under certain conditions, part of the sediment will move and part will remain immobile. This is known as partial transport. Partial transport influences the transport rate, bed forms, bed roughness and transport composition. In this study three transport models, Meyer-Peter and Müller (1948), van Rijn (2007c) and Wilcock and Crowe (2003), are tested on their performance under partial transport conditions. The first two transport models are alluvial models, whereas the third model was specifically developed for partial transport. The models are tested on flume experiments available from the literature where aspects of partial transport were studied or partial transport was observed in the measured transport rates.

Testing the models in various ways demonstrates their performance on different aspects of partial transport. In this study first a bulk grain size distribution is used with both a uniform and fractional transport calculation and secondly a surface-based grain size distribution is used with a fractional transport calculation. The surface-based grain size distribution is determined from photographs of the bed surface and bed samples. As the transport depends largely on mobile and immobile sediment present at the surface, the surface-based grain size distribution is preferable.

Two data sets, with trimodal and natural sediment are predicted well by the original transport models. However, three data sets with strong bimodal sediments cannot be predicted accurately with the transport models. Under supply limited conditions the bimodal sediment sorts into two parts, mobile and immobile sediment. This influences the functionality of the transport models. The hiding/exposure process that occurs with the strong bimodal sediment cannot be represented with the functions of the transport model. The process differs between parts where the immobile sediment is present at the surface and where the mobile sediment is present at the surface. Hiding exposure occurs mainly in the mobile sediment, but the model calculates the hiding exposure correction for the entire sediment. Therefore the calculation should be split for the mobile and immobile sediment. This should also be applied for several other represented processes in the transport models.

In the last part of this study a different approach is tested. The transport rates of only the mobile sediment is predicted and reduced with a reduction function. With different reduction functions the resulting predictions improve for the data sets with bimodal sediment.

Contents

Chapter 1

Introduction

1.1 Context

In the current world computer models are used to predict almost every aspect of the environment, including sediments transport and discharges in rivers. When new policies or measures are implemented in rivers the effects are often first predicted. This however introduces the black box problem which is often associated with models.

Inserting data, running the model and reading the results can result in a serious gap between what is predicted and what happens in reality. When modeling sediment transport various aspects can influence differences between modeled results and the real world. Many sediment transport models currently exist for many different aspects of sediment transport. Suspended transport with or without waves, bed load transport or sheet flow are examples of different forms of transport which are usually predicted using significantly different models.

Recent studies showed varying results in predicting and understanding a form of bed load transport known as partial transport (Tuijnder, 2007; Spekkers, 2008; Blom, 2000; Blom and Kleinhans, 1999). For graded sediment, part of the bed can remain immobile if the bed shear stress is large enough to mobilize the finer material but to weak to mobilize the coarser part of the material, this is known as **partial transport**. Partial transport changes the sediment transport in an intricate and complex way. Partial transport affects the dimensions of bed forms (Tuijnder et al., 2009) and can lead to development of a pavement layer (Spekkers, 2008). A pavement layer is a layer of coarser immobile sediment that can limit the amount of mobile sediment available for transport. Figure 1.1 shows an example of a flume experiment where partial transport and a pavement layer were observed. Under partial transport conditions the transported sediment is finer than the bed (or bulk) material as part of the coarse material remains immobile (Wilcock and McArdell, 1993; Blom et al., 2002). When a pavement layer limits the amount of mobile sediment available for transport, the sediment transport is supply-limited.

Figure 1.1: Example of partial transport, showing supply limited bed forms and gravel patches of a pavement layer

Struiksma (1985) already predicted partial transport rates using an alluvial transport model in combination with a reduction function. The reduction function accounts for the supply limitation caused by an immobile layer. Wilcock and Crowe (2003) developed a transport model for partial transport conditions.

1.2 Sediment transport and modeling

Water flowing in a river, carrying along sand eventually ends up in the sea. Shear stress generated at the bottom mobilizes and transports sand or gravel that is present. The shear stress, is referred to as bed shear stress, depends on the hydraulic conditions. After sediment is mobilized it is transported and can form bed forms like ripples or dunes. These affect the roughness of the river bed. This roughness in turn influences the flow velocity and water depth. Changes in velocity and water depth lead to different transport rates and possibly to changes in bed form dimensions. In turn changes the roughness of the river bed. This loop represents a simplification of the complex interaction of sediment and water. Changes in the morphologic conditions lead to changes in the transport rate. This can lead to unwanted erosion or sedimentation. Therefore accurate predictions of sediment transport rates are important.

Sediment transport is a complex process and it is not feasible to model the physical process meticulously for individual grains. Many transport models are available that include empirical relations to represent the physical processes. Including empirical relations also limits the models to a certain range of conditions: the conditions of the data on which they were calibrated.

The hydraulic conditions in combination with the sediment can lead to different modes of transport. Wilcock and McArdell (1993) defined four regimes: no-motion, partial trans-

port, fully mobile transport and suspended transport. Different models are available for the partial transport, fully mobile and suspended transport regime. In graded sediment mixture partial transport can occur if the bed shear stress only mobilizes part of the sediment: i.e. the finer fractions. The coarser fractions remain immobile or are sorted vertically into a pavement layer. A pavement layer locks in finer sediment underneath, limiting the amount of fine sediment available for transport.

Transport models represent a significant part of the processes with empirical relations because they are too complex or unknown to model theoretically. Therefore, most models are only valid for a (small) range of conditions to which the empirical relations were fitted. River managers must choose a model carefully to fit the conditions.

Problems can arise when transport models are used under different conditions than the ones they were designed for. Partial transport is a condition on which recent studies have focused. The changes in transport, bed forms and roughness under partial transport can lead to inaccurate predictions.

1.3 Problem description and research questions

River managers like to have possibilities to predict the sediment transport rate with sufficient accuracy. The processes of sediment transport are complicated and there are many different transport models available. However, for partial transport conditions currently only a few models exist. The changes caused by the immobile fractions of the sediment are accounted for in the model of Wilcock and Crowe (2003), but as with many models it is only valid for a range of hydraulic conditions and sediments. Recent studies created possibilities to test the performance of sediment transport models under partial transport conditions. Testing transport models will provide insight in the relative importance of processes of partial transport and wether these are represented sufficiently in the models. It can also show errors or opportunities for improvement. This study is guided by a set of research questions to get better understanding of partial transport and sediment transport modeling.

1. Which processes and parameters are important for sediment transport predictions? And how are they affected by partial transport?

In the Chapter 2 of the study a closer look is taken at the processes and parameters involved in sediment transport modeling. It will show some of the complex interactions between sediment and water, explain some of the terminology and provide insight to how this is represented in a transport model. It will also show how transport models represent physical processes by equations.

2. How well can currently available transport models predict transport rates under partial transport conditions?

Recent studies provide a set of data which will be used to compare predictions to measurements. The data sets are described in Chapter 3. Different studies use different hydraulic conditions and sediments and provide a broad data set to test the models. Three different models will be tested against the measured data. Analysis of the predictions will reveal their performance.

3. Can the transport models be adjusted to better represent the processes occurring under partial transport conditions?

With the knowledge and insight gained by answering research questions 1 and 2, the predictions may or may not improve. When the predictions are accurate there is no need for change. If trends can be observed in comparisons between measurements and predictions possible improvements can be suggested (or directly implemented).

1.4 Thesis outline

Before testing the transport models, first the relevant processes and parameters involved need to be understood. Chapter 2 discusses sediment transport, partial transport and modeling approaches. Analyzing the relevant processes and parameters provides insight in sediment transport and terminology needed for the rest of this study. It also discusses the three transport models that will be used in this study. The three models are:

1. the well-known model of Meyer-Peter and Müller (1948),
2. a model specifically for partial transport of Wilcock and Crowe (2003),
3. the new model of van Rijn (2007c)

The models will be applied in both a uniform and a fractional transport calculation. Each of the models is discussed on how they were developed, what processes are represented, equations and limitations. This can provide insight where the predictions may go wrong for partial transport conditions.

The models are tested on data of several flume experiments. chapter 3 discusses each data set to provide insight in differences, which may be observed later in the predictions. The goals, imposed conditions, sediment and methods of measuring parameters differ for each study.

In chapter 5 6 model predictions are compared to measured transport rates. Analyzing the predictions against different parameters provides insight in unwanted or unexpected behaviour of the models. The results will also show possible good and bad aspects of the transport models.

chapter 7 discusses some of the results of the predictions and shows a way to improve the predictions by means of a different approach and including a reduction function to account for reduced transport rates.

chapter 8 and 9 provide a discussion of all results and summarizes the conclusions and recommendations of this study.

Chapter 2

Sediment transport processes and modeling

2.1 Introduction

Models represent the physical processes occurring with sediment transport through (empirical) relations. To understand the models, the physical processes of sediment transport and in particular partial transport are discussed. In the second part of this chapter the representations of the physical processes in models are discussed.

2.2 Sediment transport

Bed shear stress

Water flowing over a river bed causes shear stress. On a plain bed, with no bed forms present and uniform flow, the bed shear stress is a simple function of the hydraulic conditions and can be calculated using equation:

$$\tau_b = \rho g h I_e \tag{2.1}$$

in which ρ is the water density, g the gravity constant, h the water depth, I_e the energy slope.

In the presence of bed forms the resistance to the flow of water becomes a two part relation. The total bed shear stress consists of the skin friction, also referred to as the effective bed shear stress, and the bed shear stress from bed forms (Figure 2.1):

$$\tau_b = \tau_b' + \tau_b'' \tag{2.2}$$

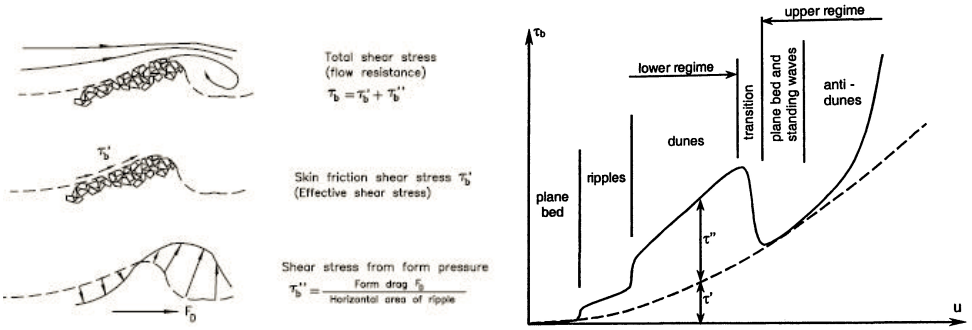

Figure 2.1: Explanatory figures of bed shear stress, skin friction and form pressure (from Yang (1996) and Engelund and Hansen (1967)))

in which τ_b is the total bed shear stress, τ_b' is the effective bed shear stress of the grains, τ_b'' is the shear stress of bed forms.

The effective shear stress and form roughness were studied by Engelund and Hansen (1967). Figure 2.1 shows the bed shear stress, effective shear stress and shear stress from bed forms as a function of average flow velocity. Transport models often account for the shear stress from bed forms through a form factor. The bed form factor corrects the bed shear stress to the effective shear stress, for example the bed form factor used in the transport model of MPM:

$$\tau_b' = \mu_{mpm}\tau_b, \qquad \mu_{mpm} = \left(\frac{C_b}{C'}\right)^{\frac{3}{2}} \tag{2.3}$$

in which C_b is the bed related Chézy roughness coefficient, C' is the grain related Chézy roughness coefficient.

2.2.1 Initiation of motion

Sediment will remain immobile when no flow is present. When flow is present, a single grain of sediment will start to move if the resisting force is overcome. A single grain starts to move when the bed shear stress is larger than the critical bed shear stress. For a single grain the balance of forces is straightforward (Figure 2.2) and the critical bed shear stress can be calculated analytically. The symbols denote F_l the lift force, F_d the drag force, F_r the resistance force and W_s the submerged weight.

However, on the river bed thousands of grains are present and the balance is not so straightforward. Then, it is not feasible to calculate the critical shear stress analytically. Shields (1936) proposed an empirical relation between the dimensionless critical shear stress (or Shields stress Eq.(2.4)) and the Reynolds number.

$$\theta = \frac{\tau_b}{\rho g(s-1)D} \tag{2.4}$$

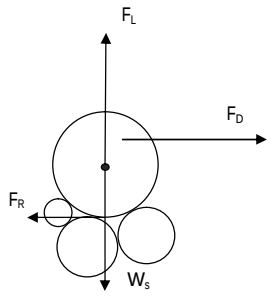

Figure 2.2: Balance of forces for a single sediment particle.

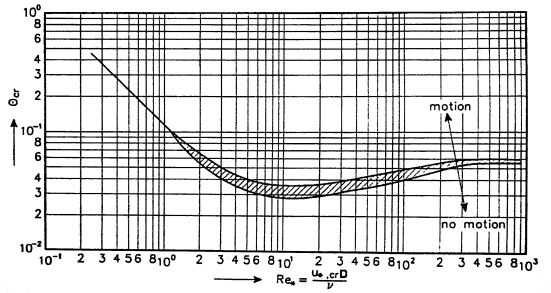

Figure 2.3: Shields parameter as a function of the Reynolds number

where ρ the density of the water, τ_b the bed shear stress, g the gravity constant, s the relative density of the sediment ($s = \rho_s/\rho$), D the grain size.

The Shields curve is often used in models to determine the point of initiation of motion (Figure 2.3).

2.2.2 Hiding/exposure

In graded sediments, a sediment mixture containing fractions of different sizes, grains can influence each other. Different grain sizes have a different critical shear stress; this will make them start to move at different values of the occuring bed shear stress. However, in a sediment mixture different grain sizes will be influenced differently by the flow. Larger grains are more exposed to the flow than smaller grains, making them more likely to start moving, whereas smaller grains can hide behind larger grains, making them less likely to start moving. This effect is known as hiding/exposure and is shown in Figure 2.4. Hiding/exposure results in smaller critical shear stresses for large grains and larger critical bed shear stresses for smaller grains. In transport models this is often accounted for by a hiding/exposure correction applied to the critical bed shear stress. An example is the hiding/exposure correction of Egiazaroff (1965):

$$\xi_i = \left[\frac{\log(19)}{\log(19D_i/D_m)}\right]^2 \tag{2.5}$$

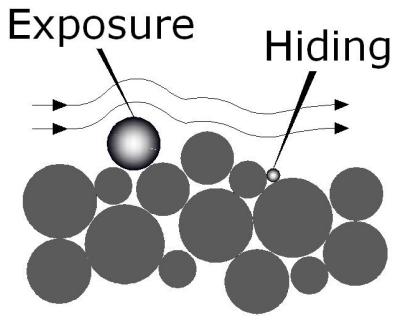

Figure 2.4: The effect of hiding and exposure

in which ξ_i is the hiding/exposure correction of fraction i, D_i the grain size of fraction i, D_m the mean diameter of the grain size distribution.

In a sediment mixture the fractions smaller than the mean diameter are corrected to a larger critical shear stress, mobilizing them at larger bed shear stresses. The reverse is applied to fractions larger than the mean diameter.

2.3 Transport models

2.3.1 General transport model

In general most sediment transport models are similar. The transport is predicted using input of hydraulic and sediment characteristics and a set of equations (Figure 2.5). The equations approximate the actual physical processes that occur in transport. What differs between the transport models are the equations and which processes are included in the transport calculation. As this study focuses on partial transport only, the transport regime is limited to bed load transport.

2.3.2 Hydraulic conditions

To describe the hydraulic conditions hydraulic parameters used in transport models. Some of the more commonly used parameters are: waterdepth (h), discharge(Q), average flow velocity(U), bed shear stress (τ_b), Chézy roughness coefficient (C), Nikuradze's roughness height ($k_{s,b}$).

2.3.3 Sediment characteristics

Sediments exist in all sorts and sizes, from fine diameters like silts or clays to extremely large diameters like gravel or boulders. In most river beds a sediment mixture is present

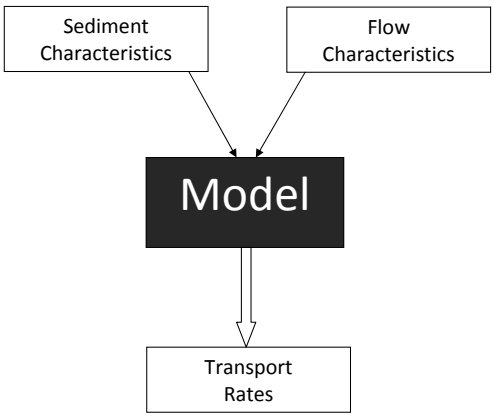

Figure 2.5: A visualization of a general transport model.

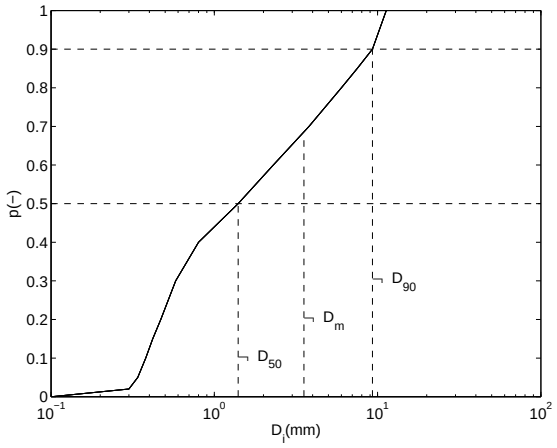

Figure 2.6: Cumulative grain size distribution of a sediment sample dredged from the Waal river.

consisting of fractions of different grain sizes. Several sediment characteristic parameters, i.e. mean and median diameter, are used to describe the sediment characteristics in models. Figure 2.6 shows a cumulative grain size distribution of sediment dredged from the Waal. This figure shows the probability of a fraction smaller in relation to the fraction diameter. Models use this information in different ways. Uniform models represent the entire sediment mixture with a single value, often the mean (D_m) or median (D_{50}) diameter. This is valid if the sediment is (nearly) uniform. However, models can also calculate the transport rate of different fractions: i.e. a fractional approach. The sediment is split into several fractions and transport is calculated for each fraction.

Transport model equations use representative diameters for the entire sediment, for example, in the hiding/exposure correction. Figure 2.6 shows three often used sediment characteristics, the D_m, the D_{50} and the D_{90}.

The mean diameter is calculated using:

$$D_m = \Sigma p_i D_i \tag{2.6}$$

in which p_i is the probability of fraction i; D_i is the grain size of fraction i.

Both the D_{50} and the D_{90} can be determined from a cumulative grain size distribution. The median diameter is the diameter of which 50% of sediment mixture has a smaller diameter by weight. The D_{90} is the diameter of which 90% is of the sediment has a smaller diameter by weight. In a cumulative grain size distribution the D_{50} and D_{90} are the diameter at p is 0.5 and 0.9 respectively.

2.3.4 Dimensionless parameters

To represent aspects of sediment transport often dimensionless parameters are used. This makes for easy comparison and excludes scale differences. Several commonly used parameters are listed below that are either used in the transport models or in the analysis of the results. The dimensionless particle size:

$$D_{*,i} = \left(\frac{(s-1)g}{\nu^2} \right)^{\frac{1}{3}} D_i \tag{2.7}$$

in which s is relative sediment density, ν is the viscosity, D_i is the grain size of fraction i.

The Shields parameter (the dimensionless bed shear stress) is expressed as:

$$\theta_i = \frac{\tau_b}{(s-1)\rho g D_i} \tag{2.8}$$

in which τ_b is the bed shear stress, s is relative sediment density ($s = \rho_s/\rho$), ρ is the density of the water.

The dimensionless transport parameter is expressed as:

$$\Phi = \frac{q_b}{\sqrt{g(s-1)D^3}} \tag{2.9}$$

in which q_b is the transport rate.

2.3.5 Meyer-Peter and Müller

The formula of Meyer-Peter and Müller is a widely used empirical formula to calculate bed load transport rates. It is based on the bed shear stress concept, which relates the sediment transport rate to the bed shear stress caused by the flow of water above the bed (Ribberink, 1998). The empirical factors of the original model are based on experiments

using both uniform and graded sediments ranging from 0.4 to 29.0 mm. The formula predicts no transport for flow conditions with low Shields values, which is caused by the critical Shields value in the formula ($\theta_{cr} = 0.047$), Eq.(2.15).

By including the hiding/exposure correction of Egiazaroff (1965) or Ashida and Michiue (1973), the formula can than also predict transports for smaller Shields values and gets increased accuracy for graded sediments. In the study by Scheer et al. (2002) the transport predictions were poor for graded beds with low Shields values ($\theta < 0.1$), with better results for larger Shields values ($\theta > 0.2$). The best results were obtained in combination with the hiding/exposure approach of Egiazaroff. However, in this study the hiding/exposure correction of Ashida and Michiue (1973) will be used as this corresponds best with the data used here. The hiding/exposure correction of Ashida and Michiue (1973) differs from Egiazaroff for $D_i/D_m < 0.4$, because a bimodal sediment is used in several data sets this range occurs often (the mean diameter of a bimodal sediment will be large compared to the finest fractions).

No initiation of motion for a fraction is calculated, the model assumes the critical Shields stress has a value of 0.047, this was determined from a broad range of data. The correction of Ashida and Michiue (1973) is used to account for hiding/exposure.

Equations for fractional transport predictions

The dimensionless transport parameter of the uniform Meyer-Peter Müller is given by:

$$\Phi_{b,i} = p_i 8(\mu_{mpm}\theta_i - \xi_i 0.047)^{1.5} \tag{2.10}$$

The volumetric transport rate can be calculated using:

$$q_{b,i} = \Phi_{b,i}\sqrt{(s-1)gD_i^3} \tag{2.11}$$

In which:

$$\theta_i = \frac{\tau_b}{(s-1)\rho g D_i} \tag{2.12}$$

$$\xi_i = \begin{cases} \left[\frac{\log(19)}{\log(19D_i/D_m)}\right]^2 & \text{for } D_i/D_m \geq 0.4 \\ 0.85D_m/D_i & \text{for } D_i/D_m < 0.4 \end{cases} \tag{2.13}$$

$$\mu_{mpm} = \left(\frac{C_b}{C'}\right)^{\frac{3}{2}} \tag{2.14}$$

$$C' = 18 \log \left(\frac{12 R_b}{3 D_{90}} \right) \tag{2.15}$$

in which D_i is the fraction diameter, D_m is the mean diameter of the sediment, ξ_i is the hiding/exposure correction for fraction i, θ_i is the Shields parameter for fraction i, μ_{mpm} is the bed form parameter, τ_b is the bed shear stress, s) is the relative sediment density, ρ is the water density, ρ_s is the sediment density, g is the gravitational constant, C' the grain related Chézy value, R_b is the hydraulic radius related to the bed.

Equations for uniform transport predictions

The dimensionless transport parameter of the uniform Meyer-Peter Müller is given by:

$$\Phi = 8(\mu_{mpm} \theta_m - 0.047)^{1.5} \tag{2.16}$$

In which:

$$\theta_m = \frac{\tau_b}{(s-1)\rho g D_m} \tag{2.17}$$

To calculate the volumetric bed load transport rate:

$$q_b = \Phi \sqrt{(s-1) g D_m^3} \tag{2.18}$$

Calculation steps

1. Calculate C' from Eq.(2.15)
2. Calculate μ_{mpm} from Eq.(2.14)
3. Calculate the hiding/exposure correction for each fraction from Eq.(2.13)
4. Calculate θ_i from Eq.(2.12)
5. Calculate Φ_i from Eq.(2.10)
6. Calculate the transport rate from Eq.(2.11)

2.3.6 Wilcock & Crowe

Wilcock and Kenworthy (2002) developed a two-fraction model for mixed size sediments. In this model the sediment mixture is split into a "sand" and a "gravel" fraction. This approach retains the practicality of a single size model like Meyer-Peter and Müller,

but includes the interactions and differences of mixed size sediments. In combination with previous research (Wilcock and McArdell, 1993; Wilcock et al., 2001; Wilcock and Kenworthy, 2002) this model was extended in Wilcock and Crowe (2003). A model that calculates bed load transport for mixed size sediments with surface based observations. Instead of the traditional critical shear stress a different threshold for initiation of motion is introduced; referred to as the reference shear stress. The reference shear stress represents the shear stress at which the transport parameter is equal to a small value ($W_i = 0.002$), a substitute for the critical bed shear stress. This approach has several advantages: the reference shear stress of fraction is easier to determine for all fractions in a mixture, and it is based on a transport rate that is on a consistent basis with the threshold between partial and fully mobile transport (Wilcock and McArdell, 1993).

The model represents initiation of motion through the reference shear stress. In their study, Wilcock and Crowe (2003) determined a relation between the sand present at the surface and the dimensionless reference shear stress. This is calculated using an empirical relation. Using data in plot of scaled reference shear stress (τ_{ri}/τ_{rm}) as a function of scaled fraction grain sizes (D_i/D_{sm}), a hiding/exposure correction was determined around the surface mean diameter. It functions similar to the hiding/exposure correction of Ashida and Michiue (1973), by reducing the critical shear stress of grain sizes larger than the mean diameter. However in the model of Wilcock and Crowe the mean surface diameter is used in the correction.

Equations for fractional transport predictions

The dimensionless transport parameter for Wilcock & Crowe is given by:

$$W_i^* = \begin{cases} 0.002\phi^{7.5} & \text{for } \phi < 1.35 \\ 14(1 - \frac{0.894}{\phi^{0.5}})^{4.5} & \text{for } \phi \geq 1.35 \end{cases} \tag{2.19}$$

In which:

$$\phi = \frac{\tau_b}{\tau_{ri}} \tag{2.20}$$

To calculate the fractional volumetric transport rate:

$$q_{bi} = \frac{W_i^* p_i u_*^3}{(s-1)g} \tag{2.21}$$

In which:

$$\tau_{rm} = \tau_{rm}^*(s-1)\rho g D_{sm} \tag{2.22}$$

$$\tau^*_{rm} = 0.021 + 0.015e^{(-20F_s)} \tag{2.23}$$

$$\frac{\tau_{ri}}{\tau_{rm}} = \left(\frac{D_i}{D_{sm}}\right)^b \tag{2.24}$$

$$b = \frac{0.67}{1 + e^{(1.5 - \frac{D_i}{D_{sm}})}} \tag{2.25}$$

$$u_* = \left[\frac{\tau_b}{\rho}\right]^{0.5} \tag{2.26}$$

in which D_{sm} is the surface mean diameter of the sediment, τ_{rm} is the mean reference shear stress, τ^*_{rm} is the dimensionless mean reference shear stress, τ_{ri} is th reference shear stress for fraction i, τ_b is the bed shear stress, $u*$ the shear velocity, F_s is the amount of sand present at the surface.

Equations for uniform transport predictions

For uniform transport calculations the fractional parts are ignored ($D_i/D_{sm} = 1$). From Eq.(2.24) it follows $\tau_{ri} = \tau_{rm}$ making the dimensionless transport parameter:

$$W^* = \begin{cases} 0.002\phi^{7.5} & \text{for } \phi < 1.35 \\ 14(1 - \frac{0.894}{\phi^{0.5}})^{4.5} & \text{for } \phi \geq 1.35 \end{cases} \tag{2.27}$$

The volumetric transport rate is calculated from:

$$q_b = \frac{W^* u_*^3}{(s-1)g} \tag{2.28}$$

In which:

$$\phi = \frac{\tau_b}{\tau_{rm}} \tag{2.29}$$

$$\tau_{rm} = \left(0.021 + 0.015e^{(-20F_s)}\right)(s-1)\rho g D_{sm} \tag{2.30}$$

Calculation steps

1. Determine F_s from the grain size distribution and calculate τ^*_{rm} from Eq.(2.23)
2. Calculate τ_{rm} from Eq.(2.22)
3. Calcutate τ_{ri} from Eq.(2.24)
4. Calculate the W^*_i from Eqs.(2.19)-(2.20)
5. Calculate the transport rate using Eq.(2.21)

2.3.7 Van Rijn 2007c

In a series of three articles, a: Initiation of motion, Bed roughness and Bed-load transport; b: Suspended transport; c: Graded beds, van Rijn (2007a,b,c) describes a new unified model for suspended and bed load sediment transport under currents and waves. It combines simple expressions and basic parameters in an attempt to include many physical processes that influence sediment transport. It is a continuation of previous work of van Rijn (van Rijn, 1984a,b).

The formulas of van Rijn in 1984 and 1993 are adjusted to incorporate waves, steady flow, silt effects, different particle size and roughness. In van Rijn (2007c) four different approaches are proposed to represent the bed shear stress paramereter. When tested against several datasets one of the approaches shows promising results, this approach is therefor the only one used in this study.

The van Rijn model calculates initiation of motion using an adjusted version of the Shields curve (van Rijn, 1984a). To account for hiding/exposure, the correction of Egiazaroff (1965) is used. Furthermore, the model of van Rijn also accounts for differences in fluid drag between different grain sizes. For small grains the fluid drag is smaller than the fluid drag of larger grains. Therefore the transport rate of the larger grain sizes is increased, and the transport of the finer grains is decreased. The fluid drag correction decreases transport for grain sizes smaller than the median diameter and increases transport for grain sizes larger than the median diameter.

Equations for fractional transport predictions

The volumetric transport rate is a function of the dimensionless bed-shear stress parameter (T_i), grain-related bed-shear stress, silt fraction, bed shear stress and the dimensionless particle diameter.

$$q_{bi} = p_i 0.5 \rho_s D_i [D^*_i]^{-0.3} [\tau'_{b,cw}/\rho]^{0.5} T_i \tag{2.31}$$

The dimensionless bed-shear stress parameter is calculated using:

$$T_i = \lambda_i \frac{\tau_b' - \xi_i (D_i/D_{50}) \tau_{b,cr,d50}}{(D_i/D_{50}) \tau_{b,cr,d50}} \tag{2.32}$$

The formula of van Rijn applies two forms of hiding/exposure the first is the well-known Egiazaroff (ξ_i).

$$\xi_i = \left(\frac{\log 19}{\log 19 \frac{D_i}{D_{50}}} \right)^2 \tag{2.33}$$

The second takes into account that larger particles are more exposed and experience larger fluid drag while smaller particles are less exposed and experience less fluid drag:

$$\lambda_i = \left(\frac{D_i}{D_{50}} \right)^{0.25} \tag{2.34}$$

$$\tau_b' = \mu_c \tau_b \tag{2.35}$$

$$\mu_c = \frac{f_c'}{f_c} \tag{2.36}$$

$$f_c = 8g / [18 \log(12 R_b / k_{s,b})]^2 \tag{2.37}$$

$$f_c' = 8g / [18 \log(12 R_b / D_{90})]^2 \tag{2.38}$$

in which f_c' is a friction coefficient based on the D_{90}, f_c a friction coefficient based on the bed roughness height ($k_{s,b}$), μ_c the current related efficiency factor, τ_b' is the effective bed-shear stress, $f_{silt,i}$ is the silt parameter.

Equations for uniform transport predictions

For uniform transport is calculated from:

$$q_b = 0.5 \rho_s d_{50} [D_i^*]^{-0.3} [\tau_{b,cw}' / \rho]^{0.5} T_i \tag{2.39}$$

With the dimensionless transport parameter:

$$T_i = \frac{\tau_b' - \tau_{b,cr,d50}}{\tau_{b,cr,d50}} \tag{2.40}$$

Calculation steps

1. Calculate the current related efficiency factor from Eq.(2.38), Eq.(2.37) and Eq.(2.36)
2. Calculate the effective bed shear stress from Eq.(2.35)
3. Calculate the fluid drag correction and hiding/exposure correction from Eq.(2.34) and Eq.(2.33)
4. Calculate the transport parameter from Eq.(2.32)
5. Calculate the transport rate from Eq.(2.31)

Chapter 3

Partial transport data sets

3.1 Introduction

To test the transport models data of six flume experiments available from the literature are used. For each dataset the goals and setup of the experiments as well as the measured and calculated parameters are described. The transport models require a set of parameters as input. For each dataset these parameters are given in figures and tables.

3.2 Data set I: Tuijnder, Spekkers(2007)

Goal

In 2007 Tuijnder and Spekkers performed a flume experiment to study bed roughness under partial transport conditions. The effects of supply limitation on bed forms and bed roughness were studied by varying the amount of sand on top of a pavement layer. Different amounts of sand on top of the pavement layer in combination with the hydraulic conditions led to different supply limitations. This dataset will be referred to as BS-I (Braunschweig - I).

Setup

The experiments were conducted in a small flume facility with dimensions of 7,5 m by 0.3 m. The experiments were a pre-study for a larger scale experiment. To maintain uniform conditions the bed was installed under a slope and the water level adjusted at the downstream end of the flume. The transported sediment was recirculated manually using a sand trap.

The experiment consisted of 26 runs that were split into two sets. In the first first set

of experiments the pavement layer consisted of gravel with larger grain sizes compared to the second set. Also the hydraulic conditions differed between the two sets.

To create partial transport conditions two types of sediment were used: sand and gravel. A gravel pavement layer was installed manually, on top sand was distributed with a predetermined thickness. The hydraulic conditions resulted in a bed shear stress which was small enough for the gravel fraction to remain immobile, but large enough to mobilize the sand. Between runs the amount of sand on top of the gravel layer was varied, while the conditions remained constant.

Measurements

Water levels were measured using six static tubes. An average water level was calculated by a fit through the measurements of the static tubes. The bed levels were measured using a laser bed profiler. From the combined measurements of water level and bed level the water depths and energy slope were calculated. The discharge was measured using an inductive discharge measurement device(IDM).

The bed shear stress was calculated and corrected for sidewall roughness as proposed by Einstein (1942) (Appendix A). To calculate the transport rate the recirculated sediment was wet weighed and return intervals registered. From the timed intervals at which the sediment was weighed and the known density of the sediment and water respectively the transport was calculated.

The measured parameters are given in Table 3.1; h denotes the waterdepth, u the depth averaged flow velocity, I_e the energy slope, R_b the hydraulic radius related to the bed, $k_{s,b}$ the Nikuradze roughness height, τ_b the bed shear stress, C_b the Chézy value related to the bed, d the average transport layer thickness (d = average bed level - average bed level of the pavement layer), f_{gravel} [1] the relative amount of gravel in the grain size distribution, q_b the sediment transport rate.

Figure 3.1 shows the cumulative grain size distributions of the three sediments used in the experiments. The first set of experiments had a pavement layer with fine gravel and a sand layer on top, while in the second set the pavement layer consisted of coarse gravel with sand on top.

[1] estimated values, calculated in chapter 4

Table 3.1: Measured parameters of the BS-I dataset.

-	**h** m	**u** m/s	I_e 10^{-3}	R_b cm	$k_{s,b}$ mm	τ_b Nm^{-2}	C_b $m^{1/2}s^{-1}$	**d** cm	f_{gravel} -	$p_{z<ztil}$ -	q_b g/s
1	0.07	0.45	2.51	6.10	6.50	1.49	36.90	0.00	1.00	1.00	0.00
2	0.07	0.49	2.72	5.80	4.90	1.55	38.80	0.03	0.98	1.00	0.00
3	0.07	0.49	2.64	5.80	4.40	1.50	39.50	0.04	0.98	1.00	0.00
4	0.07	0.51	2.81	5.60	3.80	1.54	40.40	0.12	0.93	1.00	0.78
5	0.07	0.52	2.90	5.40	3.20	1.54	41.50	0.24	0.88	1.00	2.60
6	0.06	0.55	2.90	5.00	1.70	1.42	45.70	0.43	0.72	0.00	7.80
7	0.06	0.57	2.98	4.80	1.20	1.39	47.90	0.59	0.60	0.00	14.04
8	0.06	0.56	2.91	4.90	1.50	1.40	47.00	0.67	0.55	0.17	16.90
9	0.06	0.56	3.03	4.90	1.70	1.46	45.90	0.84	0.47	0.10	18.98
10	0.06	0.56	3.20	5.00	2.00	1.56	44.60	1.09	0.39	0.05	22.62
11	0.06	0.58	3.35	4.80	1.70	1.58	45.60	1.19	0.37	0.02	25.74
12	0.06	0.57	3.27	4.90	1.90	1.56	45.30	1.64	0.28	0.00	26.00
13	0.14	0.51	1.84	10.40	11.60	1.89	36.60	0.00	1.00	1.00	0.00
14	0.13	0.50	1.84	10.00	10.50	1.80	37.00	0.00	1.00	1.00	0.00
15	0.13	0.51	1.91	9.90	10.60	1.86	36.90	0.00	1.00	1.00	0.00
16	0.13	0.51	1.73	9.60	7.30	1.62	39.50	0.01	1.00	1.00	0.21
17	0.13	0.53	2.01	9.50	8.80	1.88	38.00	0.08	0.97	1.00	1.65
18	0.13	0.54	1.84	9.00	5.30	1.62	41.70	0.16	0.95	1.00	3.72
19	0.12	0.55	1.62	8.30	2.50	1.32	47.30	0.39	0.88	1.00	6.61
20	0.12	0.57	1.89	8.10	2.90	1.51	46.40	0.58	0.83	0.58	13.23
21	0.11	0.59	2.11	8.10	3.20	1.67	45.30	0.98	0.62	0.32	19.84
22	0.12	0.56	2.18	8.90	6.50	1.90	39.90	1.26	0.53	0.22	16.95
23	0.12	0.54	2.32	9.40	10.60	2.15	36.60	1.52	0.47	0.16	17.15
24	0.12	0.54	1.84	8.90	5.30	1.59	42.80	1.81	0.41	0.11	17.15
25	0.13	0.53	2.40	9.70	13.60	2.29	35.00	2.17	0.36	0.12	17.57
26	0.13	0.53	2.46	9.80	14.70	2.36	34.50	2.65	0.30	0.04	20.67

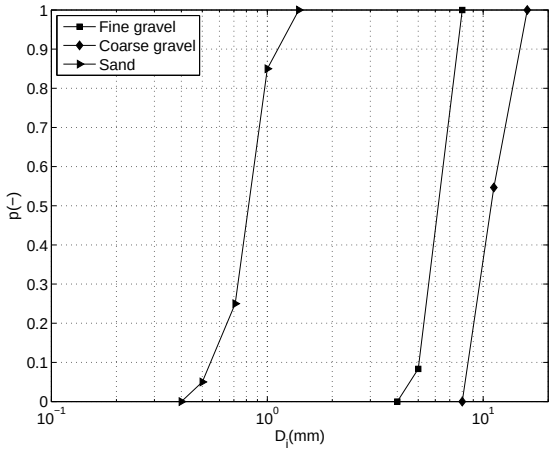

Figure 3.1: Cumulative grain size distribution of the sand and gravel fractions

3.3 Data set II: Tuijnder (2008)

Goal

Tuijnder (2007) performed a series of experiments to study the development of bed forms and bed roughness under partial transport conditions. This dataset will be referred to as BS-II.

Setup

The second data set comprises experiments that are similar to those of data set I, but were conducted in a larger flume. The experiments were conducted at the Leichtweiss Institut in Braunschweig. Not only was the scale different, also the imposed hydraulic conditions had more variation compared to data set I. The entire experiment consisted of 6 series, with a total of 37 experimental runs. Within a series only the amount of sand on top of the gravel layer was varied, while between the series the hydraulic conditions were varied. The different hydraulic conditions of the series are shown in Table 3.2, u denotes the depth averaged flow velocity, h the average waterdepth.. Series 6 consisted of three runs with alluvial conditions, two of which are used in this study.

Table 3.2: Hydraulic conditions of the different series in the BS-II dataset

Series	u	h
	m/s	m
1	0.20	0.52
2	0.30	0.52
3	0.15	0.52
4	0.20	0.58-0.67
5	0.20	0.46
6	0.25	0.52-0.58

The experiments were conducted in a flume facility with dimensions of 2 m wide and 30 m long. For the experiments the width of the flume was reduced to 1 m. The flume was equipped with a sediment recirculation system. To maintain uniform conditions, the discharge and water depth were kept at a constant by changing the water level at the downstream end of the flume and adjusting the slope of the flume.

Different supply limitations were imposed by varying the amount of sand on top a pre-installed gravel layer. At the start of a series a layer of coarse sediment was installed as a pavement layer with a D_{50} of 10.6 mm. The pavement layer remained immobile during the rest of the series. Using a laser bed profiler the bed level of the pavement layer was measured. After the installation of the gravel layer sand was distributed on top. Incrementally the amount of sand on top of the gravel layer was increased.

Table 3.3: Measured parameters of the BS-II dataset.

-	**h** m	**u** m/s	I_e 10^{-3}	R_b cm	$k_{s,b}$ mm	τ_b Nm^{-2}	C_b $m^{1/2}s^{-1}$	**d** cm	f_{gravel} -	q_b g/s
1-1	0.20	0.37	0.70	18.06	32.19	1.25	32.91	0.00	1.00	0.00
1-2	0.20	0.52	0.80	17.11	6.61	1.33	44.87	0.30	0.85	4.30
1-3	0.20	0.52	0.80	17.16	7.04	1.38	44.39	0.30	0.85	3.80
1-4	0.20	0.52	0.80	17.16	7.04	1.35	44.39	1.10	0.56	11.60
1-5	0.20	0.53	0.80	17.07	6.20	1.41	45.35	1.20	0.53	7.90
1-6	0.20	0.52	1.20	17.93	22.10	2.06	35.79	2.00	0.36	15.00
1-7	0.20	0.52	1.60	18.39	45.63	2.87	30.32	4.10	0.20	21.20
1-8	0.20	0.52	1.80	18.53	58.26	3.37	28.47	6.80	0.13	26.60
1-9	0.20	0.52	1.90	18.59	64.81	3.32	27.67	9.70	0.09	25.50
1-10(a)	0.20	0.52	2.20	18.73	82.25	3.97	25.86	16.10	0.06	31.80
2-1	0.30	0.50	0.80	25.93	35.62	2.17	34.95	0.00	1.00	0.00
2-2	0.30	0.52	0.60	24.58	12.33	1.36	42.82	0.30	0.85	3.90
2-3	0.30	0.52	0.40	22.30	2.24	0.90	55.41	1.10	0.56	6.00
2-4	0.30	0.52	0.70	25.23	20.30	1.66	39.12	1.90	0.38	9.90
2-5	0.30	0.51	0.80	25.85	33.23	2.06	35.46	3.90	0.21	13.60
2-6	0.29	0.54	1.20	25.86	60.91	3.18	30.73	6.70	0.13	20.10
2-7	0.30	0.52	0.90	26.09	39.66	2.24	34.15	9.50	0.09	16.50
3-1	0.15	0.53	1.30	13.54	10.13	1.74	39.70	0.40	0.81	4.60
3-2	0.15	0.53	1.20	13.44	8.01	1.56	41.47	1.10	0.56	10.80
3-3	0.15	0.51	1.40	13.68	14.26	1.94	37.10	2.10	0.35	15.10
3-4	0.16	0.49	1.40	14.69	22.77	1.95	34.00	3.70	0.22	18.10
3-5	0.15	0.53	2.00	13.97	29.78	2.88	31.51	6.70	0.13	15.20
3-6(a)	0.15	0.53	2.60	14.15	48.45	3.70	27.80	16.00	0.06	32.10
4-1	0.20	0.68	1.20	17.00	4.83	2.07	47.26	0.40	0.81	17.90
4-2	0.20	0.68	1.70	17.76	14.79	3.01	38.85	1.20	0.53	35.00
4-3	0.20	0.58	1.60	18.11	27.81	2.82	34.07	2.10	0.35	26.20
4-4	0.20	0.58	2.10	18.49	51.35	3.91	29.44	3.90	0.21	38.20
5-1	0.20	0.46	0.60	16.94	5.57	1.05	46.12	0.30	0.85	2.10
5-2	0.20	0.46	0.70	17.31	9.34	1.12	42.25	0.40	0.81	1.50
5-3	0.20	0.46	0.60	16.99	6.00	0.92	45.56	0.90	0.63	3.20
5-4	0.20	0.46	0.60	16.94	5.57	1.05	46.12	1.90	0.38	6.00
5-5	0.20	0.46	0.80	17.58	14.00	1.43	39.21	3.80	0.21	10.00
5-6	0.20	0.46	1.20	18.26	39.42	2.24	31.41	6.50	0.13	11.10
5-7(a)	0.20	0.47	1.50	18.53	60.35	2.84	28.19	16.00	0.06	14.50
6-1(a)	0.25	0.52	1.70	23.08	96.36	3.87	26.25	16.00	0.06	25.20
6-2(a)	0.26	0.58	2.20	24.12	117.51	5.21	25.05	16.00	0.06	45.20

Measurements

Bed and water levels were measured using echo sensors. Through the echo sensor readings trend lines were fitted to determine the average bed and water levels. From the calcualted bed and water levels, the water depth was calculated. The discharge was measured with an Inductive measurement device, or IDM.

Two turbidity sensors were installed to measure the sediment transport rates. The overall background turbidity was measured at the end of the flume, while the transport turbidity was measured in the recirculation system. At the same location more flume experiments were conducted, all flumes were supplied with water from the same water tank. Start-up of other experiments caused great variations in the turbidity of the water. Therefore, the background sensor was a necessity to filter out background turbidity. The sediment transport was calculated as the difference between total transport and background turbidity. The measurements of background turbidity assured that the influence of other experiments could be removed.

From the measured water and bed levels the bed shear stress and roughness height can be calculated. The bed shear stress is calculated and corrected for wall roughness using the Vanoni and Brooks equations (Appendix A).

The measured parameters of the BS-II dataset are given in Table 3.3.

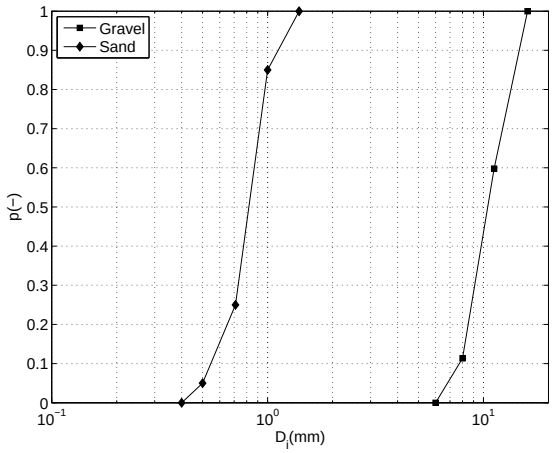

Figure 3.2: Cumulative grain size distribution of the BS-II data set.

The sediments used in this experiment consisted of two types, sand and gravel. Gravel for the pavement layer and sand on top as the transport layer. Both are given in a cumulative grain size distribution in Figure 3.2.

3.4 Data set IV: Spekkers (2008)

Goal

The third data set is similar to data set II, in that it comprises similar conditions, but with a mixed sediment composition. The experiments were conducted in the same flume as data set II at the LWI in Braunschweig. Different amounts of gravel were added to a sand bed to study the development of pavement layers. This dataset will be referred to as BS-IV, it was the fourth experiment in Braunschweig. Unfortunately the third experiment lacked accurate measurements of the transport rates and can therefore not be used in this study.

Setup

The same flume was used as in data set II, however contrary to data set II no gravel layer was pre-installed. A grain size distribution was installed with a known amount of gravel. Initially, the sediment was well-mixed, during the experiment vertical sorting of the gravel developed a pavement layer. Each of the experimental runs contained a different amount of gravel, that was increased with consecutive runs.

Uniform conditions were maintained by keeping the water depth and discharge constant and changing the downstream water level and slope of the flume.

Measurements

The discharge was measured with an IDM. The bed and water levels were measured with echo sensors. Trend lines were fitted through the echo sensor readings to determine the average bed and water level. From the average bed and water levels, the water depth and flow velocity were calculated. The bed shear stress was calculated and corrected for wall friction using the equations of Vanoni-Brooks. The bed roughness and roughness height were calculated using the Chézy equations and White-Colebrook correction (Appendix A). At the end of each experimental run, photographs and laser profiles were taken of the final state of the bed. These can be used to determine the surface based grain size distribution. The measured parameters of data set IV are given in Table 3.4. The grain size distribution of the two sediments used in this experiment are shown in Figure 3.3.

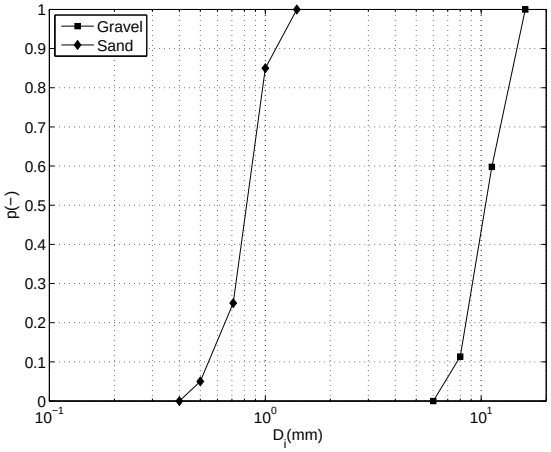

Figure 3.3: Cumulative grain size distributions of for the BS-IV dataset.

Table 3.4: Measured parameters of the BS-IV dataset.

	h	**u**	I_e	R_b	$k_{s,b}$	τ_b	C_b	**d**	f_{gravel}	$p_{z<ztil}$	q_b
-	m	m/s	10^{-3}	cm	mm	Nm^{-2}	$m^{1/2}s^{-1}$	cm	-	-	g/s
1	0.20	0.52	1.50	18.30	45.10	2.81	31.39	7.00	0.05	0.00	17.96
2	0.20	0.52	1.30	18.09	30.70	2.31	33.91	4.64	0.10	0.02	18.83
3	0.20	0.52	1.10	17.81	18.30	1.93	37.15	3.44	0.15	0.06	18.33
4	0.30	0.52	0.60	24.58	12.90	1.50	42.82	2.57	0.15	0.12	9.56
5	0.20	0.52	1.70	18.46	27.30	2.98	29.35	3.06	0.15	0.09	33.03
6	0.20	0.52	0.90	17.42	9.90	1.54	41.53	1.58	0.20	0.19	11.79

3.5 Data set V: Blom(2000)

Goal

The fifth data set is a study conducted at the flume facility of WL Delft Hydraulics (Blom, 2000). The experiments conducted by Blom were a study of grain size selective transport and sorting using a tri-modal sediment mixture. Different conditions and

sediment compositions were used: both partial transport and pavement layers were observed. This dataset will be referred to as Blom.

Setup

In a large flume, dimensions of 50 m long and 1 m wide different sediment mixtures were tested under different conditions. Two different starting conditions were tested; first a fully mixed sediment and second a mixed surface layer on top of fine sediment (finest of the three fractions). The latter series was to study entrainment and redistribution of the sediment over depth of the flume. Conditions were kept uniform by a constant discharge and changing the downstream water level.

Measurements

Water and bed levels were measured with conductivity sensors. Sediment was recirculated using a hydrocyclone. At the end of the flume sediment was collected and transported to the hydrocyclone at the begin of the flume. The sediment was released back into the flume when the hydrocyclone reached a certain weight. By timing the intervals of release and the known release weight the transport rate was calculated.

At the start and end of the equilibrium stages of the experiment the sediment was sampled. The sediment was sampled with a specially developed core sampler, in the center and both sides of the flume. From these samples and bed level measurements van der Scheer et al. (2002) determined surface based grain size distributions.

From measurements of the water and bed level the bed shear stress and hydraulic roughness were calculated. The bed shear stress and hydraulic radius were calculated and corrected for side-wall roughness with the Vanoni and Brooks. Figure 3.4 shows the cumulative grain size distributions of the three sediment fractions used in the experiments. Table 3.5 shows the parameters that will be used in the model calculations.

Table 3.5: Measured parameters of the Blom dataset.

	h	**u**	I_e	R_b	$k_{s,b}$	τ_b	C_b	q_b
-	m	m/s	10^{-3}	cm	mm	Nm^{-2}	$m^{1/2}s^{-1}$	g/s
A1	0.15	0.64	2.00	14.20	13.53	2.78	37.80	29.61
A2	0.32	0.83	1.80	28.52	25.50	4.63	38.30	113.45
B1	0.16	0.63	1.90	14.24	12.10	2.62	38.70	30.65
B2	0.39	0.69	2.20	36.44	178.59	7.39	25.00	116.59

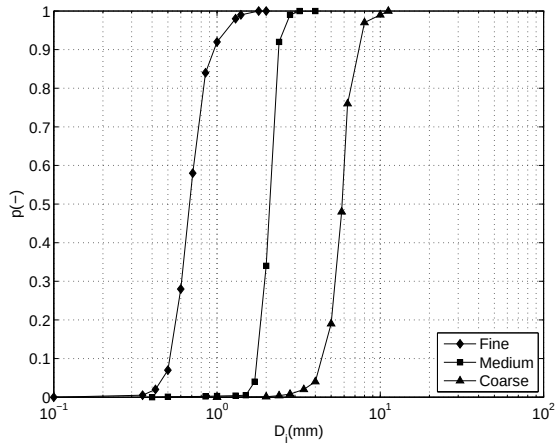

Figure 3.4: Cumulative grain size distributions of the three fractions used in the Blom experiments.

3.6 Data set VI: Blom and Kleinhans(1999)

Goal

The sixth dataset is a flume experiment conducted at the WL Delft Hydraulics flume facility by Blom and Kleinhans (Blom and Kleinhans, 1999). Similar to Dataset V this is a study in grain size selective sorting and transport, but with a different sediment mixture and conditions. A sediment mixture dredged from the river Waal was used under different conditions. The transported sediment was much finer than the original composition indicating partial transport. This dataset will be referred to as BK.

Setup

The experiments were conducted in a large flume, with dimensions of 50 m long and 1.5 m wide. Uniform conditions were maintained by varying both the discharge and downstream water level and keeping flow velocity constant. Four experimental runs were set up to represent a flood hydrograph, increasing and decreasing flow velocity.

Measurements

Water and bed levels were measured with conductivity sensors. Sediment transport rates were determined in the same way as data set V. Also, at the start and end of the equilibrium stages of the experiment the sediment was sampled.

From bed and water level measurements the bed shear stress and hydraulic radius were calculated. The bed shear stress and hydraulic radius were calculated and corrected for side-wall roughness with the Vanoni and Brooks equations. Figure 3.5 shows the

cumulative grain size distribution and Table 3.6 shows the measured and calculated parameters.

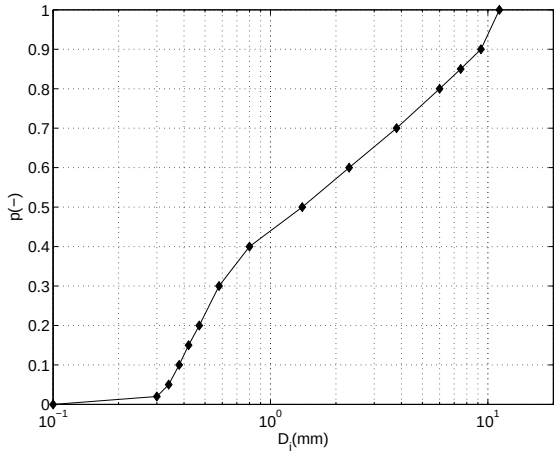

Figure 3.5: Cumulative grain size distributions of for the BK dataset.

Table 3.6: Measured parameters of the BK dataset.

	h	**u**	I_e	R_b	$k_{s,b}$	τ_b	C_b	q_b
-	m	m/s	10^{-3}	cm	mm	Nm^{-2}	$m^{1/2}s^{-1}$	g/s
T5	0.25	0.69	1.50	22.40	23.11	3.40	37.18	123.93
T7	0.35	0.79	1.50	31.60	38.70	4.80	35.84	214.58
T9	0.26	0.70	1.80	24.00	36.91	4.10	34.06	148.29
T10	0.19	0.59	1.20	17.60	10.54	2.00	41.43	45.06

Chapter 4

Data preparation

4.1 Introduction

For the transport model calculations more parameters are needed than are known for some data sets. In the BS-I and BS-II data sets the grain size distribution of the individual fractions are known. However, no sediment composition, a combination of the fractions, was determined during the experiments. Also for the BS-IV dataset the sediment transport rate was not measured due to failure of the one of the sensors. In this chapter these additional parameters are estimated from the available data of the experiments.

4.2 Sediment compositions

The transport models require input of either a representative sediment characteristic parameter (e.g. D_{50}) or a sediment composition. For the BS-I and BS-II datasets this is estimated using the transport layer thickness (d).

BS-I

To calculate transport rates the sediment characteristic parameters like the D_{50} and D_{90} need to be calculated. The parameters need to represent the sediment in transport, but also contain information of the immobile sediment, to account for partial transport effects like supply limitation.

To determine a representative sediment composition both sand and the immobile gravel layer are included. Figure 4.1 shows roughly the three situations that occured during the experiments. Also alluvial conditions were observed, in that case the gravel layer is completely coverd with sand.

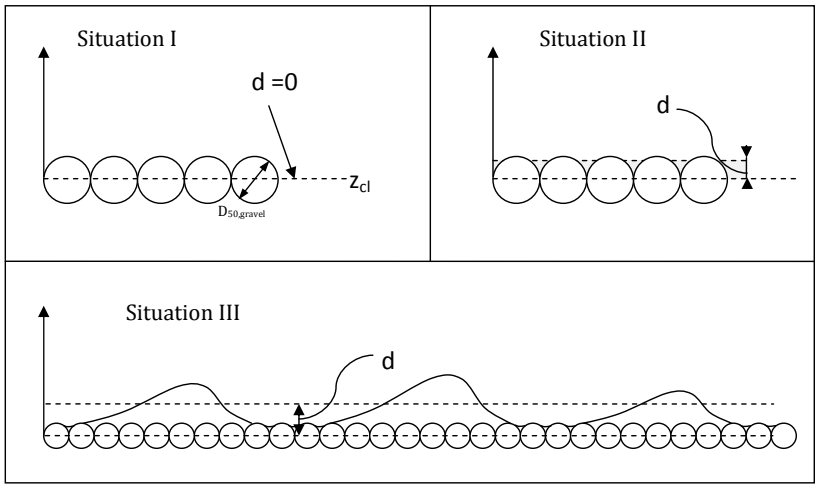

Figure 4.1: Three situations of supply limited conditions, situation I: only gravel present (z_{cl} is the average bed level of the gravel layer), situation II: very small amount of sand present, situation III: supply limited bed forms present

For this study it is chosen to include a layer of gravel with a thickness of one average grain diameter. The gravel at the top of the layer directly influences the sand on top, while the gravel below the surface layer is locked in a pavement layer and cannot influence the sand under the observed circumstances. The transport layer thickness is the difference between the average bed level during transport and the average bed level of the gravel layer (d in Figure 4.1). The transport layer thickness is combined with one layer of gravel into a sediment composition that is used in the model calculations. To create the sediment composition a relative amount of gravel is calculated based on volumes of sand and gravel:

$$f_{gravel} = V_{gr}/(V_{gr} + V_s) \tag{4.1}$$

where f_{gravel} is the relative amount of gravel in the sediment composition, V_{gr} the volume of gravel (without pores), V_s the volume of sand (without pores).

However, this is difficult to determine because the porosity of the sand/gravel mixture depends on the relative amount of sand and gravel. Sand will occupy the pores of the gravel fraction decreasing the porosity of the mixture. Spekkers (2008) measured porosities of sand/gravel mixtures for the sediments of BS-I. Without the presence of sand the porosity of the gravel is 0.42, the porosity of the sand is 0.35. In a mixture of sand and gravel, sand will occupy the pores of the gravel reducing the porosity to a minimum of 0.2, where all the pores of the gravel are maximally filled with sand.

With sand on top of the gravel layer, two situations are observed: for very small amounts of sand first the pores of the gravel are filled up (Situation II in Figure 4.1), the porosity of this mixture varies between 0.42 for gravel only and 0.2 for gravel maximally filled

up with sand. After the pores are filled sand will accumulate on top of the gravel layer (Situation III in Figure 4.1). In this case two different porosities exist, first the layer of gravel filled with sand with a porosity of 0.2 and second the sand on top with a porosity of 0.35.

In an example, a box of $1m^3$ filled with gravel contains $0.58m^3$ gravel (1 - 0.42 = 0.58). A box of $1m^3$ filled with sand contains $0.65m^3$ sand (1 - 0.35 = 35). If the pores in the box of gravel are filled with sand the total amount of sediment in the m^3 increases to $0.8m^3$. Therefore the volume of sand in a m^3 of sand and gravel is estimated $0.22m^3$ (0.8 - 0.58 = 0.22).

In the flume experiment the gravel layer was pre-installed, therefore the volume of gravel does not change. An average layer of gravel without pores has a volume of:

$$V_{gr} = D_{50,gr}(1 - \epsilon_{gr}) \tag{4.2}$$

where $D_{50,gr}$ the median diameter of the gravel, ϵ_{gr} the porosity of the gravel.

The layer of sand on top of the gravel layer is expressed as the average transport layer thickness or d. Figure 4.1 shows the three situations;

- situation I: no sand is present (d = 0)
- situation II; the pores of the gravel layer are filled up with sand ($0 < d \leq 0.5D_{gr}$), for increasing d the amount of sand slowly adds up to 0,22 for completely filled pores of the gravel fraction.
- situation III: is the situation where bedforms are present on top of the gravel layer ($d > 0.5D_{gr}$).

The volume of sand is calculated using Equation 4.3.

$$V_s = \begin{cases} 0 & \text{for } d = 0 \\ 0.22d & \text{for } d \leq 1/2D_{50,gr} \\ \left(d\left(\frac{1}{2}D_{50,gr}\right)\right)(1 - \epsilon_s) + 0.22\frac{1}{2}D_{50,gr} & \text{for } d > 1/2D_{50,gr} \end{cases} \tag{4.3}$$

where V_s is the volume of sand without pores, d is the average transport layer thickness, $D_{50,gr}$ the median diameter of the gravel fraction, ϵ_s the porosity of the sand fractions.

With the calculated volumes of sand and gravel the relative amount of gravel is calculated using Equation 4.1. The sediment composition is calculated by multiplying the grain size distribution of the gravel (Figure 3.1) with the estimated f_{gravel} and the sand grain size distribution with $1 - f_{gravel}$. The estimated grain size distributions are given in Figure 4.2, the values are given in Appendix B.

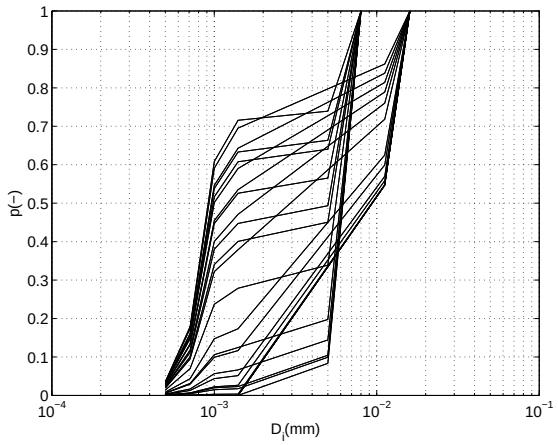

Figure 4.2: Cumulative grain size distributions of for the BS-I dataset.

BS-II

The sediment composition is calculated in the same way as data set I. However, in the experiments of data set II only one type of gravel was used compared to two for data set I. The relative amount of gravel in the sediment is calculated from Equation 4.1 and combined with the distributions of the sand and gravel fraction respectively (Figure 3.2). Figure 4.3 shows the cumulative grain size distributions that will be used in the transport model calculations, the calculated values are given in Appendix B.

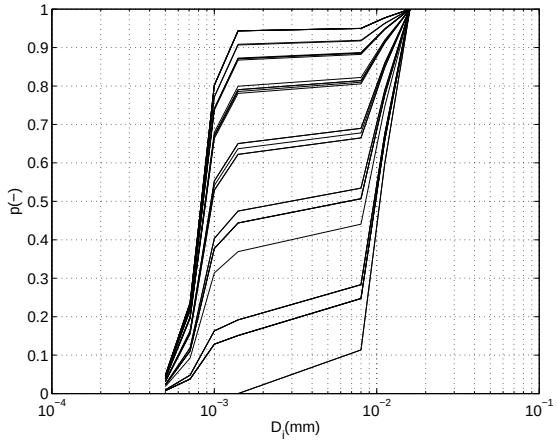

Figure 4.3: Cumulative grain size distributions of for the BS-II dataset.

BS-IV

The sediment composition for the BS-IV experiment were predetermined. For the experiments a pre-determined amount of gravel was added to a known amount of sand.

The grain size distributions are given in Figure 4.4, the calculated values in Appendix B.

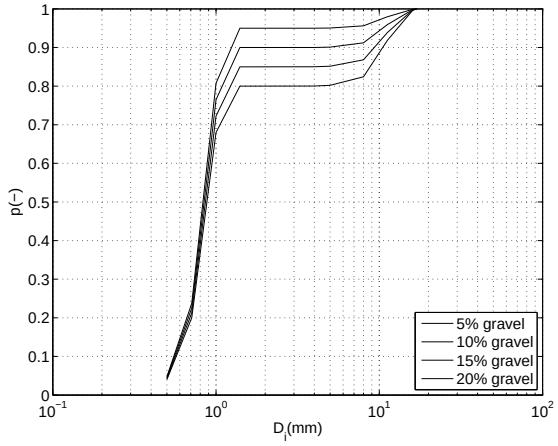

Figure 4.4: Cumulative grain size distributions of for the BS-IV dataset.

Blom

For the Blom dataset the sediment compositions at the start of the experiments were known. The first three experimental runs were conducted with a mixture of one third of each fraction (fine, medium and coarse), while the last experimental run was done with a 80:10:10 mixture (80% fine, 10% medium and 10% coarse). The sediment compositions are given in Figure 4.5 and the calculated values are given in Appendix B.

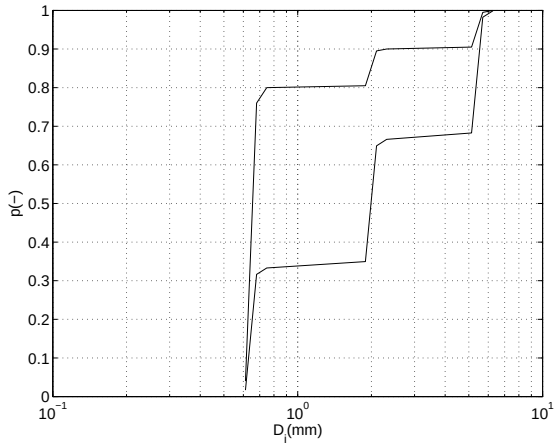

Figure 4.5: Cumulative grain size distributions of for the Blom dataset.

4.3 Transport rate

Sediment transport rates

In the experiment of data set the BS-IV the background turbidity sensor failed, no transport rates could be calculated accurately. At the location where the experiments were conducted other flume experiments influenced the turbidity of the water.

This dataset can only be used if the transport rates are estimated, this is done using a technique known as dune tracking. The dune tracking method was used by Blom et al. (2002) and proved fairly accurate. In the dune tracking method the transport rate can be calculated on the basis of several assumptions developed by Bagnold (1942). If (1) the dunes migrate at a constant speed, (2) there is no flux between dunes and (3) there is no change in dune dimensions, the transport rate is calculated using:

$$q_b = cc_b\alpha\Delta \tag{4.4}$$

in which c is the celerity of the bed form; c_b is the sediment concentration within the bed ($c_b = 1 - \epsilon_p$, where ϵ_p is the porosity); α is the form factor; Δ is the bedform height (Blom et al., 2002).

In this equation the transport rate, bed form celerity and form factor are unknown. The bed form factor (α) is calibrated using data set II. In this dataset similar conditions, sediments and bed forms were observed. In data set II transport rates were measured and bed form celerity calculated from the bed level measurements. Using a sum of least squares fitting method, the bed form factor is calibrated on the BS-II dataset with $\alpha = 0.41$. It is assumed that for the similar conditions and sediments of BS-IV this value is also valid. With the bed form factor determined, the transport rate and bed form celerity are still unknown. The bed form celerity can be determined from echo sensor readings. From plots of bed levels in time and space, as shown in Figure 4.6, the bed form celerity can be determined as the solid black line in the figures. Each line follows a crest or trough of a bed form through time and space. The angle of the solid line is the bed form celerity, the determined values are shown in Table 4.1. From the celerities and Equation 4.4 the transport rates are calculated and shown in Table 4.1

Table 4.1: Celerities and transport rates determined using dune tracking

Experiment (-)	Celerity (m/h)	Sediment transport (g/s)
1	1.60	18.0
2	2.00	18.8
3	2.20	18.3
4	1.20	9.6
5	3.80	33.0
6	2.10	11.8

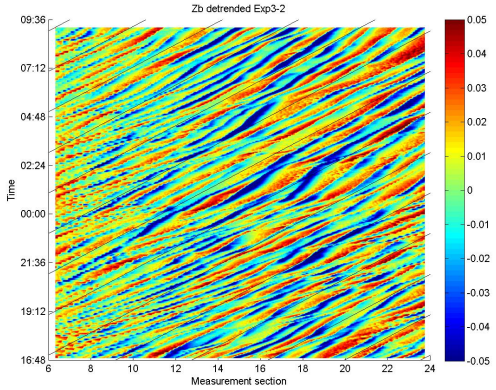

(a) Exp 1.

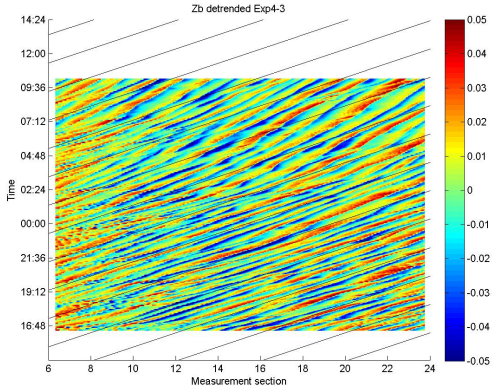

(b) Exp 2.

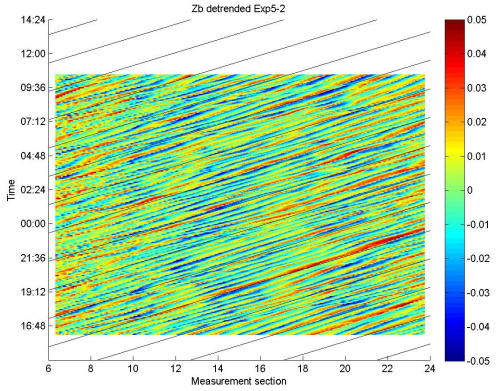

(c) Exp 3.

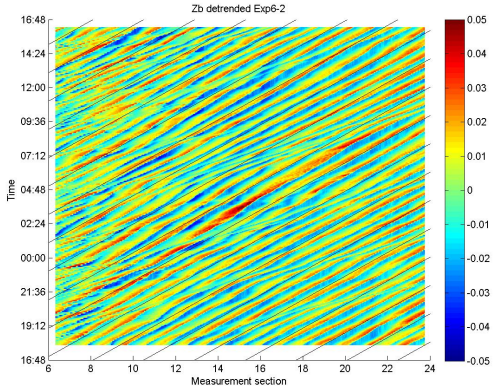

(d) Exp 4.

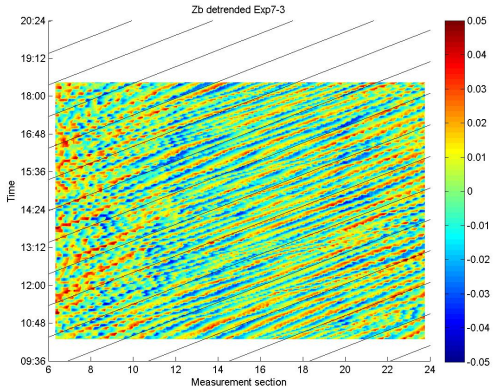

(e) Exp 5.

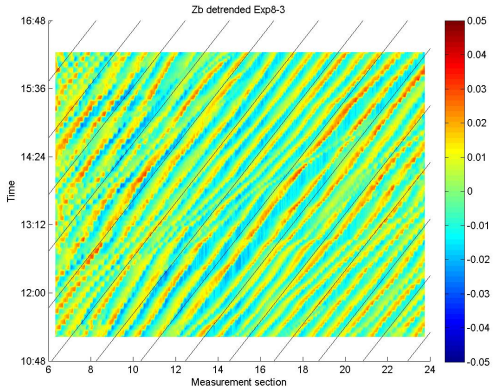

(f) Exp 6.

Figure 4.6: Bed levels in time and space for 6 runs of the BS-IV data set. The solid black lines indicate the bedfrom celerity.

Chapter 5

Sediment transport rate predictions, Bulk-based

5.1 Introduction

In this chapter the transport models' performance is tested using the bulk grain size distributions. The bulk grain size distributions were determined in chapter 4. Different approaches are used; both uniform and fractional transport calculations for each transport model. A uniform transport calculation represents the entire sediment mixture with one representative diameter, often the mean or median diameter. In the fractional transport calculation the transport rate of each fraction is predicted. To demonstrate the performance of the transport models, the predicted transport rates are compared to the measured transport rates.

5.2 Bulk based transport predictions

Each transport model calculates transport rates from a combination of sediment characteristic parameters and hydraulic conditions. In chapter 2 a calculation procedure for each transport model is given that is combined with measured and calculated data from chapter 3 and 4. In chapter 3 the hydraulic conditions for each dataset are given in Table 3.1, 3.3, 3.4, 3.5, 3.6. The sediment characteristics are derived from figures of the grain size distributions (Figure 4.2, 4.3, 4.4, 4.5, 3.5). The values of the grain size distributions are also given in tables in Appendix B.

In sections 5.2.1 - 5.2.3 the three models are used in a uniform transport calculation, in sections 5.2.4 - 5.2.6 in a fractional transport calculation. For the uniform transport calculation the predictions consist of a total transport rate prediction only ($q_{b,pred}$), that is compared to the measured total transport rate ($q_{b,meas}$). For the fractional transport

calculation the model predicts transport rates for each fraction, therefore the predictions can both be compared to the measured total transport rate as well as the measured fractional transport rate. However, for the BS data sets only the total transport was measured and the predictions of the fractional transport rates cannot be compared to measurements. It is known that only the sand fraction was mobile, which was also the set-up of the experiment, thus the fractional transport rates can be analyzed on mobility of the sand and gravel fractions only.

In the analysis of the performance of the transport models several aspects are checked:

- Predicted total transport rate is compared to measured transport rates.
- Transport composition is checked (for fractional transport calculations only)
- For the BS data sets (BS-I, BS-II and BS-IV) the predictions are analyzed on supply limitation
- Analyze different parameters in the transport calculations.

5.2.1 Meyer-Peter and Müller (1948) (uniform)

Figure 5.1 shows the predicted and measured total transport rates for the uniform transport calculation. The uniform model has trouble predicting transport for the data sets with the bimodal sediment (BS-I, BS-II and BS-IV). A transport rate of zero is predicted for 100% of the BS-I datapoints, 75% of the BS-II datapoints and 50% of the BS-IV datapoints. The predictions for the Blom and BK data set are too low, but almost all within a factor 2, which in the literature is considere a good prediction.

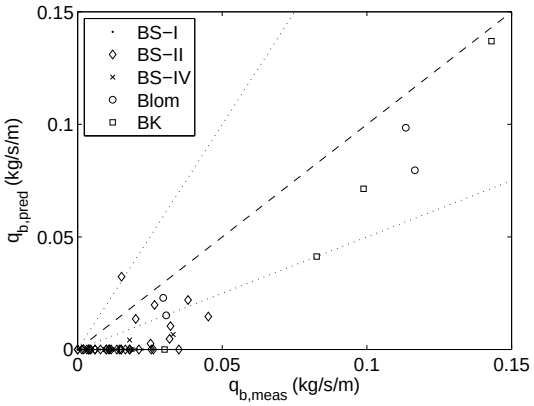

Figure 5.1: Predicted and measured transport rates for all data sets with the uniform model of Meyer-Peter and Muller. The dashed line depicts perfect agreement between measurement and prediction, the dotted line a factor two deviation.

Figure 5.2 shows the transport predictions in relation to the supply limitation for the BS datasets. Note that the figure is on a log-scale, so zero transport predictions are

not shown. In Figure 5.2 only the predictions for the BS data sets are given, too little information is available on the data sets of Blom and BK to calculate transport layer thickness. It can be seen that all the transport rates are underpredicted, except for one point of the BS-II data set. No obvious difference can be seen between predictions under supply limited conditions or under alluvial transport.

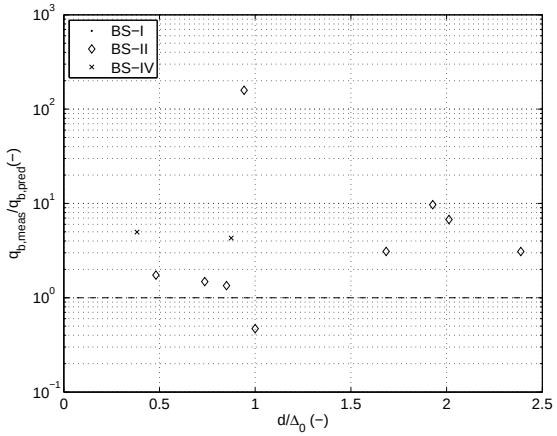

Figure 5.2: Transport ratio as a function of the relative transport layer thickness for BS data sets using the uniform Meyer-Peter and Müller model.

Figure 5.3 shows two parameters used in the transport calculation as well as the total transport ratio. The first row of graphs shows the bed shear stress that, in combination with the second row (mean Shields stress), explains why a lot of transport rates cannot be predicted. A zero transport prediction occurs when $\mu_{mpm}\theta_m - 0.047$ from Equation 2.10 is below zero. Although the bed shear stress is fairly similar for each of the data sets, ranging from approximately 2 - 4 Nm^{-2}. The mean Shields stress (θ_m) decreases rapidly if the mean diameter is larger. In the first three columns (the BS data sets), the mean diameter is always above 1 mm, while during the experiment only the sand was mobilize (mean diameter of the sand is approximately 0.9 mm). The large mean diameters are caused by the estimated amount of gravel in the grain size distribution. Because the sediment of the BS data sets is strongly bimodal, including even small amounts of gravel will give a large increase the mean diameter of the grain size distribution. Large mean diameters in turn result in a small mean Shields stress (Equation 2.17), that in turn results in either zero transport prediction or very small transport rates. This is demonstrated in last row, where most of the predicted ratios are above 1, overpredicting the transport.

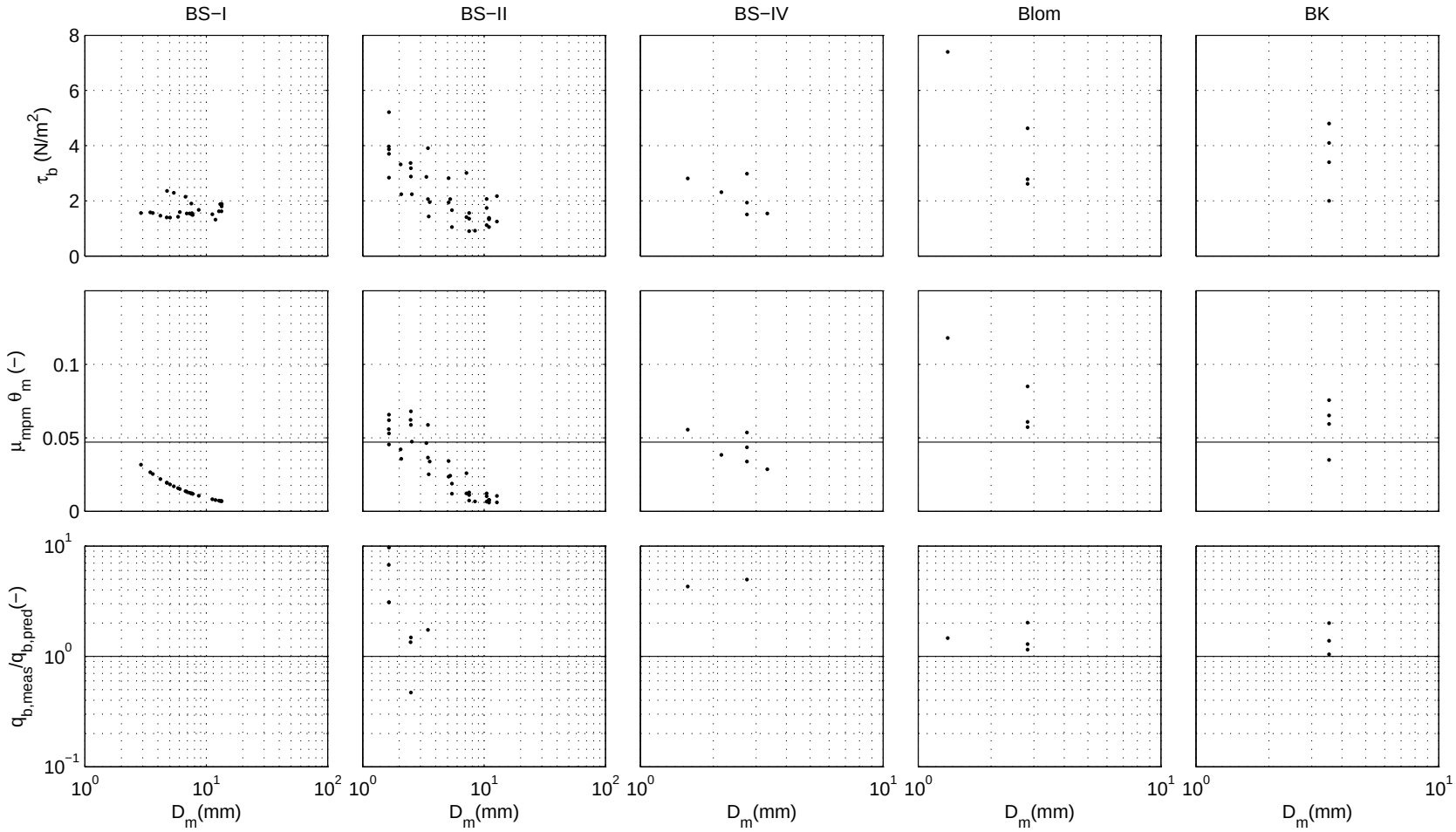

Figure 5.3: The bed shear stress, mean Shields stress and transport ratio of the uniform model of Meyer-Peter and Müller

A lot of the bad or zero transport predictions are due to the 'choice' of the mean diameter in the transport model in combination with the bimodal sediment of the BS-datasets. One option is to use the median diameter instead of the mean diameter. However, in the original model this was not the case and therefore it has not been changed here. Figure 5.4 shows the mean Shields stress as a function of the mean diameter. An average bed shear stress from the BS-II data set is used to demonstrate variations of the mean Shields stress. The dashed horizontal line depicts the critical Shields stress of the Meyer-Peter and Müller model ($\theta_{cr} = 0.047$). For a mean diameter above approximately 2 mm the mean Shields stress is below the critical Shields stress of the model and zero transport is predicted. For the bimodal sediments of the BS-data sets a mean diameter above 2 mm occurs often, resulting in a zero transport prediction.

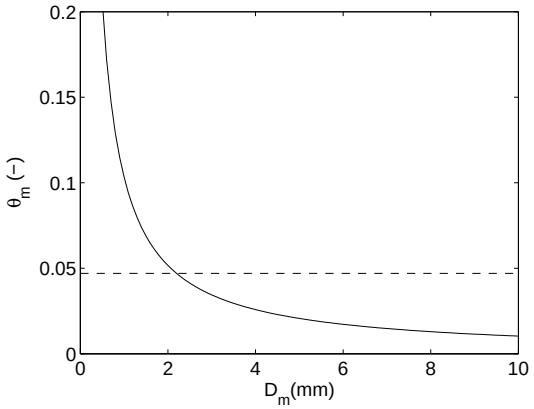

Figure 5.4: Shields stress as a function of the mean diameter

5.2.2 van Rijn (uniform)

Figure 5.5 shows the predicted and measured transport rates of the uniform model of van Rijn. For the Blom and BK data set it gives fairly accurate predictions, while showing both overpredictions and underpredictions for the BS-data sets, as well as a number of zero transport predictions.

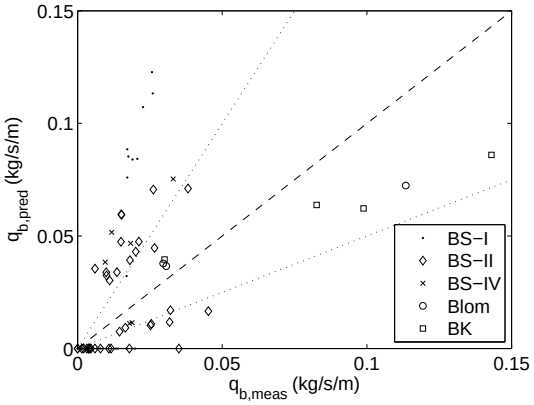

Figure 5.5: Predicted and measured transport rates for all data sets with the uniform model of van Rijn

Figure 5.6 shows the transport ratio in relation to the supply limitation. For all data sets the total transport rates are predicted too high. For supply limited conditions, $d/\Delta_0 < 1$, the model strongly overpredicts the transport rates, while for nearly alluvial conditions the model predicts transport rates that are too low.

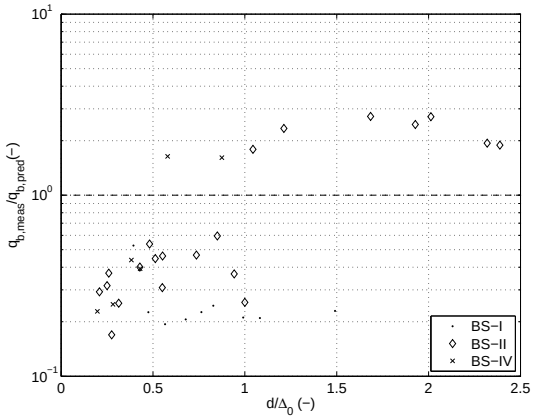

Figure 5.6: Transport ratio as a function of the supply limitation using the uniform van Rijn model.

Figure 5.7 shows the transport ratio as well as some of the parameters of the model calculation in relation to the median diameter of the sediment. The first row of graphs depicts the grain related bed shear stress. The grain related bed shear stress is calculated with the current related efficiency factor (μ_c). Equation 2.38 shows that the current related efficiency factor is calculated from the grain related friction factor. The D_{90}

used in this calculation is affected by the relative amount of gravel in the grain size distribution. For most of the points of the BS data sets more than 10% gravel is present in the grain size distribution. In that case the D_{90} is a gravel diameter and this results in current related efficiency factors that are extremely high. This directly affects the grain related bed shear stress that will also be too large resulting in transport predictions that are often too high. In the case of better sorted sediment this will occur less. On the other hand the bulk grain size distribution is coarser than the actual transported material. This affects the grain related bed shear stress, resulting in predicted transport rates that are too low. This can be seen for the Blom and BK data sets.

The second row in Figure 5.7 shows the critical bed shear stress. In combination with the grain-related bed shear stress this determines the transport from the bed shear stress parameter (T_i). Since the grain related shear stress is too high compared to the critical shear stress, the predicted transport rate becomes too high.

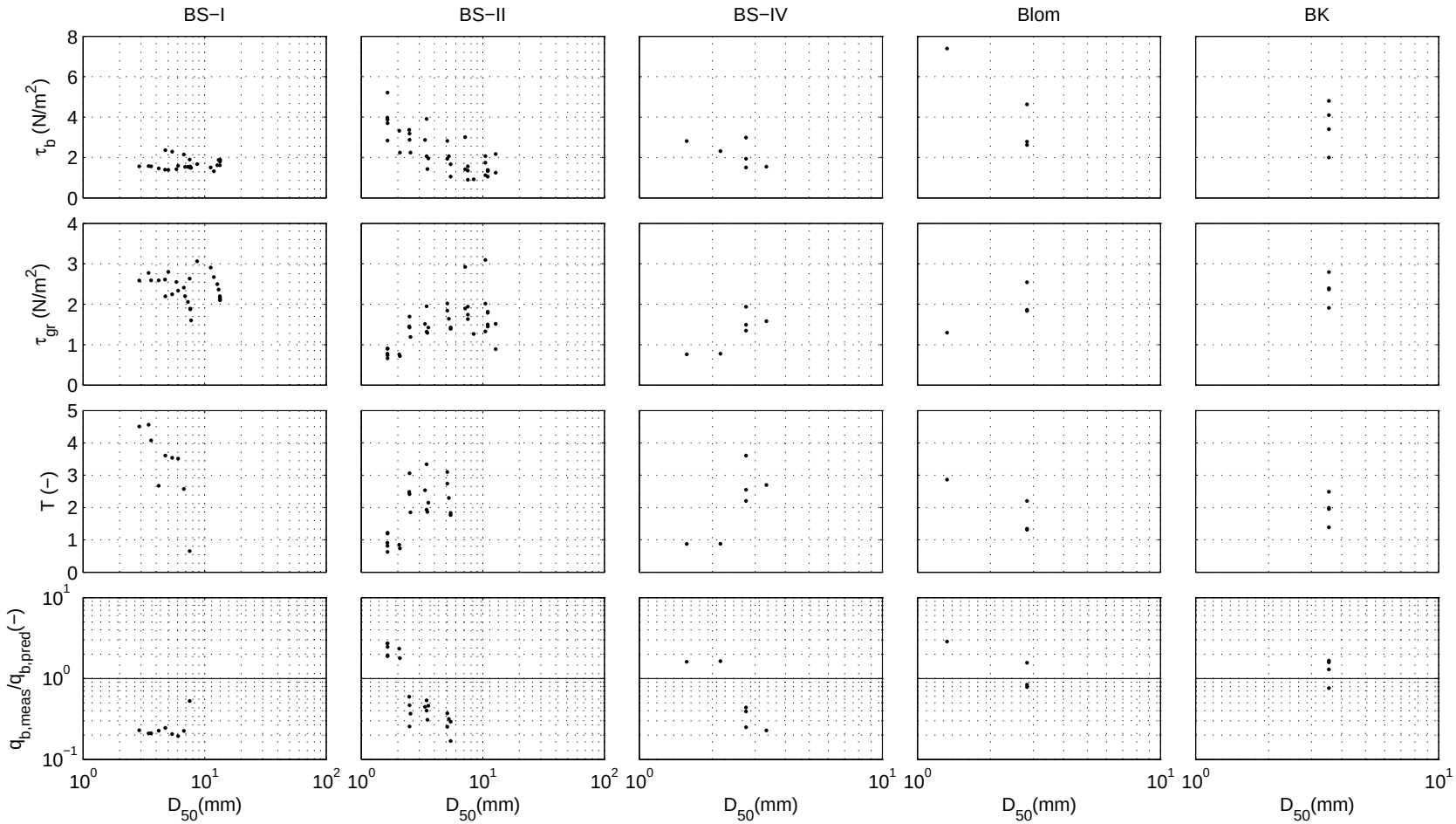

Figure 5.7: The grain related bed shear stress, critical bed shear stress for the median diameter, bed shear stress parameter (T_i) and the transport ratio as a function of the median diameter for the uniform van Rijn model.

5.2.3 Wilcock and Crowe (uniform)

Figure 5.8 shows the predicted and measured transport rates for the uniform Wilcock and Crowe model. This model predicts the Blom data set well, the data sets of BS and Blom are predicted poorly. Most of the transport rates are predicted too low.

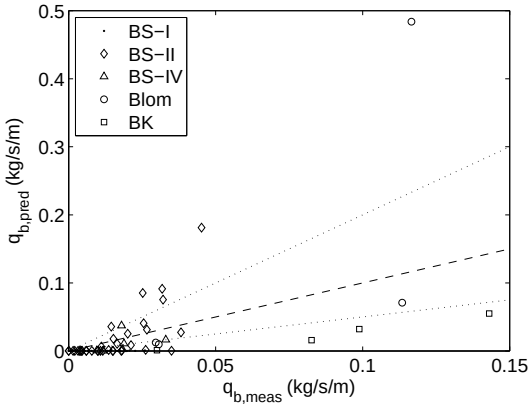

Figure 5.8: Predicted and measured transport rates for all data sets with the uniform model of Wilcock and Crowe

Figure 5.9 shows the transport ratio in relation to the supply limitation for the BS data sets. The transport model of Wilcock and Crowe is designed for partial transport conditions. For supply limited conditions however, the model underpredicts the transport rates of the BS data sets strongly, while for more alluvial conditions ($d/\Delta_0 > 0.5$) the predictions for the BS-II data set are nearly accurate.

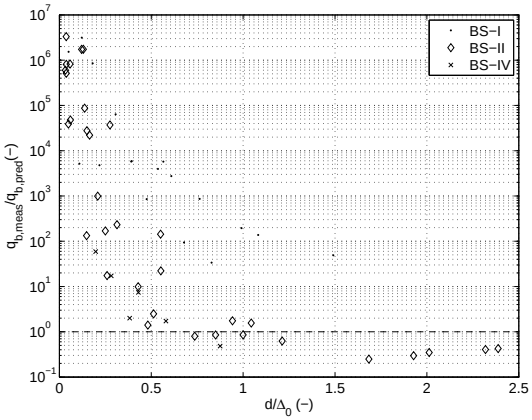

Figure 5.9: Transport ratio as a function of the supply limitation using the uniform model of Wilcock and Crowe.

Figure 5.10 shows the bed shear stress, the mean reference shear stress and transport ratio as a function of the mean diameter for the uniform Wilcock and Crowe model. The first row of graphs depicts the occuring bed shear stress of the experiments. The second

row shows the mean reference shear stress as a function of the mean diameter, this increases steeply for increasing mean diameters. The model predicts transport based on the ratio of the bed shear stress and reference shear stress. With a large mean diameter of the sediment the mean reference shear stress becomes large and a very small transport rate is predicted. This results in many underpredictions of the total transport rate. The third row shows the transport parameter (ϕ_i). For increasing mean diameters it is shown that the transport parameter decreases. For grain size distributions with a mean diameter approximately above 3 mm the transport parameter is approximately zero. However, in the fourth row the total transport ratio shows extreme underpredictions, which means that the predicted transport rate is very small.

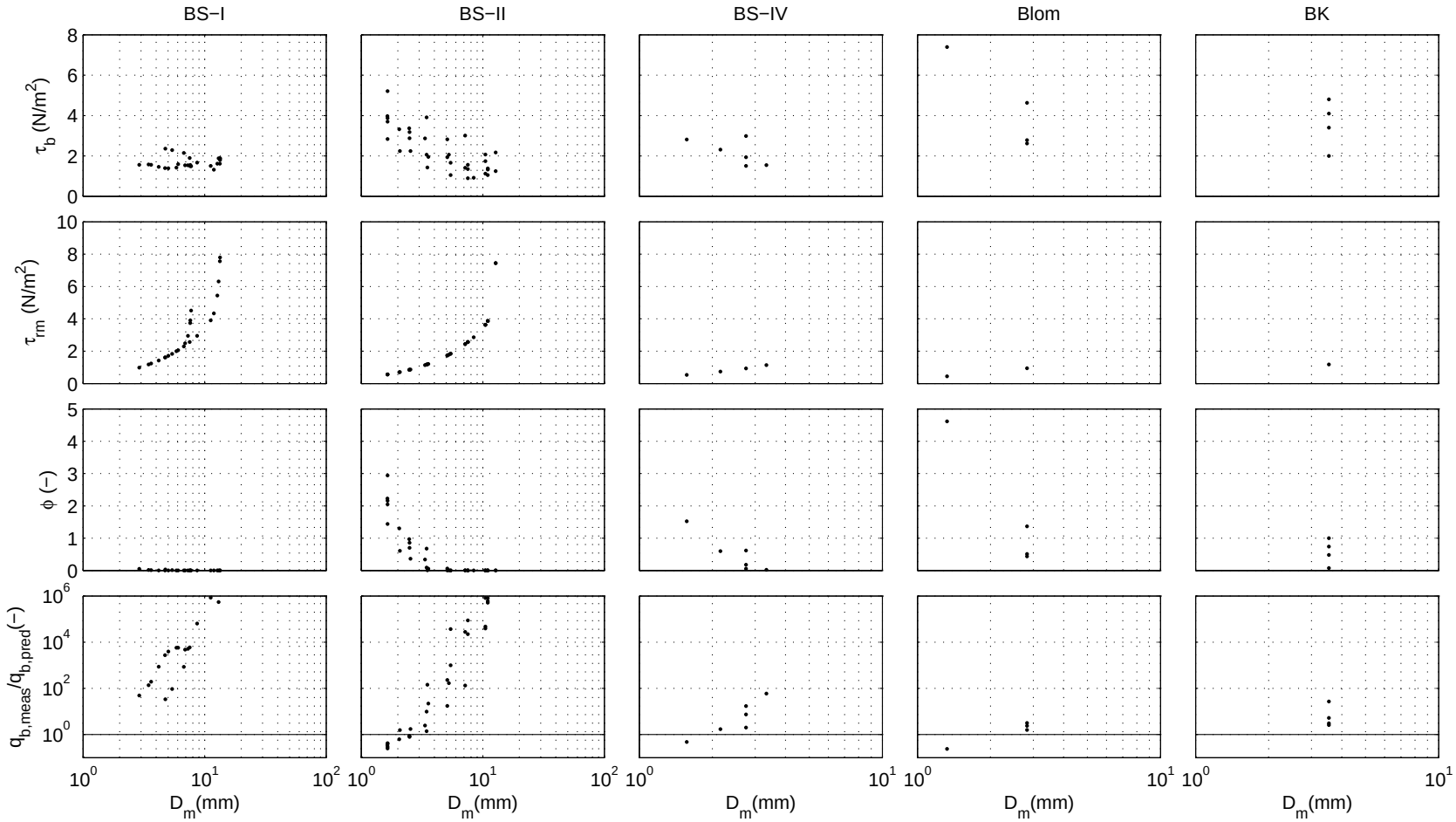

Figure 5.10: The bed shear stress, mean reference shear stress and transport ratio as a function of the mean diameter for the uniform Wilcock and Crowe model

5.2.4 Meyer-Peter and Müller (fractional)

Figure 5.11 shows the predicted and measured total transport rates (left) and the total transport ratio and transport composition ratio (right). The data sets of Blom and BK are predicted fairly accurately, while most of the BS data points are still predicted at zero transport. Compared to the uniform model, the predictions of the total transport rate have improved.

The prediction of the transport composition is demonstrated by comparison of the mean diameter of the transported material with the mean diameter of the predicted material. In Figure 5.11b the transport ratio is shown as a function of the transport composition ratio.

All of the BS-data sets have predicted transport compositions with a mean diameter very near the mean diameter of the transported sediment. Therefore the model accurately predicts immobility of the gravel fractions as observed in the experiments. Both the Blom and BK data sets are predicted too fine ($D_{m,pred} > D_{m,meas}$).

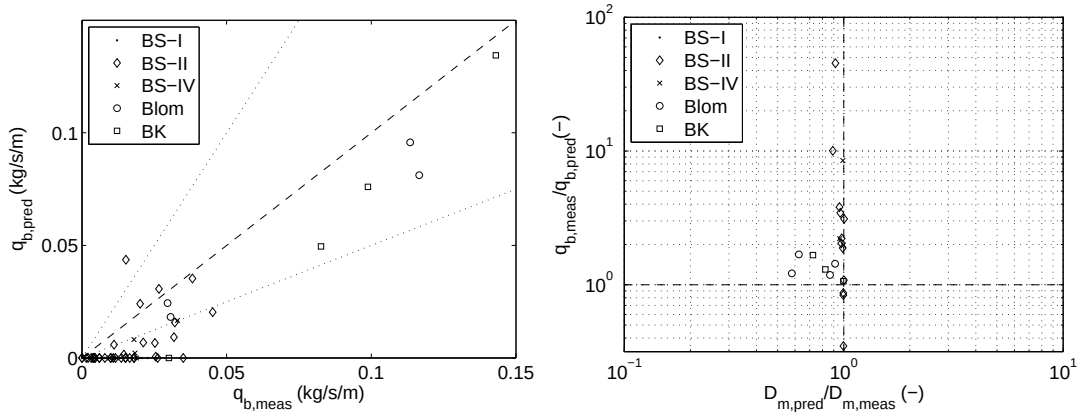

Figure 5.11: Predicted and measured transport rates (left) and transport ratio and transport composition (right) for all data sets with the fractional model of Meyer-Peter and Muller

Figure 5.12 shows the total transport ratio in relation to the supply limitation for the BS data sets. It is shown that the transport rates are (nearly) all underpredicted, both for supply limited and near alluvial conditions. Compared to the uniform predictions the results have improved a little: more points are predicted and more accurately for the entire range.

Figure 5.13 shows the transport ratio as a function of the fraction diameter, as well as several parameters used in the transport calculation. For clarity of the figure only one experimental run of each data set is shown. The runs shown are, for BS-I: 18, BS-II: 1-7, BS-IV: 3, Blom: 2, BK:2. Each run is chosen to explain some of the flaws in the transport models.

The first row shows a graphs depicting the Shields stress for each fraction, a horizontal

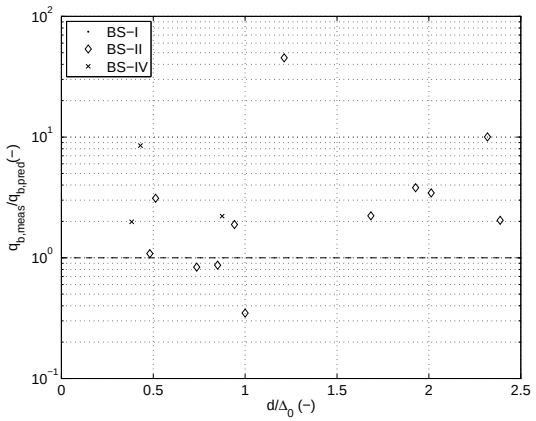

Figure 5.12: The transport ratio as a function of the supply limitation using the fractional model of Meyer-Peter and Müller.

dashed line is included for the critical Shields stress of the model ($\theta_{cr} = 0.047$). For the BS data sets it can be seen that the Shields stress for the sand fractions (with a diameter smaller than approximately 1 mm) is larger than 0.047. The smaller fractions are mobilized, while the coarse fractions fall below the critical Shields stress and thus remain immobile. This is somewhat simplified as in the fractional transport calculation a hiding/exposure correction is included. The hiding/exposure correction is calculated with the mean diameter of the grain size distribution (Equation 2.13). For the bulk sediments the mean diameter is very large (because gravel is included in the grain size distribution), which results in extreme hiding/exposure corrections. In the second row (depicting the hiding/exposure correction) extreme values are seen that reduce the Shields stress of even the finest fractions of the BS-I data sets to below the critical Shields stress of the model. The third row shows the dimensionless transport parameter. It can be seen that the hiding/exposure correction hides the fine fractions too much, resulting in very small values. Which can also seen in the transport ratio in the fourth row.

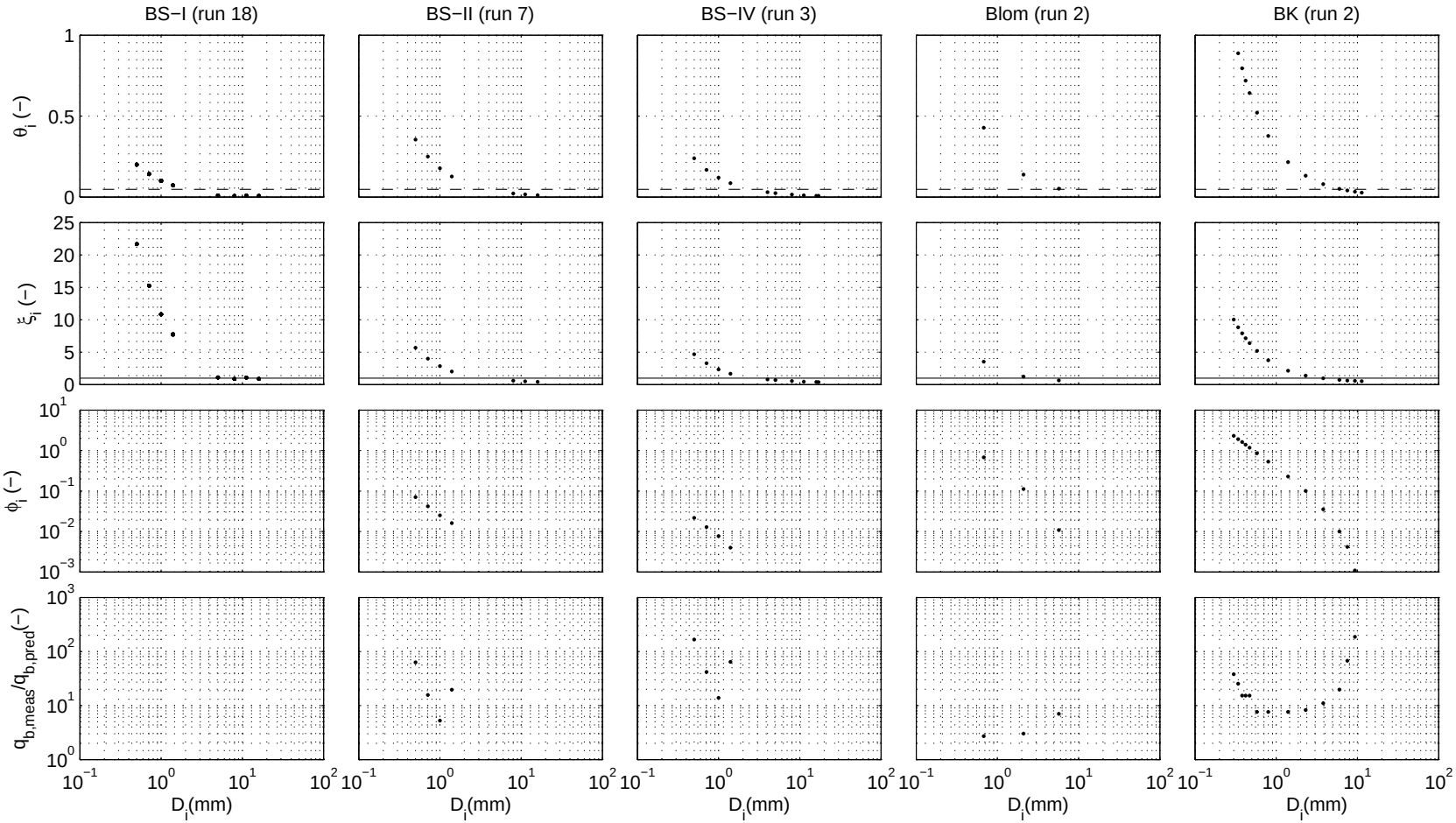

Figure 5.13: The Shields stress, hiding/exposure correction, transport parameter and transport ratio of the model of Meyer-Peter and Müller (showing runs BS-I: 18, BS-II: 1-7, BS-IV: 3, Blom: 2, BK:2)

5.2.5 van Rijn (fractional)

Figure 5.14 shows the measured and predicted transport rates, as well as the total transport ratio and transport composition ratio. The data of Blom and BK are predicted fairly accurately (nearly all within a factor two), while the predictions for the BS-data sets shows two trends: part of the predictions is too low and part is too high. For both BS-I and BS-II several data points are predicted at zero transport.

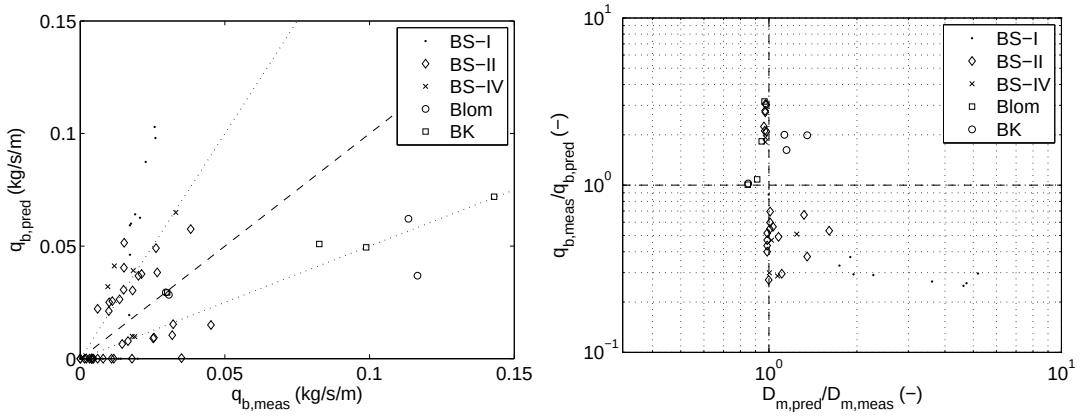

Figure 5.14: Predicted and measured transport rates (left) and transport ratio and transport composition (right) for all data sets with the fractional model of van Rijn

Figure 5.15 shows the transport ratio in relation to the supply limitation of the BS data sets. For supply limited conditions the model over predicts the transport rates, for near alluvial conditions the model underpredicts the transport rates.

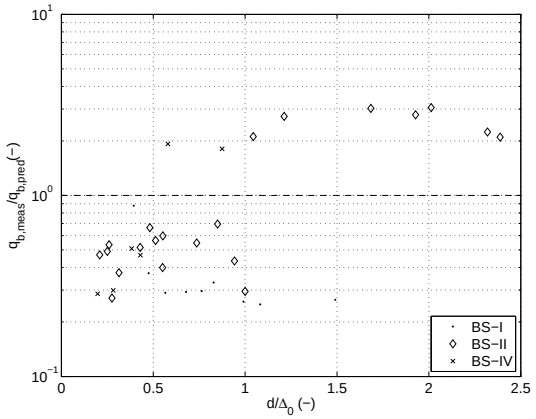

Figure 5.15: Transport ratio as a function of the supply limitation with the fractional model of van Rijn.

Figure 5.16 shows the transport ratio as a function of the median diameter, as well as several parameters that are used in the transport calculations. The first row shows the hiding/exposure correction as a function of the fraction diameter (D_i). It can be

seen that for the BS-data sets the hiding/exposure correction functions within the sand fraction (D_{50} is approximately 1 mm). It shows values above one for fraction diameters below 1 mm, hiding the finest sand fractions. It exposes the larger sand fractions, with diameters of approximately 1 - 4 mm; and exposes the gravel fractions, with diameters above 5 mm. It also shows sensible hiding/exposure correction between 0 and 2.

The second row shows the fluid drag correction. The correction increases transport of fractions coarser than the D_{50}, and decreases for transport fractions smaller than the D_{50}. The fluid drag correction balances out some of the hiding/exposure correction.

The third row shows the bed shear stress parameter (T). It shows decreasing values for larger fraction diameters. With the extreme hiding/exposure corrections the bed shear stress parameter is zero for the BS-I data set, and small for larger diameters (Equation 2.32).

The fourth row shows the transport ratio as a function of the transport diameter. It can be seen that for the BS-data sets the transport of the fine fractions is overpredicted. The van Rijn model is an alluvial model and cannot account for the supply limitation observed in the BS experiments. Supply limitation will result in smaller transport rates, therefore the predicted transport rates are in line with the expectations of using an alluvial model under partial transport conditions.

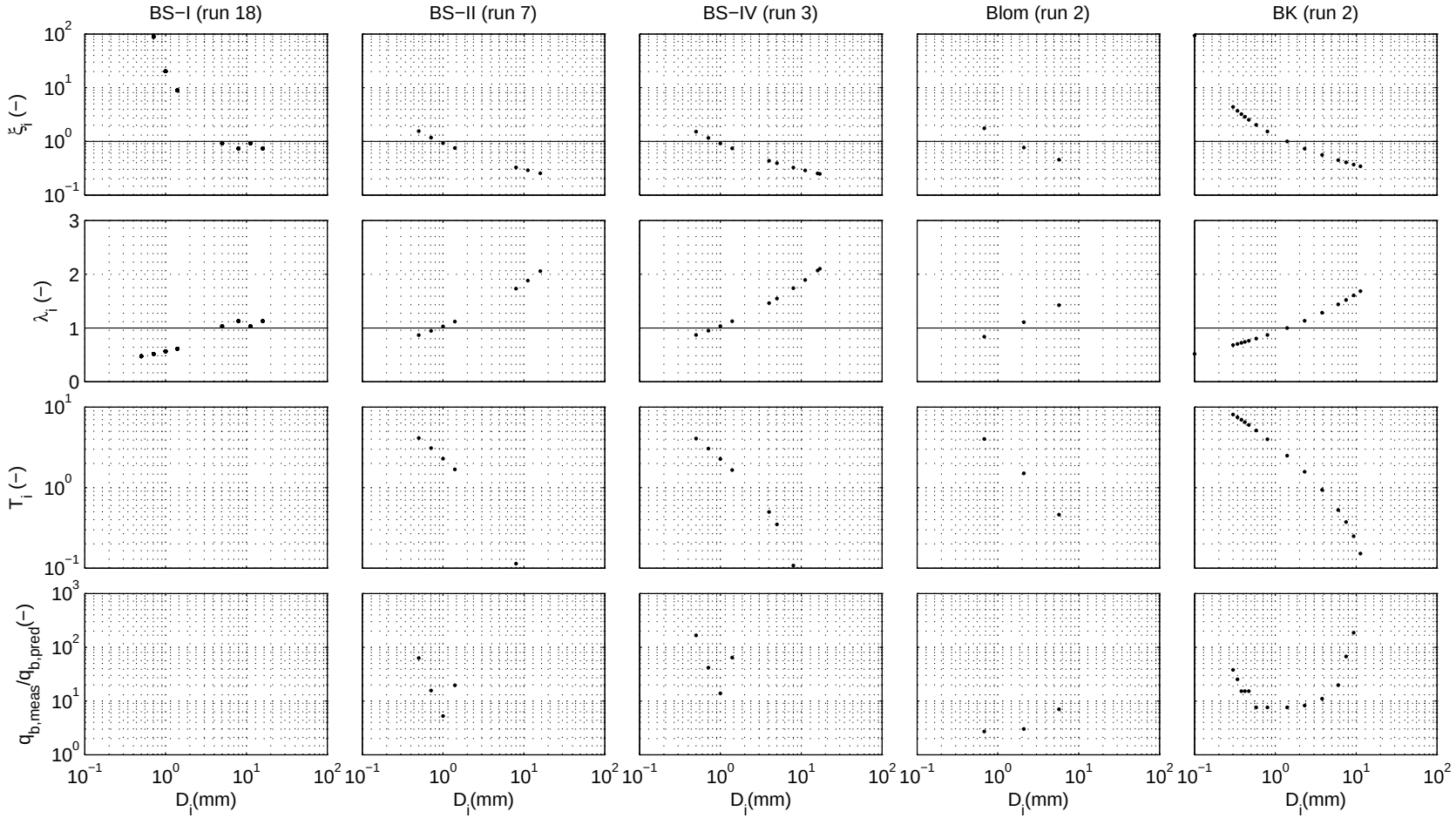

Figure 5.16: The hiding/exposure correction, fluid drag correction, bed shear stress parameter and transport ratio of the fractional van Rijn model ().

5.2.6 Wilcock and Crowe (fractional)

The model of Wilcock and Crowe predicts the transports of Blom and BK too low, with one exception for one data point of Blom. The BS data sets are mostly underpredicted.

Figure 5.17 shows the transport ratio in relation to the transport composition ratio. The mean diameter of the predicted transport of the Blom and BK data sets is predicted accurately. In the BS-I and BS-II data sets the transport is predicted too coarse.

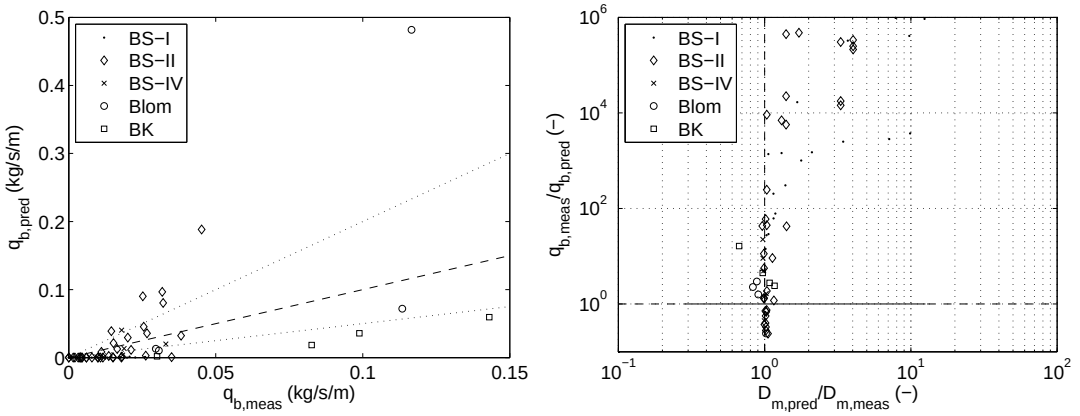

Figure 5.17: Predicted and measured transport rates (left) and transport ratio and transport composition (right) for all data sets with the fractional model of Wilcock and Crowe

Figure 5.18 shows the transport ratio in relation to the supply limitation. For extreme supply limitation ($d/\Delta_0 < 0.5$), the model undepredicts all transport rates. For less supply limitated conditions and near alluvial conditions (approximately $0.5 > d/\Delta_0 > 1.5$) the BS-II data set is predicted with reasonable accuracy.

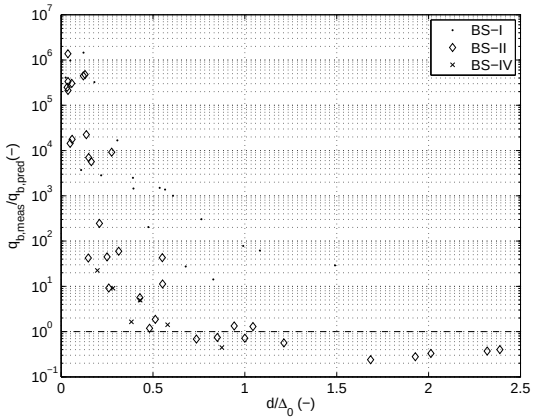

Figure 5.18: Transport ratio as a function of the supply limitation using the fractional model of Wilcock and Crowe.

Figure 5.19 shows the transport ratio as a function of the fraction diameter, as well as several parameters that are used in the transport calculation. For clarity only one example run of each data set is shown in the figures.

The graphs in the first row depict the reference shear stress as a function of the fraction diameter. A horizontal solid line is included for the measured bed shear stress for that experimental run and a dashed line for the mean reference shear stress (τ_{rm}). The reference shear stress for each fraction is calculated with Equation 2.24. In the first row it is seen that the reference shear stress for nearly all data sets is equal, except for the BS-I data set. In run 18 of the BS-I data set hardly any sand is present in the grain size distribution. The mean diameter of this grain size distribution is high (gravel diameter) therefore through Equation 2.23 and 2.22 the reference mean shear stress is also high.

In the transport model of Wilcock and Crowe transport is predicted on basis of the ratio τ_b/τ_{ri}, larger ratios lead to larger transport predictions. For the BS-I data set the ratio is small and therefore the predicted transport rate is almost zero. This is also shown in Figure 5.17 where the predicted transport composition has a mean diameter that is too large. This is also visible in the second row of Figure 5.19 which shows the transport parameter as a function of the fraction diameter.

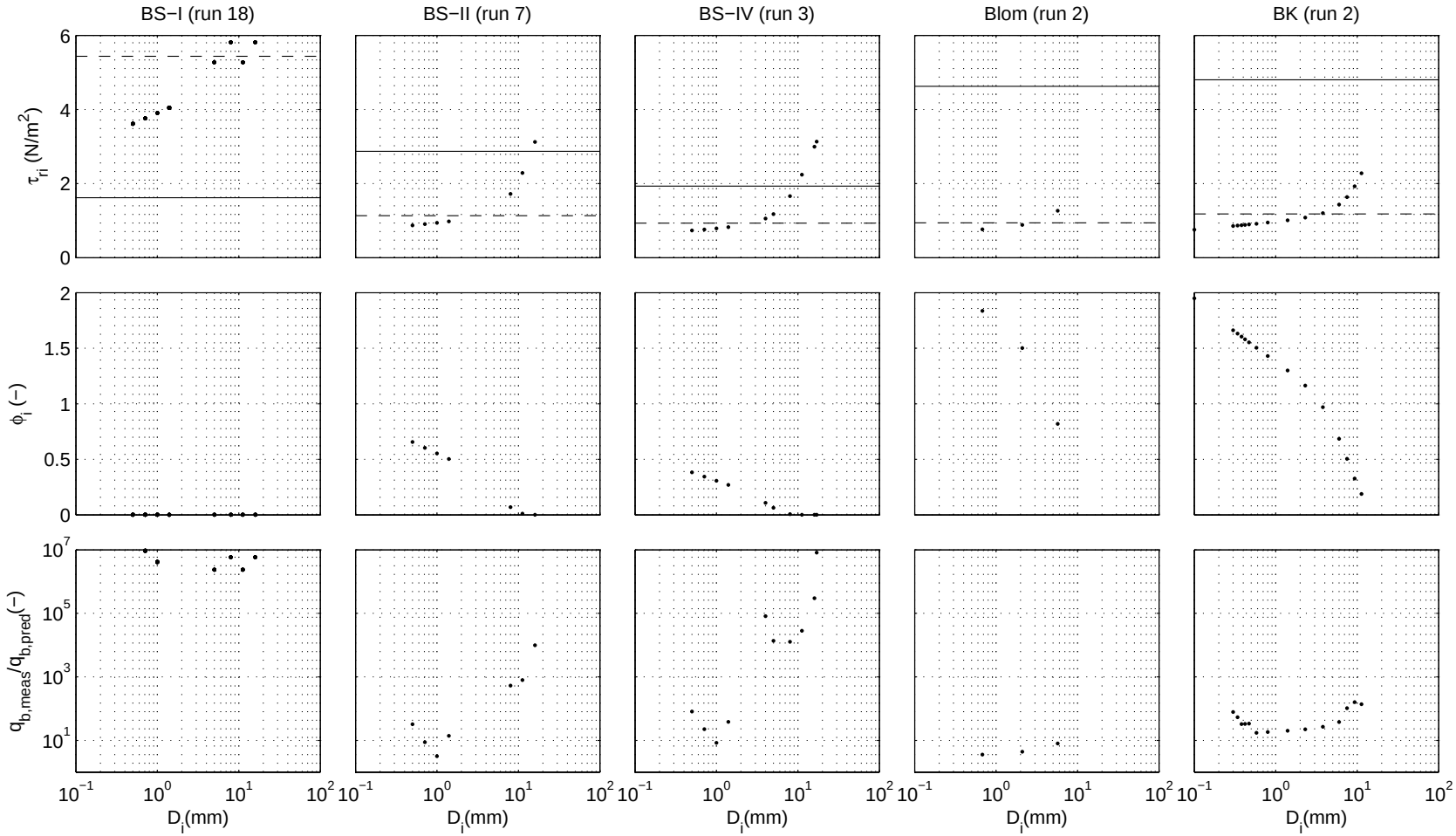

Figure 5.19: The reference shear stress, transport parameter and transport ratio of the fractional model of Wilcock and Crowe

5.3 Discussion

The predictions from the transport models using the bulk grain size distributions are poor, especially for the BS data sets. To compare the performance of the transport models a scoring method is used, adapted from van der Scheer et al. (2002). The method is explained in Appendix C, a score of 1 represent a perfect prediction. Table 5.1 gives the scores for each transport model and data set. Overall the fractional transport model of van Rijn performs best with a score of only 0.44, the uniform model of Wilcock and Crowe performs worst with a score of 0.24. All transport models have problems predicting the BS-I data set, while the Blom data set is predicted fairly well by all transport models.

Table 5.1: Scores of the uniform and graded transport predictions.

	BS-I	BS-II	BS-IV	Blom	BK	Overall(ranking))
Meyer-Peter and Müller (uniform)	0.00	0.09	0.07	0.70	0.54	0.26(5)
van Rijn (uniform)	0.09	0.23	0.42	0.65	**0.69**	0.41(2)
Wilcock and Crowe (uniform)	0.00	0.21	0.30	0.40	0.23	0.24(6)
Meyer-Peter and Müller (fractional)	0.00	0.15	0.18	**0.74**	0.58	0.31(3)
van Rijn (fractional)	**0.12**	**0.27**	**0.44**	0.70	0.65	0.44(1)
Wilcock and Crowe (fractional)	0.01	0.21	0.35	0.41	0.27	0.27(4)
Overall	0.04	0.19	0.29	0.60	0.49	0.32

van der Scheer et al. (2002) predicted transport rates for the Blom and BK data sets using the uniform and fractional models of Meyer-Peter and Müller and the model of Wilcock and Crowe. When compared to the predictions in this study the results are the same for the (uniform and fractional) model of Meyer-Peter and Müller, but a bit worse for the model of Wilcock and Crowe. In the study of van der Scheer et al. (2002) a different (older) version of the model is used.

Sediment characteristics and model parameters

For the experiments with the bimodal sediments the predictions are best using the fractional approach of the van Rijn transport model. The sediment characteristics (D_m, D_{50} and D_{90}) of a strongly bimodal sediment are the cause of most of the errors in the predictions of the BS data sets. These parameters are supposed to represent the sediment in transport, then the model parameters calculated determine mobility, transport rate etc. that are predicted.

For the bulk sediment the mean diameter of the grain size distribution is always larger than the sediment in transport (D_m diameter of sand fraction), which for the van Rijn and Wilcock and Crowe model leads to prediction of mobile gravel in the BS data sets. The hiding/exposure correction (ξ_i), bed form factor (μ) and current related efficiency factor (μ_c) are greatly affected by the large mean diameters, resulting in extreme values.

The extreme values of the mean diameter are mostly due to the gravel in the grain size distribution. In the bulk grain size distribution gravel was included for all the BS data

sets. Although the gravel remains immobile it does influence the transport with the pavement layer supply limitation. Figure 5.20 shows the effect of different amounts of gravel on the sediment characteristics in bimodal sediment of the BS data sets. For increasing amounts of gravel in a sediment composition the mean diameter steadily rises. For amounts above approximately 5% gravel the mean diameter is larger than the diameter of the sand fraction. The D_{50} and D_{90} show jumps when the amount of gravel exceeds 50 and 10 % respectively. At those points the parameters jump from diameters in the sand fraction to the gravel fraction. This results in jumps in the predictions as well.

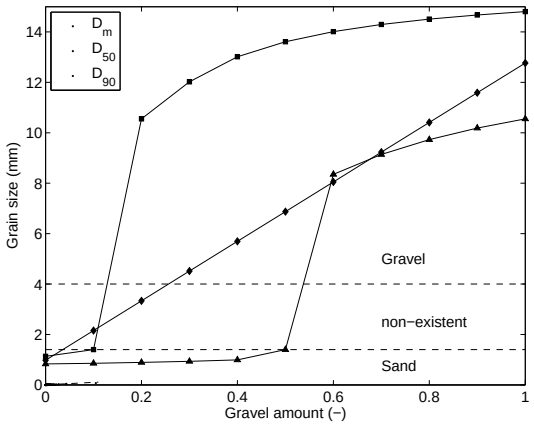

Figure 5.20: Sediment characteristic parameters as a function of the relative amount of gravel in the grain size distribution for the BS data sets.

For the BK and Blom data sets the sediment characteristic parameters are less jumpy (for D_{50} and D_{90}) or better representative for the sediment. Both the sediments for BK and Blom are more or less a continuous distribution. Therefore, the mean diameter is a diameter in one of the mobile fractions. Figure 5.21 shows two grain size distributions of the BS-II and BK data sets that demonstrate the difference for the mean diameter between a strongly bimodal and a natural sediment.

The parameters and functions in the transport models that are calculated with the mean diameter are for the sand and gravel fraction combined (in the case of the BS data sets). However, in reality it is more a split process. For example the hiding/exposure process differs between parts where the gravel is exposed and where it is covered. When the gravel is exposed the sand hides in the pores of the gravel and the gravel fraction is exposed. However, for parts where the gravel layer is covered the hiding/exposure process shifts to the sand fraction, the fine sand is hidden and the coarse sand is exposed. This also counts for the use of the D_{90} in the bed form factor of Meyer-Peter and Müller and the current related effiency factor of van Rijn.

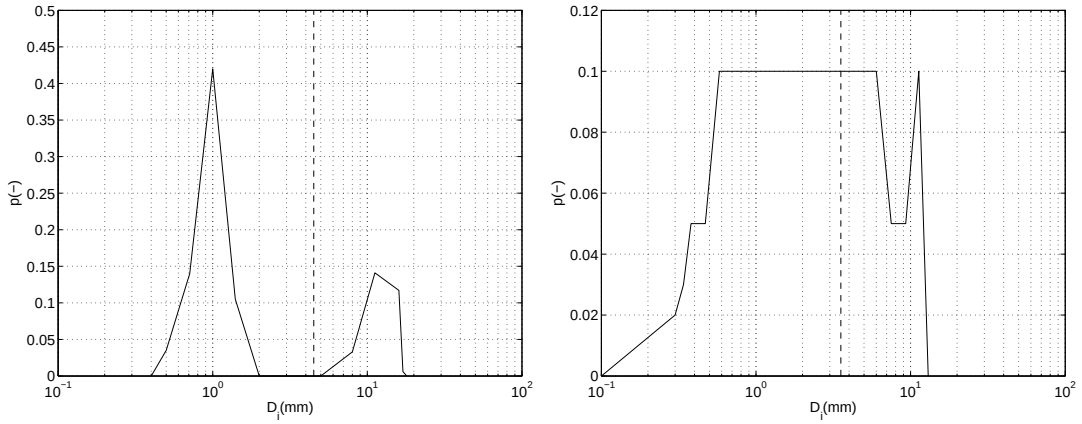

Figure 5.21: Grain size distributions of the BS-II (left) and BK (right) data sets. The dashed line shows the mean diameter of the sediment.

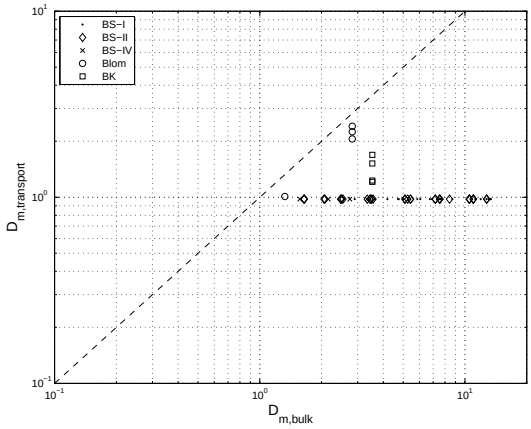

Figure 5.22: Comparison of the mean diameter of the transported material and the bulk material

Bulk sediment versus transported sediment

In this chapter the bulk sediment was used for the predictions, the bulk grain size distribution is coarser than the transported sediment (Figure 5.22), which is one of the effects of partial transport. The coarser fractions are either immobile or less mobile than the finer fractions. This affects the predictions because it causes the sediment characteristic parameters are higher than the sediment characteristic parameters of the transported sediment ($D_{m,bulk}$ $D_{m,transport}$).

Chapter 6

Sediment transport rate predictions, Surface-based

6.1 Introduction

Under partial transport the sediment present at the bed surface differs in composition from the bulk sediment. The coarse, less mobile sediment will vertically sort down, away from the surface. The transported material is therefore finer than the bulk material and thus the transport depends on the material present at the bed surface.

Surface based grain size distributions can be determined in various ways, for example by sampling the surface material but also from photographs like Wilcock and Crowe (2003) did. Each fraction of the sediment was painted in a different color and was counted manually, a very time consuming task. In this study, a surface based sediment composition is determined from photographs of the final state of the bed of BS-II data set.

In the Blom experiments surface sediment samples were taken during and at the end of the experiments. van der Scheer et al. (2002) determined the surface based sediment composition from these samples.

In this chapter the surface based grain size distributions are determined and used to predict the transport rates with the three fractional versions of the transport models.

6.2 Surface based sediment composition

BS-II

In the experiments of BS-II two types of sediment were used: sand and gravel. During the experiments, the gravel fraction remained immobile in a pavement layer while the sand fraction was transported on top of the pavement layer in small bed forms. Figure 6.1 shows an example photograph from the final bed surface. Patches of sand and gravel can be distinguished clearly. Using Matlab (R2007b) the relative amount of gravel visible at the surface is estimated.

Figure 6.1: Example photograph of the final bed state in the BS-II experiments.

To determine the relative amount of gravel present at the surface colored photographs are converted to black and white images, where the gravel is painted white and the sand black. Creating the black and white images is done in several steps. First each photograph is cropped to remove overlap; and lighting corrected for sidewall shadows. A photograph contains several million pixels. Each pixel has a color value on the rgb-scale expressed in the luminance of the color (red green and blue). To distinguish sand from gravel the color layers are separated. In Figure 6.2(b-d) the luminance of each of the layers is depicted in a gray-scale image. The sand and gravel can be distinguished, because the sand looks gray and gravel is either dark gray or nearly white.

The images are converted based on a threshold value of the luminance between the sand and gravel (threshold 1) using the average grayness value (Otsus method (Otsu, 1979)). When the red layer is converted (Figure 6.3(a)) most of the gravel can be distinguished. However, the lighter colored gravel fraction is also filtered out. Therefore another threshold is applied to the red layer, a threshold between the sand and lighter gravel fraction (threshold 2). This reveals some of the light colored gravel (Figure 6.3(b)). The last bit of lighter colored gravel is revealed from the green layer, also with a threshold between sand and lighter colored gravel (threshold 2). When the blue layer is converted it no longer contributes to the amount of gravel revealed from the photos, therefore it is neglected.

When the images are combined, all gravel is revealed from the photograph. This was checked visually for all photographs. The amount of gravel at the bed surface is calcu-

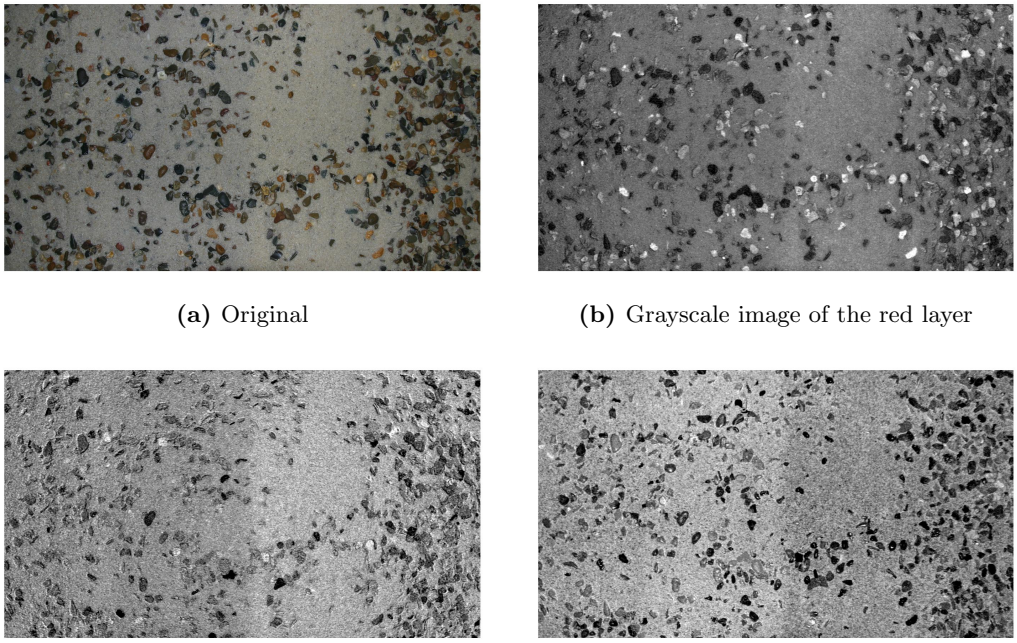

(a) Original

(b) Grayscale image of the red layer

(c) Grayscale image of the green layer

(d) Grayscale image of the blue layer

Figure 6.2: Example images of the bed surface showing, the original (a) and the red, blue and green color layers as grayscale images (b-d)

lated as the white area relative to the entire surface. All original and converted images are given in Appendix B.

Photographs for six runs of the BS-II data set are available; these are converted to a relative amount of gravel present at the surface. To obtain an entire set of gravel amounts present at the surface, the six gravel amounts from the photographs are used to create a model to predict gravel amounts based on the transport layer thickness. The model consists of two parts: first with little sand available the pores of the gravel fraction are filled, second the layer of sand on top of the gravel layer is described. For the first part a 2D equation for the description of a circle is used[1] , only 2D is used for simplicity (Figure 6.4). For the second part an exponential function is fitted to the gravel amounts determined from the photographs using least sum of squares fitting. The complete two part equation is described with:

$$f_{gravel} = \begin{cases} \frac{\sqrt{(r_{gravel}^2 - d^2)}}{r_{gravel}} & \text{for } d < r_{gravel} \\ 0.283 * \exp^{-64.1d} & \text{for } d >= r_{gravel} \end{cases} \tag{6.1}$$

in which r_{gravel} is the radius of a gravel particle, d the average layer thickness. This is also shown in Figure 6.5. With the calculated gravel amounts at the surface and the grain size

[1] mathematical description of a circle $x^2 + y^2 = r^2$, where r is the radius of the circle

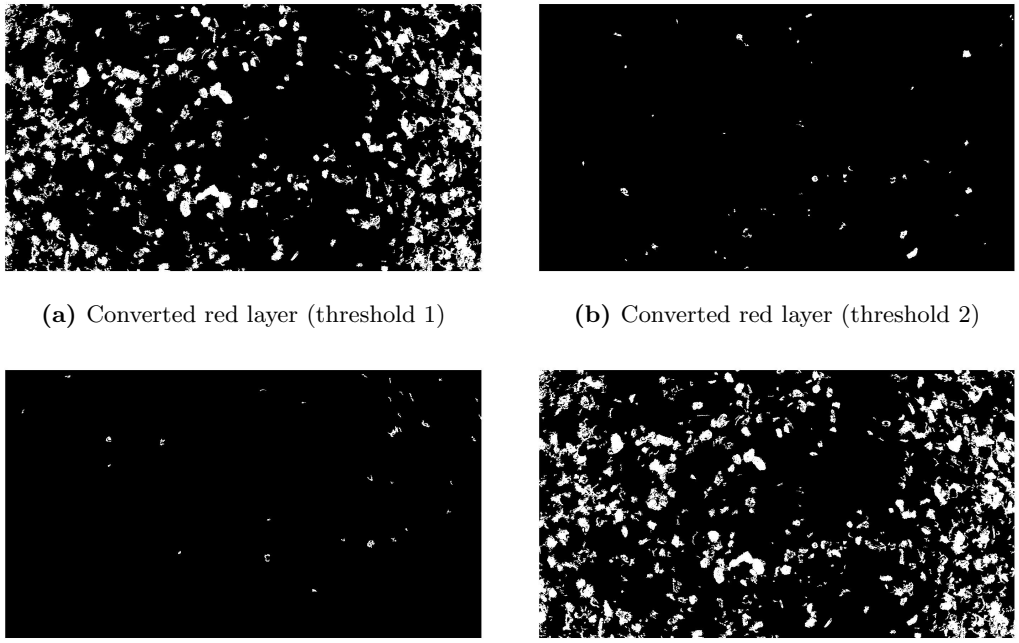

(a) Converted red layer (threshold 1)

(b) Converted red layer (threshold 2)

(c) Converted green layer (threshold 2)

(d)

Figure 6.3: Example images of converted bed surface photographs showing: converted red layer (a,b), the converted green layer(c) and the final converted image (d).

distributions of the sand and gravel fraction, the surface based grain size distributions are calculated from the measured transport layer thickness and Equation 6.1. The surface grain size distributions of the BS-II data set are shown in Figure 6.6(left) and given in Appendix E.

Blom

Surface based grain size distributions were determined by van der Scheer et al. (2002) for the Blom data set. During and at the end of experiments samples were taken from the surface, both in troughs and crests of dunes, which were averaged over the length of the flume. From the samples and bed level elevations the surface grain size distributions were determined. The surface grain size distributions are given in Figure 6.6(right), the values are also given in Appendix E.

Bulk versus surface grain size distribution

The surface grain size distributions determined in the previous section are coarser than the bulk grain size distributions. Figure 6.7 shows a comparison of the grain size distribution for all fractions between the bulk and surface material. It can be seen that

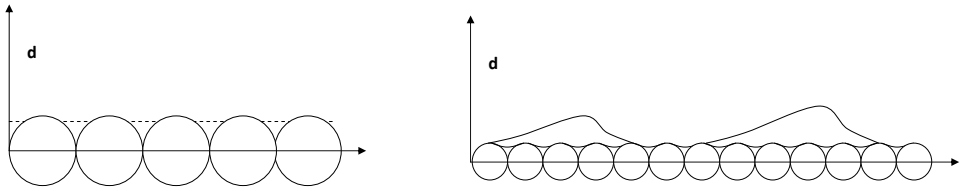

Figure 6.4: Sand filling up the pores of the gravel fraction (left) and formation of supply limited bed forms (right)

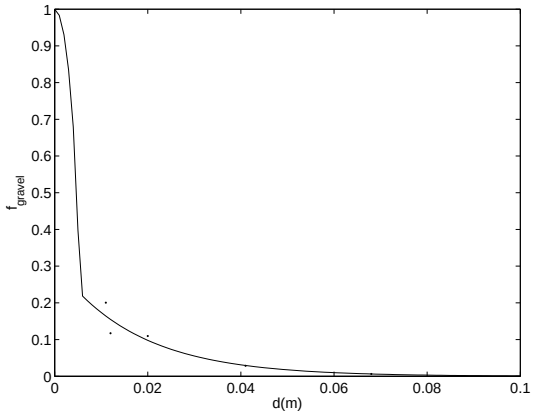

Figure 6.5: Gravel amount at the surface in relation to the average transport layer thickness

the surface grain size distribution contains more fine fractions and less coarse fractions compared to the bulk grain size distributions.

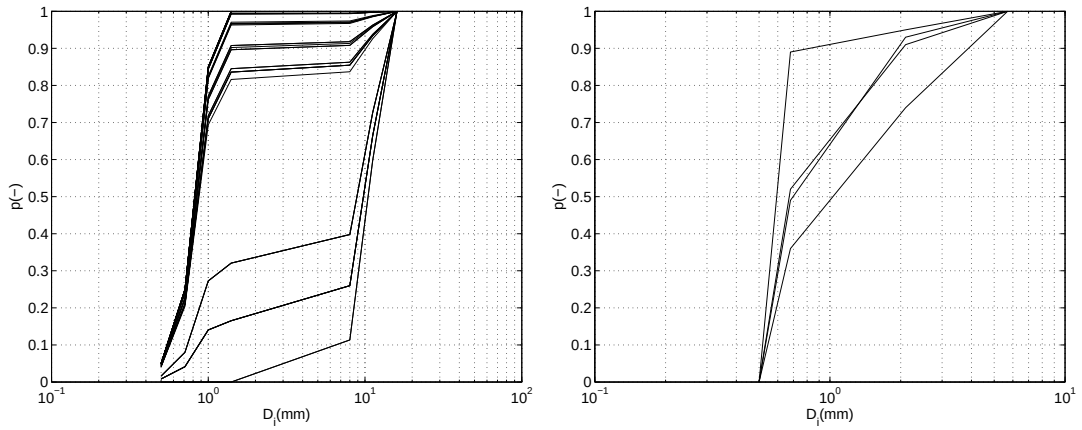

Figure 6.6: Cumulative surface grain size distribution of the BS-II (left) and Blom (right) data set.

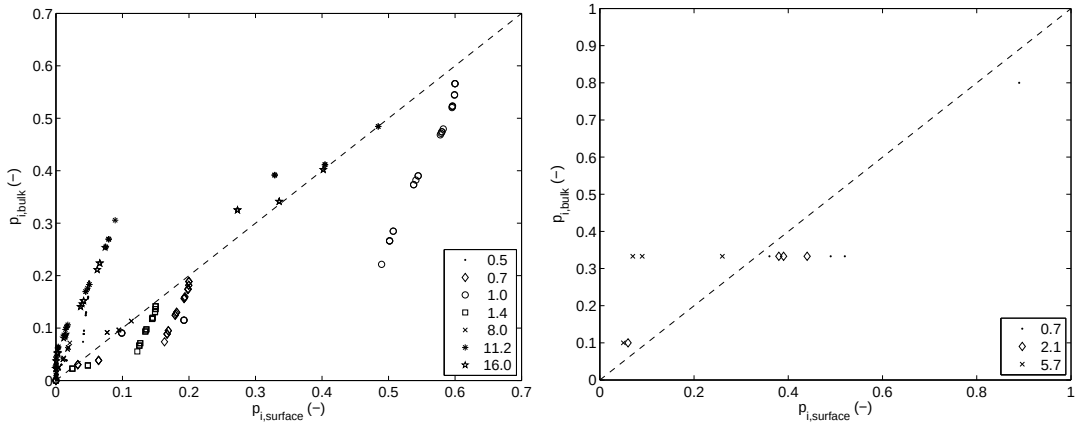

Figure 6.7: Comparison of the mean diameter of the bulk and surface grain size distributions for the BS-II data set (left) and Blom data set (right)

6.3 Surface based transport predictions

The surface based transport is predicted with the calculation steps provided in chapter 2, the data provided in chapter 3 and the grain size distributions provided in Appendix E.

Similar to chapter 5 the predictions are checked on total transport, transport composition and supply limitation. The results are also compared to the bulk based predictions to check if the model performance improves with the surface grain size distribution.

6.3.1 Meyer-Peter and Müller (fractional)

Figure 6.8 shows the predicted and measured transport rates, as well as the transport rate and transport composition ratio for the BS-II and Blom data set using the surface based grain size distributions. Except for very small transport rates the model is fairly accurate (within a factor 2) for both the BS-II and Blom data set. Compared to the bulk based predictions, the BS-II data set predicitions improve much (39% within a factor two compared to 11% with the bulk distribution), whereas there is only a small difference for the Blom dataset. For the BS-II dataset a smaller number of points is predicted at zero transport, because the mean diameter of the surface based sediment is finer, resulting in smaller Shields stresses and less extreme hiding/exposure corrections.

The mean diameter of the transport is predicted accurately for nearly all data points with the exception of one point in the Blom data set. Compared to the bulk based predictions little difference can be seen.

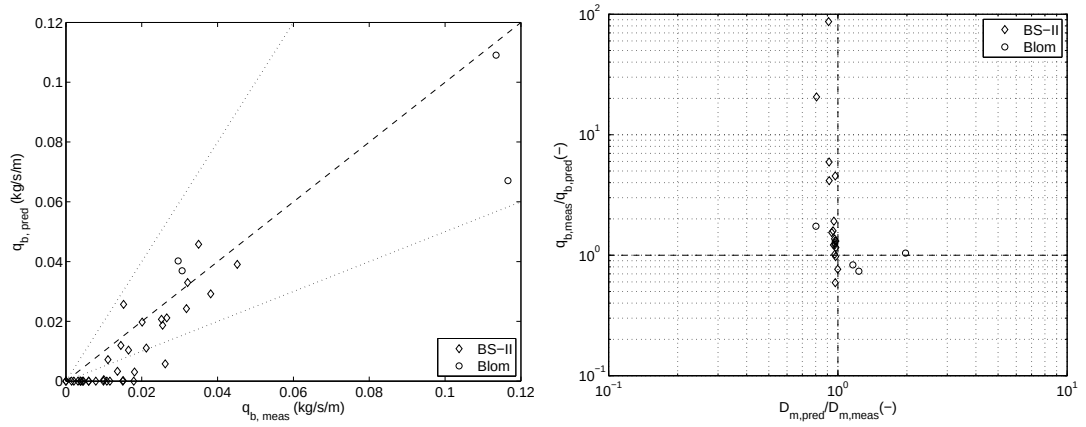

Figure 6.8: Predicted and measured transport rates (left) and a comparison of the total transport and transport composition ratio (right) for the surface based sediment usign the Meyer-Peter and Müller model

Figure 6.9 shows the total transport ratio in relation to the supply limitation for the BS-II data set. For extreme supply limitation the transport model underpredicts the transport rates ($d/\Delta_0 > 0.5$) the transport rate is predicted accurately (within a factor

2). Compared to the bulk predictions the results are much better, more points are predicted especially for more alluvial conditions the predictions are all within a factor 2.

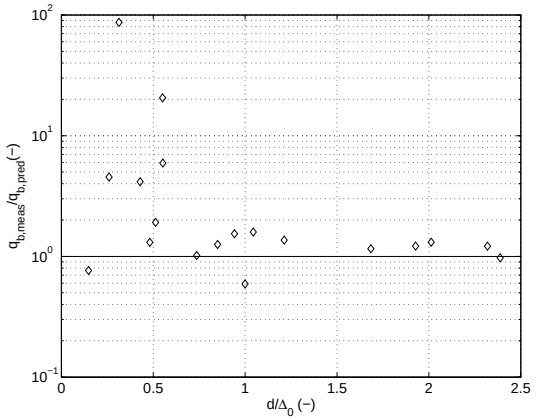

Figure 6.9: Transport ratio as a function of the supply limitation using the model of Meyer-Peter and Müller.

Figure 6.10 shows the transport ratio and several parameters used in the transport calculation as a function of the fraction diameter. For clarity only two experimental runs from both the BS-II and Blom data sets are shown. For the BS-II data set one run is a nearly alluvial condition and one a supply limited situation, for the Blom data set run 1 is compared to run 2. In both cases (BS-II and Blom) these runs were chosen to demonstrate a good and poor prediction.

For the BS-II dataset the first two rows (Shields stress and hiding/exposure correction) explain why there are still many zero predictions. A combination of low Shields stress and extreme hiding/exposure correction results in zero transport prediction. This is still the result of the mean diameter in the hiding/exposure correction. The same happens as with the bulk based predictions.

For the Blom data set the differences are less extreme. In run 1 coarse layers were observed, indicating partial transport and possibly supply limitation. Although in run 1 the Shields value of the coarsest fraction is below the critical value, the hiding/exposure correction reduces the critical Shields value to below the occuring value. Under the assumption that the pavement layer existed the coarsest fraction should be immobile.

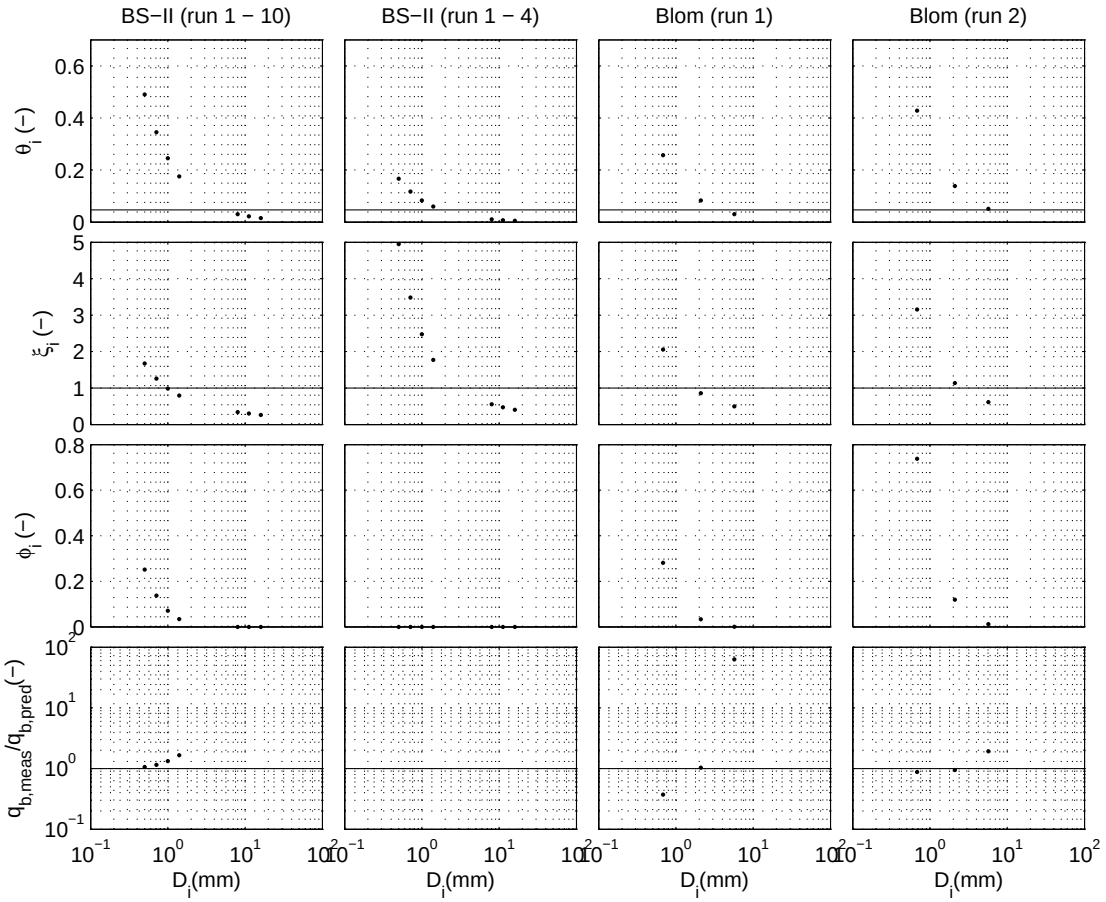

Figure 6.10: Shields parameter, hiding/exposure correction and transport ratio of the surface based predictions of the fractional model of Meyer-Peter and Müller

6.3.2 van Rijn (fractional)

Figure 6.11 (left) shows the predicted and measured transport rates for both the BS-II and Blom data set with surface based grain size distributions. For small transport rates, the model of van Rijn strongly overpredicts transport for the BS-II data set, while for larger transports the model consistently underpredicts the transport rate. For the Blom data set one point is underpredicted, the rest is predicted accurately (within a factor 2). Compared to the predictions with the bulk grain size distribution the BS-II data set improved with less zero transport predictions, however very small transport rates are overpredicted more extremely. For the Blom data set the predictions are slightly worse for the small transport rates and slightly better for the larger transport rates.

Figure 6.11 (right) shows the total tranpsort ratio in relation to the transport composition ratio. For the BS-II data set the predictions improved, while for the Blom data set the results are slightly worse with small overpredictions and underpredictions of the transport composition ratio.

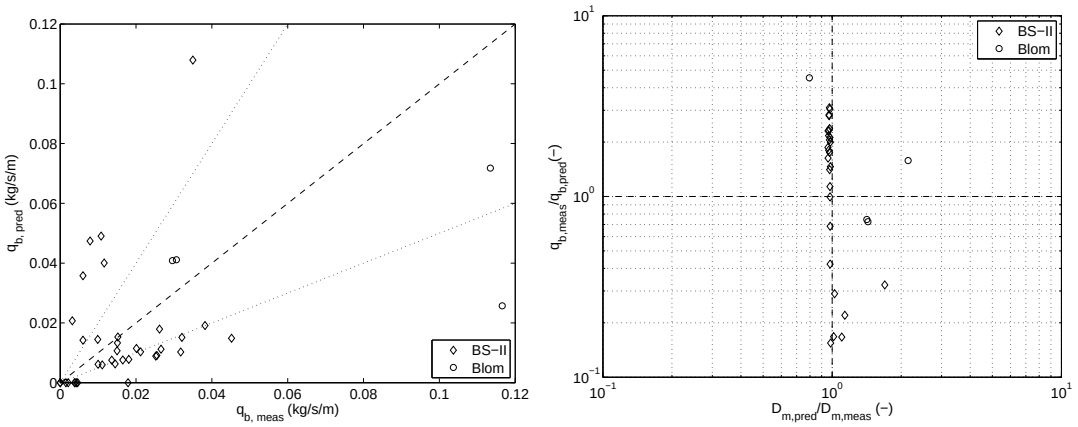

Figure 6.11: Predicted and measured transport rates (left) and transport ratio and transport composition ratio (right)

Figure 6.12 shows the transport ratio in relation to the supply limitation for the BS-II data set. For extreme supply limited conditions the model overpredicts transport rates, while for values of $d/\Delta_0 > 0.5$ the model underpredicts transport rates.

Figure 6.13 shows the transport rate ratio, as well as several parameters used in the transport calculation. For clarity only two of the experimental runs from the BS-II and Blom data sets are shown.

The first row of graphs in Figure 6.13 shows the hiding/exposure correction as a function of the fraction diameter. For both runs of the BS-II data set the hiding/exposure correction hides two of the fine sand fractions (ξ_i is larger than 1 for $D_i < 1mm$). For the rest of the sediment it decreases the critical bed shear stress. For the Blom data set only the critical shear stress of the finest fraction is increased. In the second row (fluid

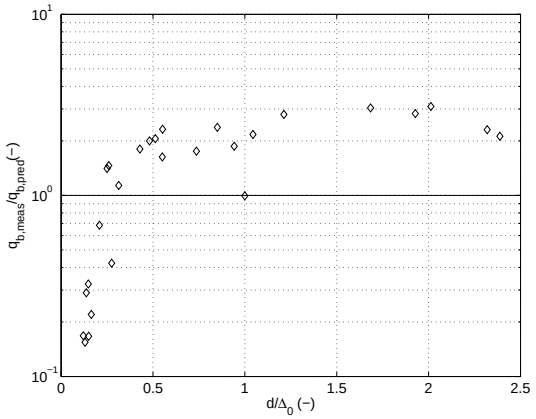

Figure 6.12: Transport ratio as a function of the supply limitation of the van Rijn model.

drag correction) the opposite is seen compared to the hiding/exposure correction.

Although the graphs from the first three rows are nearly the same, the fourth shows a large difference. With the fractional van Rijn model two errors mainly occur: extreme hiding/exposure corrections (Eq.(2.33))and extreme efficiency factor corrections (Eqs.(2.36)-(2.38)) due to the use of the D_{90} in the calculation. The hydraulic conditions for both runs of the BS-II data set are similar: the bed shear stresses are 1.43 and 1.41 Nm^{-2} respectively. The difference between the two runs is in the sediment composition and the calculated sediment characteristics. For run 5-6 the gravel amount is low and the D_{90} is a diameter in the sand range of the sediment. However, for run 1-5 the gravel amount is larger and the D_{90} shifts to a diameter in the gravel fraction.

For the Blom data set the differences are fairly small. In run 4 more fine sediment is present in the grain size distribution, this results in a small D_{90}, small current related efficiency factor and a transport rate that is underpredicted (Eqs.(2.38)-(2.35)).

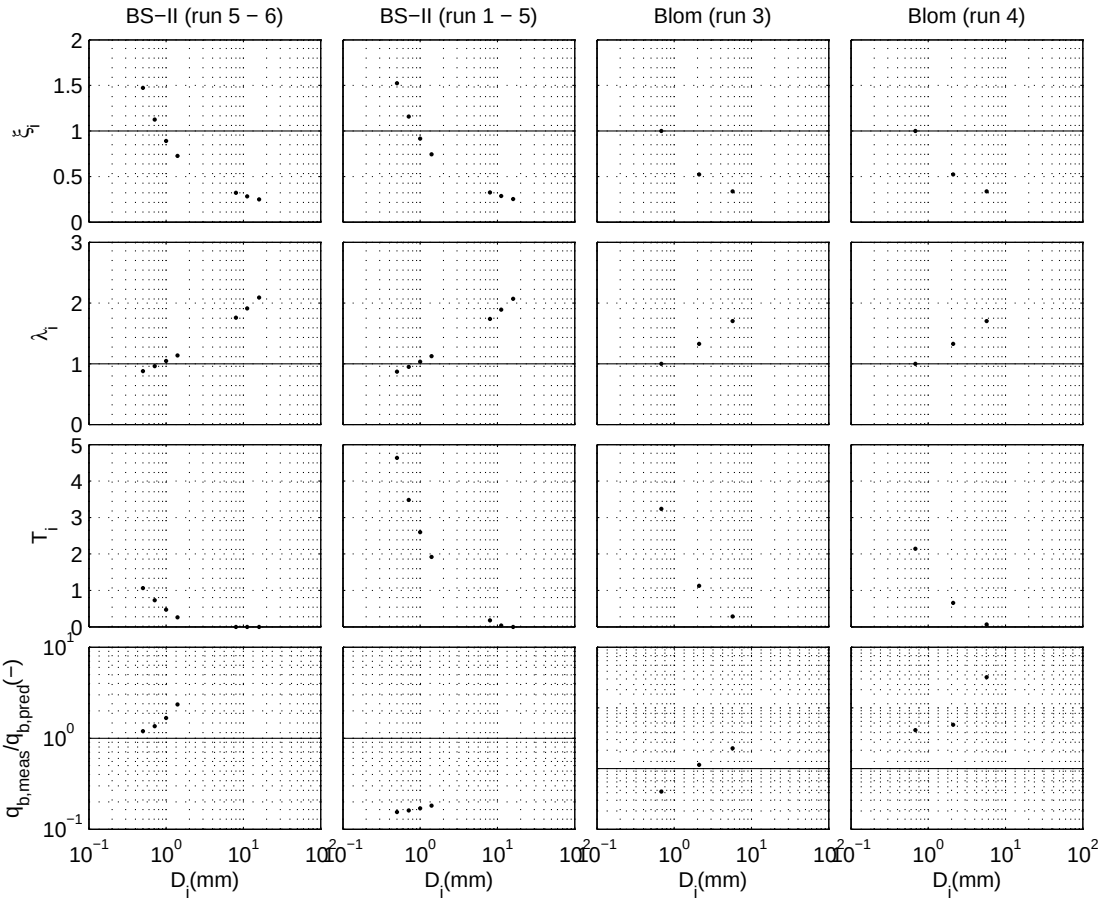

Figure 6.13: Hiding exposure correction, fluid drag correction, transport parameter and transport ratio of the surface based predictions of fractional van Rijn model

6.3.3 Wilcock and Crowe (fractional)

Figure 6.14 shows the predicted and measured transport rates (left) and the transport rate and transport composition ratios (right). For small transport rates the model underpredicts the transports of the BS-II data set, while for larger transport rates it overpredicts the transport. The data set of Blom is predicted within a factor 2 except for one data point. Compared to the predictions using the bulk grain size distribution the predictions of the BS-II data set have improved. The transport rates are more often within a factor 2 and there are less extreme underpredictions. For the Blom data set three points improve and one point is overpredicted more extremely.

The mean diameter of the transport is predicted well for the BS-II data set, it improved slightly compared to the bulk based predictions. The predicted transport composition ratio for the Blom data set is slightly worse compared to the bulk based predictions, a little too fine.

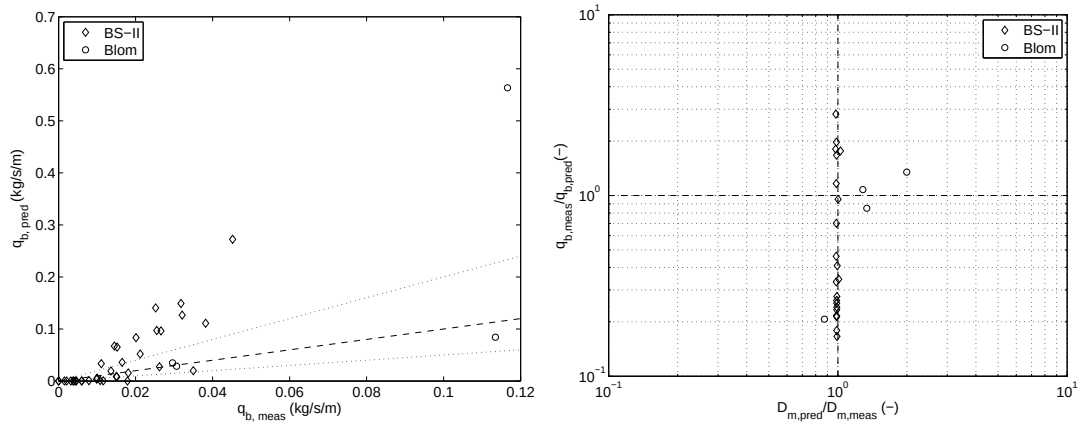

Figure 6.14: Predicted and measured transport rates (left) and transport ratio and transport composition ratio (right)

Figure 6.15 shows the total transport ratio in relation to the supply limitation for the BS-II data set. Under extreme supply limited conditions the model of Wilcock and Crowe underpredicts transport rates by up to a factor 10^6. For less supply limitation and near alluvial conditions ($d/\Delta_0 > 0.5$) the model overpredicts transport rates.

Figure 6.16 shows the transport ratio as a function of the fraction diameter, as well as two parameters used in the transport calculation. The first row of graphs depicts the reference shear stress of each fraction. Two horizontal lines are also shown: one for the occuring bed shear stress (dashed line) and one for the mean reference shear stress (solid line). The mean refence shear stress (τ_{rm}) for both of the BS-II runs is nearly the same, while the actual bed shear stress differs almost a factor 2. The resulting reference shear stress of the fractions (τ_{ri}) after hiding/exposure correction is therefore too low, which results in a high transport parameter (ϕ, from Equation 2.20. This results in transport

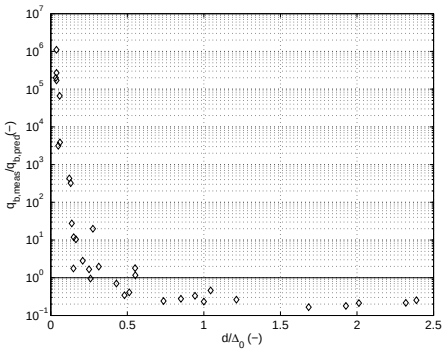

Figure 6.15: Transport ratio as a function of the supply limitation of the model of Wilcock and Crowe.

predictions that are too high.

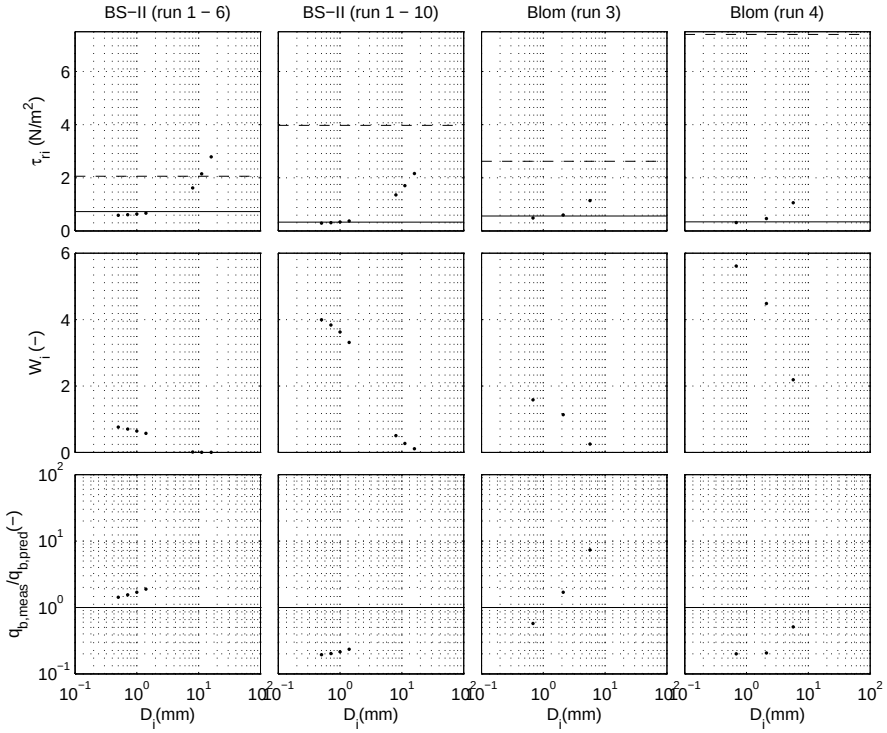

Figure 6.16: Reference shear stress, hiding/exposure correction and transport ratio for the surface based predictions of the fractional Wilcock and Crowe model

6.4 Discussion

The predictions of the model of Meyer-Peter and Müller and van Rijn improve compared to the bulk grain size distribution. Only the Blom data set using the van Rijn model is predicted slightly worse (Table 6.1). Overall the data set of BS-II has a score that is 48% higher (a score of 0.31 compared to 0.21), while the Blom data set improves only 13% (a score of 0.68 compared to 0.60).

Table 6.1: Scores of the surface based predictions

	BS-II		Blom	
	bulk	surface	bulk	surface
Meyer-Peter and Müller	0.15	0.32	0.74	0.78
van Rijn	0.27	0.35	0.70	0.58
Wilcock and Crowe	0.21	0.25	0.41	0.68
Overall	0.21	.31	0.60	0.68

van der Scheer et al. (2002) also used the surface grain size distribution of the data set of Blom to predict the transport with the model of Wilcock and Crowe. Similar to the predicitons with the bulk grain size distribution the predictions are a bit worse, because a different version of the model is used.

Surface grain size distribution and sediment characteristics

Using photographs the surface grain size distribution was determined. This better represents the sediment that will be transported, but is not perfect. The determined gravel amounts may be optimized further with more data. A better relation independent of transport layer thickness, which is often unavailable, may be determined from more photos and research.

To accurately predict the transport rates it would seem logical to predict transport based on a relation based of sediment available for transport (the surface). The model of Wilcock and Crowe is such a model, but it performs poorly for the bimodal sediment because of the use of the mean diameter in the transport calculation. However, the predictions show that the chosen grain size distribution (bulk or surface) influences the predictions greatly. It is therefore important to use a grain size distribution that represents the sediment and conditions best. Similar to the bulk based predictions the use of certain sediment characteristic parameters (D_{50}, D_{90} and D_m) results in extreme values of parameters and jumps in values of parameters. In turn this explains some of the errors in the predictions.

Chapter 7

Predictions, adjusted

7.1 Introduction

The predictions with the bulk and surface based grain size distributions are not satisfying. The predictions improve with the surface grain size distribution, but the results for supply limited conditions are still poor. For partial transport conditions with larger amounts of immobile sediment the mean and median diameter of the grain size distribution are either too high, resulting in extreme model parameters.

The models of Meyer-Peter and Müller and van Rijn cannot account for the effects of partial transport, since they are meant for alluvial transport conditions. In the previous two chapters the models were used unadjusted to test if the transport could be predicted, here a different approach is tested. In the previous predictions a lot of the problems are caused by the immobile fractions that are included in the transport calculations. A different possibility is to predict only the transport rates of the mobile fractions and account for partial transport with a reduction function. Struiksma (1985) predicted transport rates of mobile sediment on top of an immobile layer and developed a reduction concept to account for the lower transport rates under partial transport. Kleinhans and van Rijn (2002) reduced transport rates using a hindrance factor to account for the hindered movement of finer fractions by larger immobile grains. Tuijnder (2010) reduced transport rates based on the exposure of the coarse layer, which was predicted with a 'coverage of the immobile layer model'.

Three reduction functions are tested in this chapter: first the Struiksma reduction function, secondly the hindrance factor of van Rijn and lastly the exposure of the coarse layer concept of Tuijnder.

7.2 Mobile sediment

Reduction functions are applied to predictions of the mobile part of the sediment, therefore only the mobile part of the sediment is used as input for the transport model. Determining the mobile part of the sediment and an accompanying grain size distribution is done with several methods. Often the Shields curve (or adjustments of the Shields curve) is used to determine the point of initiation of motion for a sediment fraction, this neglects hiding/exposure however. A different option would be to use the functionality of the transport model. This includes hiding/exposure correction and provides a sediment composition that can be used as input. In a second model run the transport rates can be predicted, a double model run.

Shields curve

Figure 7.1 shows an adjusted version of the Shields curve (van Rijn, 1984a). It also shows the critical bed shear stress ($\tau_{b,cr}$)) values of each of the fractions used in both the BS-II and Blom data sets. In the BS-II experiments the bed shear stress varied from 0.9 - 5.21 N/m^2. From the Shields curve it follows that the gravel fractions (diameter 2 mm) are immobile. Because the gravel fraction is immobile the grain size distribution of only the sand is used as input for the new transport prediction.

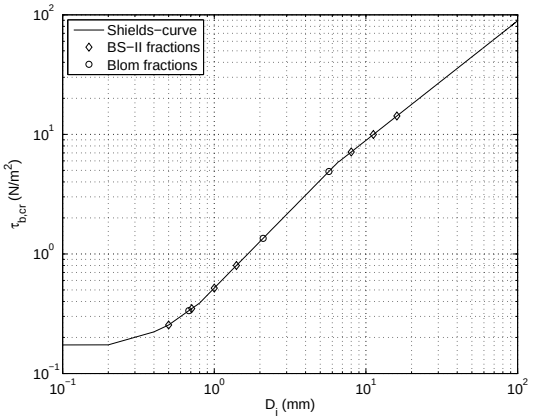

Figure 7.1: Adjusted Shields curve depicting the critical bed shear stress as a function of fraction diameter.

For the Blom data set the bed shear stress varies from 2.61 - 7.39 N/m^2. When compared with the critical bed shear stresses of the fractions (Figure 7.1), it shows that in three out of four experimental runs the coarsest fraction (diameter of 5.7 mm) remains immobile. In the last run the bed shear stress is large enough to mobilize all fractions. This information is used to determine new grain size distributions that are used as input for the adjusted transport predictions. The surface based grain size distribution is adjusted to create teh new grain size distributions, by removing the immobile fractions.

The adjusted grain size distributions are given in Figure 7.2. Using the adjusted grain

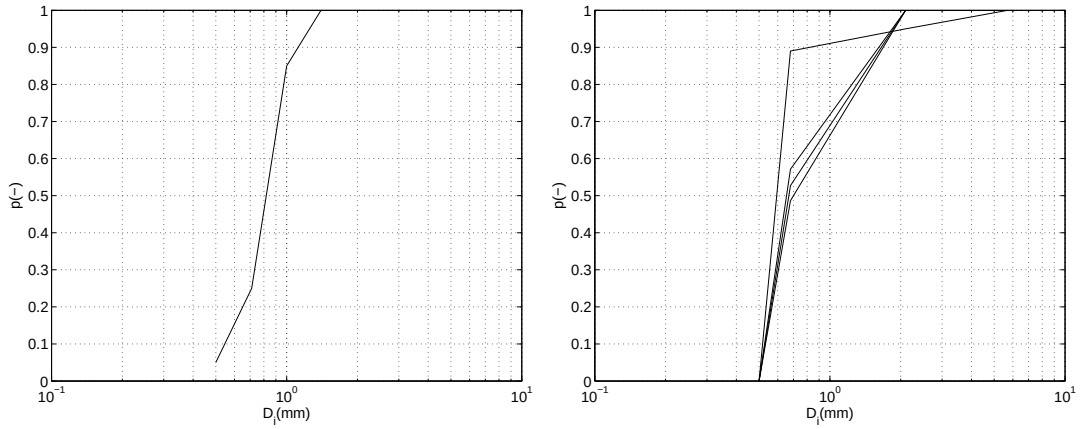

Figure 7.2: Grain size distributions for the mobile sediment of the BS-II (left) and Blom (right) data sets.

size distributions and the hydraulic conditions from chapter 3 the transport rates are predicted with the transport models of Meyer-Peter and Müller and van Rijn. Figure 7.3

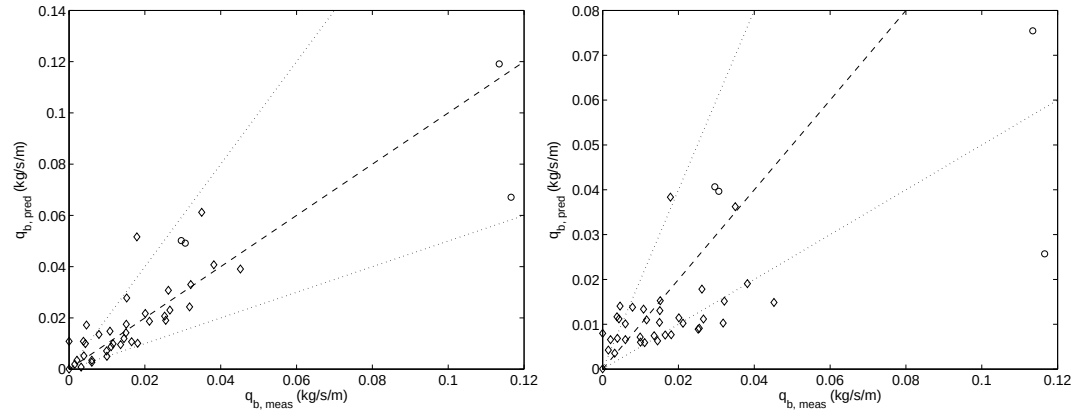

(a) Meyer-Peter and Müller **(b)** van Rijn

Figure 7.3: Predicted and measured transport rates, with only the mobile fractions as input

shows the predicted and measured transport rates for the BS-II and Blom data set using two transport models. The results for the model of Meyer-Peter and Müller are good, no zero transport predictions and 78% is within a factor two. For the model of van Rijn the results are not satisfying since only 50% is within a factor two.

Double model run

In the double model run approach, the transport model is first used to determine the transport composition and then to predict the transport rates. With the surface based

grain size distribution a fractional transport calculation is done to determine the grain transport composition only. The surface based predictions from chapter 6 can be used for this purpose. They consist of fractional and total transport rates. The grain size distribution is now determined as the ratio of the fractional transport rate in relation to the total transport rate. For a single fraction the probability of the new grain size distribution is given by:

$$p_i = \frac{q_{b,i}}{q_{b,t}} \tag{7.1}$$

This is done for each model and the BS-II and Blom data sets only. This results in the grain size distributions shown in Figure 7.4 The resulting grain size distribution

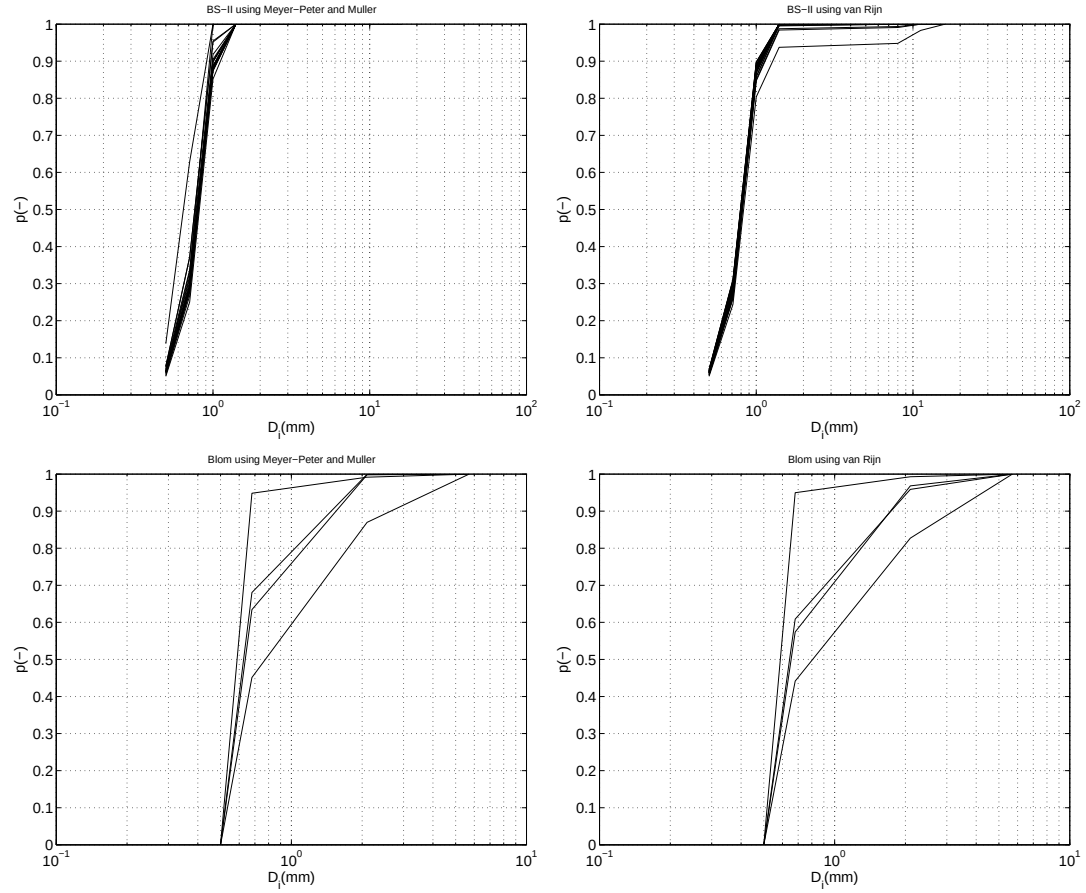

Figure 7.4: Grain size distributions determined from a transport model prediction using the surface based grain size distribution, showing both the BS-II (top row) and Blom data sets (lower row).

is nearly the same as when using the Shields curve, with (nearly) only sand in the distribution. However, when the model has a zero transport prediction no grain size distribution can be determined. Using the grain size distributions determined from the transport compositions and the hydraulic conditions from chapter 3 the transport rates are predicted. Compared to the predictions with the grain size distribution determined

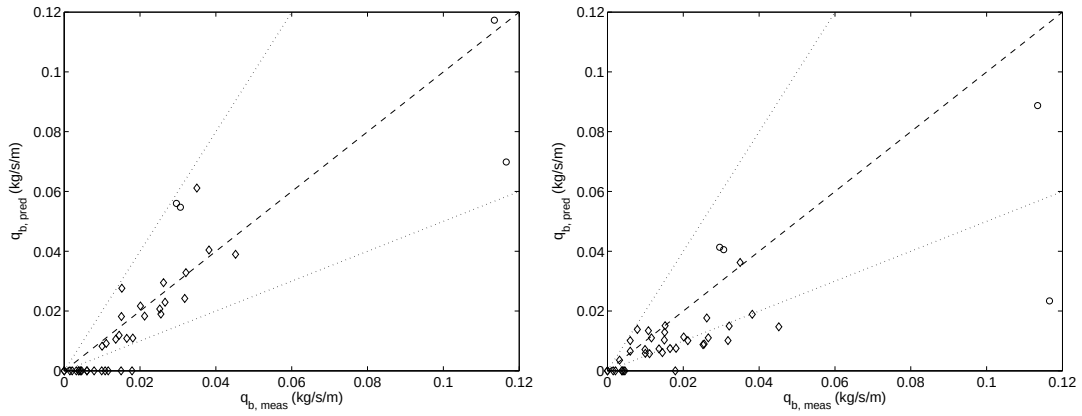

Figure 7.5: Predicted and measured transport rates, with the double model run for both the model of Meyer-Peter and Müller (left) and van Rijn (right)

with the Shields curve the results are worse for both the model of Meyer-Peter and Müller and van Rijn. For the model of Meyer-Peter and Müller only 63% of the predictions are within a factor two and 53% for van Rijn.

7.3 Struiksma reduction functions

In the study of Struiksma (1985) a reduction function is proposed to account for the reduced transport rates as a result of an immobile layer. The transport reduction is related to the relative transport layer thickness through a reduction function, given by:

$$q_b = \psi * q_{b,a} \tag{7.2}$$

where q_b is the predicted partial transport rate, ψ is the reduction function, $q_{b,a}$ is the predicted alluvial transport rate.

The reduction function can be described in two ways: the linear and reduction function and the sinusoid reduction function described below.

$$\psi = \frac{d}{d_a} \qquad \text{for } d < d_a \tag{7.3}$$

Sinusoid reductiion function:

$$\psi = sin\left(\frac{\pi}{2}\frac{d}{d_a}\right) \qquad \text{for } d < d_a \tag{7.4}$$

where d is the average transport layer thickness, d_a the transport layer thickness required for alluvial conditions. The transport layer thickness is half the bedform height ($d_a = 0.5\Delta_0$, (Struiksma, 1985)).

The reduction function requires input of d and Δ_0, which are known for the BS data sets only. Therefore the results with the BS-II data set are shown only. Figure 7.6 shows the results of the reduction functions, using both approaches. Both reduction function cannot accurately account for the measured transport reduction of the BS-II data set. The transport rates are reduced too much. With the reduction functions the model of Meyer-Peter and Müller predicts 58% within a factor two using the linear reduction and 67% with the sinusoid reduction function. For the model of van Rijn 25% is within a factor two with the linear reduction and 39% with the sinusoid reduction.

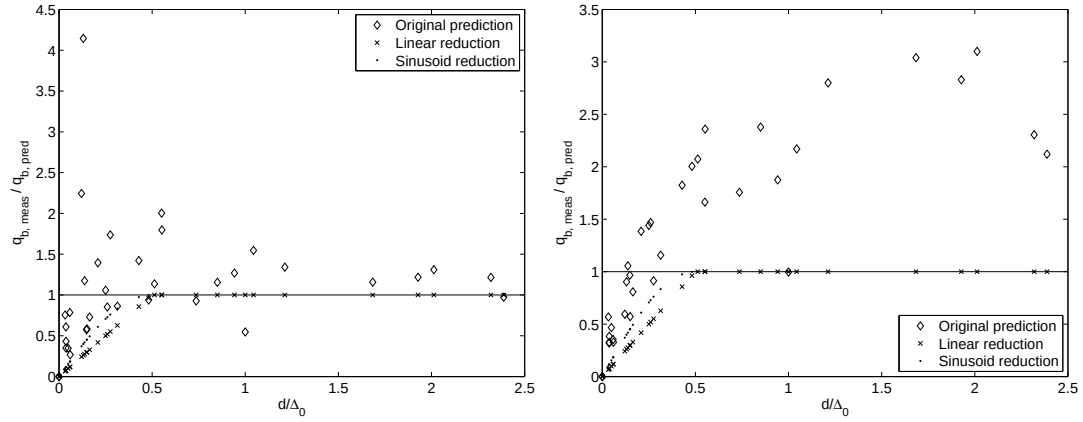

Figure 7.6: Transport ratio in relation to the supply limitation, also showing the two reduction functions of Struiksma, with the models of Meyer-Peter and Müller (left) and van Rijn (right)

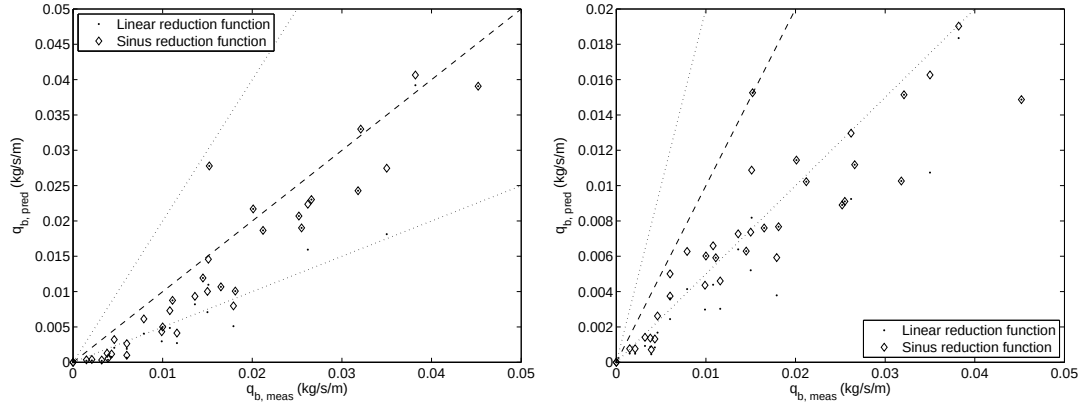

Figure 7.7: Predicted and measured transport rates with the reduction functions of Struiksma, Meyer-Peter and Müller (left) and van Rijn (right)

7.4 Hindrance factor

Kleinhans and van Rijn (2002) propose a different approach to account for the transport reduction using a hindrance factor. It is assumed that for partial transport conditions the small grains are hindered by coarse grains and can also be shielded by an immobile layer (Kleinhans and van Rijn, 2002). To account for this effect the hindrance factor is assumed to be related to the area of transported coarse grains compared to the area of immobile coarse grains. The hindrance factor is calculated with:

$$q_b = f_h q_{b,a} \tag{7.5}$$

With:

$$f_h = 1 - e^{-7.2\left(\frac{D_{90,bedload}}{D_{90,bed}}\right)^2} \tag{7.6}$$

where q_b is the reduced transport rate, f_h is the hindrance factor, $q_{b,a}$ is the predicted transport rate, $D_{90,bedload}$ the D_{90} of the transported bedload, $D_{90,bed}$ the D_{90} of the grain size distribution used in the transport calculation.

The $D_{90,bedload}$ is determined from the predicted transport composition. In the experiments of BS-II only the sand fraction was mobile, therefore the $D_{90,bedload}$ is a constant factor: the D_{90} of the sand fraction ($D_{90,bedload} = 1.2$ mm).

The ratio of $\frac{D_{90,bedload}}{D_{90,bed}}$ represents the transport condition, as it becomes unity for large bed shear stresses. For the poorly sorted bimodal sediment of BS-II the ratio of $\frac{D_{90,bedload}}{D_{90,bed}}$ functions similarly, however not the way the transport actually occurs. For very large bed shear stresses the gravel fraction will become mobile. However,for the sand fraction alluvial conditions are reached for lower bed shear stresses. The hindrance factor should become unity for alluvial conditions of the sand fraction to represent the transport of the BS-II experiment.

For the bimodal sediment of BS-II the $D_{90,bed}$ approximates two values. When little gravel is in the grain size distribution the $D_{90,bed} = D_{90,sand}$ and for amounts of gravel above 10% $D_{90,bed} = D_{90,gravel}$. For that situation the ratio of $\frac{D_{90,bedload}}{D_{90,bed}}$ is smaller than 1 and the hindrance function works. When the relative transport layer thickness increases the amount of gravel in grain size distribution decreases and the ratio of $\frac{D_{90,bedload}}{D_{90,bed}}$ becomes 1. The transport of finer fractions is no longer "hindered" and the hindrance factor becomes one. Therefore the hindrance factor can also approximately be two values. The hindrance factor cannot account for the measured transport reduction of BS-II (Figure 7.8). For the Blom data set similar results are seen for both transport models: two runs are corrected a little bit, one run is corrected a lot and one run is not corrected at all.

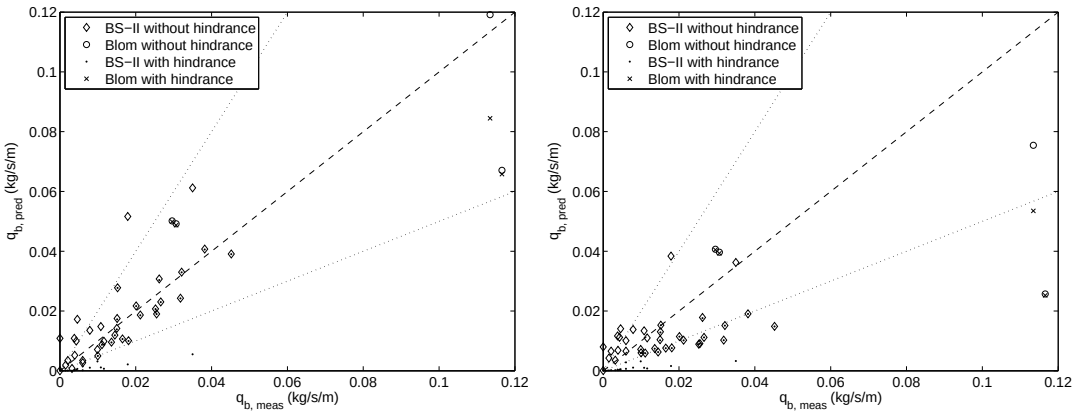

Figure 7.8: Predicted and measured transport rates for the model of Meyer-Peter and Müller (left) and van Rijn (right) with hindrance factor correction

7.5 Exposure of the coarse layer

Tuijnder (2010) calculated the exposure of the coarse layer for the BS-II experiments. Under alluvial conditions the bed levels of a bed with ripples or dunes usually can be predicted by a Gaussian distribution. With this assumption and the bed level measurements of data set BS-II, the exposure of the coarse layer was approximated using (Tuijnder, 2010):

$$p = \frac{1}{\sigma\sqrt{2\pi}} \int_{-\infty}^{z_{til}} e^{\frac{(z-\mu)^2}{2\sigma^2}} dz \tag{7.7}$$

where p the exposure of the coarse layer, $\sigma = \frac{\Delta}{2.5}$, Δ is the bedform height, z is the bedlevel, $\mu =$ d is the transport layer thickness.

The predicted exposures of the coarse layer are shown in Appendix F. On the exposed parts of the coarse layer no transport takes place, therefore it is assumed that predicted transport rates need to be reduced by the area of exposed gravel. The exposure reduction function is calculated from:

$$q_b = q_{b,a}(1 - p) \tag{7.8}$$

where q_b is the reduced transport rate, $q_{b,a}$ is the predicted transport rate, p is the fraction of the bed where the immobile layer is exposed. It can be seen that the exposure of the coarse layer does not account for the measured transport reduction. For supply limited situations, d/Δ_0 smaller than approximately 1, the measured reduction in transport is greater than is accounted for by the exposure of the coarse layer.

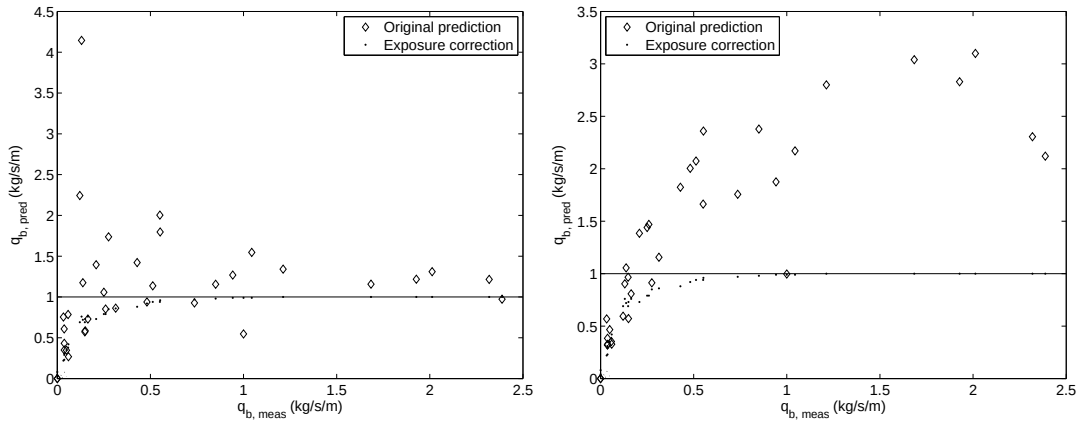

Figure 7.9: Transport ratio as a function of the relative transport layer thickness, also showing the exposure correction, of the models of Meyer-Peter and Müller (left) and van Rijn (right).

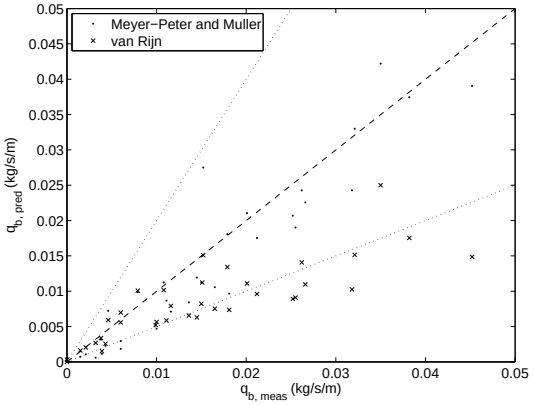

Figure 7.10: Predicted and measured transport rates of the models of Meyer-Peter and Müller and van Rijn with the exposure correction.

Concept validation

For the other data sets with bimodal sediment the necessary input for the exposure correction can be calculated. The data sets of BS-I and BS-IV can thus be predicted as well. The Shields curve approach is used to determine the mobile fractions, this results in only mobility of the sand fractions (same as the BS-II data set). Using Equation 7.7 the exposure of the coarse layer is predicted, this is included in Table 3.1 and Table 3.4.

With the input of the grain size distribution from the Shields curve, the p from Equation 7.7 and hydraulic conditions from chapter 3 the transport rates are predicted with the fractional models of Meyer-Peter and Müller and van Rijn. Figure 7.11 shows the predicted and measured transport rates of both models, with and without the exposure of the coarse layer correction. The predictions with the mobile sediment only (MPM and van Rijn in Figure 7.11) improve the predictions of the BS-I data set greatly for the Meyer-Peter and Müller model, with the (estimated) bulk grain size distribution all predictions were zero. For the model of van Rijn also improve greatly, nearly all predictions are within a factor two of the measurements, compared to a single prediction within a factor two in the bulk predictions. For the BS-IV data set a large increase in performance is also seen, for both the models.

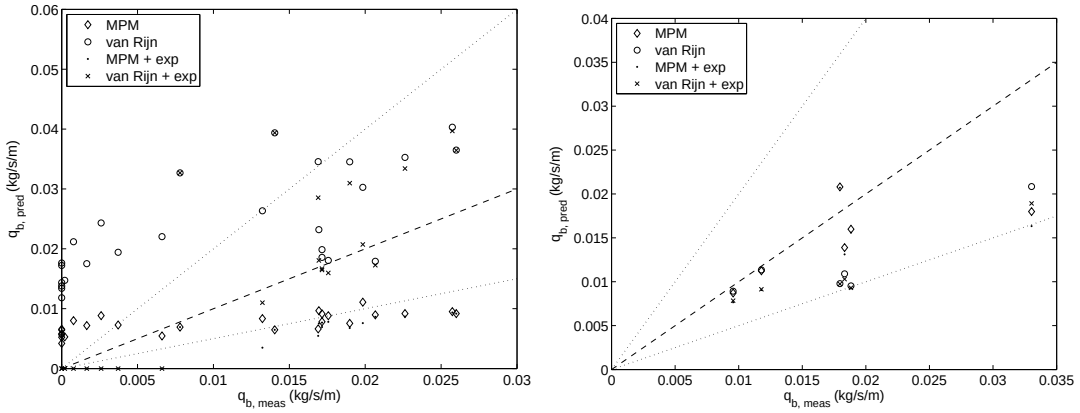

Figure 7.11: Predicted and measured transport rates for the BS-I (left) and BS-IV (right) data set with the exposure of the coarse layer correction.

7.6 Discussion

For the bimodal sediment of the BS-II data set the predictions with only the mobile sediment improve the performance of the transport models greatly. When extended with a reduction function the performance increases further, Table 7.1. The best results are obtained with the exposure of the coarse layer approach of Tuijnder (2010).

Table 7.1: Overview of the scores of all the prediction for the BS-II data set, including several reduction corrections like Struiksma and Hindrance correction.

	Bulk	Surface	Shields	Double-run	Struiksma-lin	Struiksma-sin	Hindrance	Exposure
MPM	0.15	0.32	0.65	0.42	0.50	0.58	0.46	**0.66**
van Rijn	0.27	0.35	0.53	0.45	0.38	0.46	0.33	**0.58**

For the data set of Blom the predictions show a different outcome. The Struiksma reduction and Tuijnder exposure correction are not possible, due to lack of data. The predictions with the surface grain size distribution using the transport model of Meyer-Peter and Müller give the best results, while the model of van Rijn performs best with the bulk sediment composition.

Table 7.2: Overview of the scores of all the prediction for the Blom data set, including the correction of the hindrance factor of van Rijn.

	Bulk	Surface	Shields	Double-run	Hindrance
MPM	0.74	**0.78**	0.69	0.66	0.63
van Rijn	**0.70**	0.58	0.60	0.61	0.55

The reduction functions of Struiksma cannot give the right transport reduction. However, a trend is visible in the figures that may be found using a different mathemathical function, for example a logarithmic function. Also, the reduction functions of Struiksma require knowledge of the transport layer thickness. Finding a similar function using different parameters, for example bed form height, could make the reduction function more broadly applicable.

The hindrance factor of Kleinhans and van Rijn (2002) cannot account for the transport reduction in the BS data sets. This is mostly due to the strong bimodal sediment, the hindrance factor is approximately two values. Changing the parameters for the hindrance calculation may improve this.

The exposure of the coarse layer from Tuijnder (2010) performs well for bimodal sediment. However, if a more natural sediment is used the calculation of the exposure of the coarse layer may not be straightforward. For the prediction the diameter of the coarse layer is needed as input as well as the transport layer thickness, information that is not always available or can be hard to determine.

Chapter 8

Discussion

Different approaches, different result

Partial transport presents a problem for the choice of the sediment grain size distribution. With strong bimodal sediment, like in the BS experiments, the grain size distribution influences the functionality of the transport model and therefore the predicted transport rates. With a more continuous grain size distribution, like the data set of BK, the functionality of the model is not affected as strongly. The strong bimodal sediment combined with the conditions that lead to strong supply limitation require a different approach and transport model than a natural sediment with similar conditions. While for the data sets of Blom and BK the original transport models (using the bulk and surface grain size distribution) were able to predict the transport rates fairly well, the BS data sets required both a different approach and a reduction function to predict the transport rates accurately.

Furthermore, the models of Meyer-Peter and Müller and van Rijn have no functionality included to account for effects of partial transport, like transport reduction. However, they perform better than the model of Wilcock and Crowe which was developed for partial transport conditions.

Sediment characteristic parameters

The used sediment composition is of great influence on the performance of the transport models. Especially grain size distributions with gaps, like the bimodal sediment (Figure 5.21), will result in extreme values of the sediment characteristic parameters. For the D_{50} and D_{90} this results in jumps in the value for different compositions. Also, the D_{90} is a diameter in the gravel fraction of the BS data sets for (nearly) all predictions. Only if no gravel is included in the grain size distribution will the D_{90} be a diameter of

the transported sediment. Excluding the gravel from the grain size distribution improves the performance of the transport models, but also excludes the ability to account for the effects of the gravel on the sand fraction. This can be accounted for with a reduction function however.

Alternatively the mean diameter is used; however this also leads to erratic behavior. For the strong bimodal sediment, if gravel is included in the grain size distribution, the mean diameter is a diameter that does not exist in the mixture, it being larger than the diameter of the sand fraction and smaller than the diameter of the gravel fraction. For more natural sediments like that of the Blom and BK data sets, the influence of these parameters (D_{50}, D_{90} and D_m) is smaller. The mean diameter is (nearly) always existent in the sediment and the D_{50} and D_{90} will not jump.

Although it may not be a serious problem that the these parameters are too high or too low, in the transport models it results in different functionality than occurring physically in transport.

Model parameters and functions

The sediment characteristics influence the model parameters and functions that represent physical processes, like hiding/exposure. Erratic effects in the mean and median diameter directly translate to erratic effects for example the hiding/exposure correction. This applies to the hiding/exposure correction of Meyer-Peter and Müller and of Wilcock and Crowe, the bed form factor of Meyer-Peter and Müller; and the current related efficiency factor of van Rijn.

Furthermore, the physically represented processes present a problem with the BS data sets. For example, if the coarse layer is exposed the hiding/exposure correction functions well, hiding the sand and exposing the gravel fraction. However, when the gravel layer is covered with sand the hiding/exposure correction should hide the fine sand fractions and expose the coarse sand fractions, ignoring the gravel fractions. However, in the transport models the hiding/exposure correction is calculated based on the mean or median diameter of the entire sediment. This results in extreme hiding/exposure corrections that more or less represent the hiding/exposure of the situation where the coarse layer is exposed. Splitting the hiding/exposure correction into two parts can be a solution to increase its functionality. However, this requires knowledge of the area of exposed gravel. For the the bed form factor of Meyer-Peter and Müller and current related efficiency factor of van Rijn this is also the case. These parameters are calculated with the D_{90} of the grain size distribution. Both parameters represent the correction for the effective bed shear stress, which is related to the grains. When calculated with a D_{90} of the gravel fraction this represents the process occurring when the gravel layer is exposed. Using a substitute like the D_m (for example $(D_m)^n$) may improve predictions, also in

the development of the transport model van Rijn proposes to use the D_i in stead of D_{90}.

In the adjusted model predictions (chapter 7) the split calculation is partly demonstrated. With the predictions of the mobile fraction only, the performance for the BS data sets improves greatly. Also, the hiding/exposure correction functions closely to how it occurs in reality, hiding the coarser sand fractions and exposing the finer sand fractions. However, the second part of the split calculation is not performed in this study. For the coarser fractions no transport will be predicted, because the occurring bed shear stress is too low to mobilize the gravel.

Surface grain size distribution

The surface grain size distribution for the BS-II data set improves the predictions a somewhat. However, they were determined on a basis of only six sets of photographs for 36 data points. The determined relation could therefore be improved if more data is available, while it may also be improved by making it independent of the transport layer thickness. The transport layer thickness is not always known.

Chapter 9

Conclusions

This chapter summarizes the conclusions of this study by revisiting the three research questions posed in chapter 1.

1. Which processes and variables are important when predicting sediment transport rates? And how are they affected by partial transport?

All three transport models calculate the transport rate with the bed shear stress, which in two of three models is corrected for bed forms (Meyer-Peter and Muller) or current efficiency (van Rijn). The bed shear stress is compared to a critical value that indicates initiation of motion of the sediment or sediment fraction. This critical value is corrected for hiding/exposure effects by all three models, but in three different ways. For accurate predictions the corrections have to be valid, adjusting the process to the way it occurs in reality.

Under partial transport the effect of hiding/exposure changes, most noticeably if a pavement layer develops. Where the pavement layer is exposed, hardly any or no transport takes place and the finer fractions hide inside the pores of the pavement layer. Where the pavement layer is covered, the effect of hiding/exposure occurs only within the fine fraction. Therefore the hiding/exposure correction should be split into two calculations, which is not done in the transport models.

Furthermore, the pavement layer limits the amount of fine sediment available for transport. The transport therefore depends on the amount of mobile sediment available at the surface (Wilcock and McArdell (1993)). To accurately predict transport rates under partial transport this would have to be accounted for in the transport models.

From the predictions it is that the functions that correct for the physical processes, like hiding/exposure, need to be included. However, it is important to make sure that parameters are used to ensure the functionality for the actual occurring processes. For

Table 9.1: An overview of which model performs best for each of the data set for both the bulk and surface based grain size distribution.

	Bulk grain size distribution	Surface grain size distribution
BS-I	van Rijn (fractional)	-
BS-II	van Rijn (fractional)	van Rijn (fractional)
BS-IV	van Rijn (fractional)	-
Blom	Meyer-Peter and Müller (fractional)	Meyer-Peter and Müller (fractional)
BK	van Rijn (uniform)	-

example, with the BS data sets the hiding/exposure correction malfunctioned if gravel was included in the grain size distribution. This also occurred with other correction factors like the bed form factor and current-related efficiency factor.

2. How well can currently available transport models predict transport rates under partial transport conditions?

With the currently available transport models two approaches were tested: a bulk grain size distribution as input and a surface based grain size distribution. Overall it can be concluded that the used approaches, both the bulk and surface based grain size distributions, cannot accurately predict the measured transport rates of the used data sets. The fractional approaches predict the transport composition well in most cases, especially with the surface based grain size distributions. It can be concluded that the transport models have trouble predicting the transport rates for the bimodal sediment of the BS data sets. For the tri-modal sediment of Blom and the natural sediment of BK all the models predict the transport rates with greater accuracy.

With the bulk grain size distribution the performance of the transport models is poor for the BS data sets and slightly better for the data sets of Blom and BK. Table 9.1 shows which model performs best for each data set with the bulk and surface based grain size distribution.

In previous chapters the performance was shown in the form of scores. For the data sets with the bimodal sediment the predictions with both the bulk and surface based grain size distribution were poor, with a maximum score of 0.44. With the surface based grain size distribution the performance of the transport models improved a little bit. The biggest problem when predicting the transport of the BS data sets is the effect of the sediment parameters (D_{50}, D_{90} and D_m). In bimodal sediment the fractions, sand and gravel, are far apart in diameter and therefore functions in the models do not work as intended. For each of the transport models the poor performance is caused by different functions:

- Meyer-Peter and Müller: hiding/exposure correction (use of D_m) and bed form factor (use of D_{90})
- Van Rijn: current-related efficiency factor (use of D_{90})

- Wilcock and Crowe: hiding/exposure correction (use of D_m) and mean reference shear stress (use of D_m).

Alternatively the parameter in question (D_m or D_{90}) could be replaced by for example the D_{50}, this however has a drawback when more than 50% gravel in in the grain size distribution (jump).

Furthermore, the models of the Meyer-Peter and Müller and van Rijn have no included functionality for partial transport like the model of Wilcock and Crowe. The model of Meyer-Peter and Müller underpredicts transport rates for both supply limited and near alluvial conditions, this is caused by the hiding/exposure correction. The van Rijn model over predicts supply limited conditions, it cannot account for the occurring supply limitation. However, for near alluvial conditions the model predicts transport rates that are too low. For the bimodal sediment of BS-II this due to the current related efficiency correction factor.

3. Can the transport models be adjusted to better represent the processes occurring under partial transport conditions?

By changing the approach and determining the mobile sediment before predicting the transport rates the performance of the models improve greatly for the BS data sets. By including a reduction function the performance of the transport models improves further, except for the BS-IV data set.

For the data sets of Blom the predictions with the surface based grain size distribution cannot be improved by using a different approach and including a reduction function. The prediction of the Meyer-Peter and Müller model is best. For both the Blom and BK dataset (nearly) all predictions are within a factor two, except for the model of Wilcock and Crowe.

Bibliography

Ashida, K. and Michiue, M. (1973). Studies on bed load transport rate in alluvial streams. Sediment Transportation, volume 1.

Blom, A. (2000). Flume experiments with a natural and a trimodal sediment mixture-data report sand flume experiments 1999/2000. Technical report 2000R-004/MICS-013, University of Twente.

Blom, A. and Kleinhans, M. (1999). Non-uniform sediment in morphological equilibrium situations. data report sand flume experiments 97/98. Technical report Cit 99R-002/MICS-001, University of Twente, Rijkswaterstaat RIZA, WL/Delft Hydraulics.

Blom, A., Ribberink, J. S., and Vriend, H. d. (2002). Vertical sorting in bed forms. flume experiments with a natural and a trimodal sediment mixture. Water Resources Research.

Egiazaroff, I. (1965). Calculation of nonuniform sediment concentrations. Journal of the Hydraulics Division, ASCE, 91:225–248.

Engelund, F. and Hansen, E. (1967). A monograph on sediment transport in alluvial streams. Teknisk Forlag.

Kleinhans, M. and van Rijn, L. (2002). Stochastic prediction of sediment transport in sand-gravel bed rivers. Journal of Hydraulic Engineering, 128(4).

Meyer-Peter, E. and Müller, R. (1948). Formulas for bed-load transport. In Proceedings 6th Congress IAHR.

Otsu, N. (1979). A threshold selection method from gray-level histograms. IEEE Transactions on Systems, Man, and Cybernetics.

Spekkers, M. (2008). Laboratory study on the development of a pavement layer beneath river dunes. Data report, University of Twente.

Struiksma, N. (1985). Celerity and deformation of bed pertubations travelling over a non-erodible layer.

Tuijnder, A. (2010). Sand in short supply : modelling of bedforms, roughness and sediment transport in rivers under supply-limited conditions. PhD thesis, Twente University.

Tuijnder, A., Ribberink, J., and Hulscher, S. (2009). An experimental study into the geometry of supply-limited dunes. Sedimentology.

Tuijnder, A. P. (2007). Experiments with sand over an immobile gravel at the lwi braunschweig july - december 2007. Data report, University of Twente.

van der Scheer, P., Ribberink, J., and Blom, A. (2002). Transport formulas for graded sediment. Technical report, Civil Engineering University of Twente.

van Rijn, L. (1984a). Sediment transport, part i: Bed load transport,. Journal of Hydraulic Engineering.

van Rijn, L. (1984b). Sediment transport, part ii: Suspended load transport. Journal of Hydraulic Engineering.

van Rijn, L. (1993). Principles of sediment transport in rivers, estuaties and coastal seas. Aqua Publications.

van Rijn, L. (2007a). Unified view of sediment transport by currents and waves, i: Initiation of motion, bed roughness, and bed-load transport. Journal of Hydraulic Engineering, 133(6):649 – 667.

van Rijn, L. (2007b). Unified view of sediment transport by currents and waves, ii: Suspended transport. Journal of Hydraulic Engineering, 133(6):668 – 689.

van Rijn, L. (2007c). Unified view of sediment transport by currents and waves, iii: Graded beds. Journal of Hydraulic Engineering, 133(7):761–775.

Wilcock, P. and Crowe, J. (2003). A surface-based transport model for mixed-size sediments. Journal of Hydraulic Engineering, 29(2).

Wilcock, P. and Kenworthy, S. (2002). A two-fraction model for the transport of sand/gravel mixtures. Water Resources Research, 38(10).

Wilcock, P., Kenworthy, S., and Crowe, J. (2001). Experimental study of the transport of mixed sand and gravel. Water Resources Research, 37(12):339–3358.

Wilcock, P. R. and McArdell, B. W. (1993). Surface based fractional transport rates: Mobilization threshold and partial transport of a sand-gravel sediment. Water Resources Research.

Yang, C. (1996). Sediment Transport: Theory and Practice. McGraw-Hill.

List of notations

p_i	probability (volume fraction) of size fraction i (-)
F_s	proportion of sand in surface size distribution (-)
D_i	diameter of bed material of fraction i (m)
D_m	geometric mean diameter (m)
D_{sm}	mean grain size of bed surface (m)
C_b	Chézy related to the bed ($m^{1/2}s^{-1}$)
C'	Chézy related to the grains ($m^{1/2}s^{-1}$)
f_c	friction coefficient based on $k_{s,b}$ (-)
f'_c	friction coefficient based on D_{90} (-)
$k_{s,b}$	current related roughness heigth (m)
Φ	Dimensionless transport parameter (-)
τ_b	bed shear stress (N/m^2)
τ'	bed shear stress related to the grains (N/m^2)
τ_{ri}	reference shear stress of size fraction i (N/m^2)
τ_{rm}	reference shear stress of mean size of bed surface (N/m^2)
τ^*_{rm}	reference dimensionless Shields stress for mean size of surface (-)
f_{gravel}	amount of gravel in the sediment composition (-)
q_b	bed load sediment transport (kg/s)
θ	Shields stress (-)

Appendix A

Bed shear stress and sidewall roughness

In the flume experiments different methods are used to calculate the bed shear stress according to the flume facility. For the small flumes of BS-I the roughness of the wall is corrected for with the equations of Einstein (1942). For the large flumes of BS-II and BS-IV the wall roughness is corrected with the Vanoni-Brooks (1957) equations.

Bed shear stress calculation with Einstein (1942) correction for sidewall roughness:

$$\tau_b = -\rho g \bar{h} I_e \left(1 - 0.0012 \frac{\bar{u}^{1.4}}{-I_e^{0.8}}\right) \tag{A.1}$$

$$k_{s,b} = \frac{12 R_b}{10^{C_b/18}} \tag{A.2}$$

$$C_b = \sqrt{\rho g \bar{u}^2 / \tau_b} \tag{A.3}$$

in which h the water depth, I_e the energy slope, $\bar{u}$ the depth-average flow velocity, R_b the hydraulic radius related to the bed.

Bed shear stress calculation with the Vanoni-Brooks (1957) correction for sidewall roughness:

$$\tau = \rho g R I_e \tag{A.4}$$

$$C = \sqrt{\frac{\rho g u^2}{\tau}} \tag{A.5}$$

$$f = \frac{8g}{C^2} \tag{A.6}$$

$$Re = \frac{4uR}{\nu} \tag{A.7}$$

$$f_{wall} = [20\frac{Re}{f}^{0.1} - 39]^{-1} \quad \text{original equation} \tag{A.8}$$

$$f_{wall} = 0.0026(\log(Re/f))^2 - 0.0428\log(Re/f) + 0.1884 \quad \text{wall-roughness, van Rijn (1993)} \tag{A.9}$$

$$f_b = f + \frac{2h}{B}(f - f_{wall}) \tag{A.10}$$

$$C_b = \sqrt{\frac{8g}{f_b}} \tag{A.11}$$

$$R_b = \frac{f_b}{f}R \tag{A.12}$$

$$\tau_b = \rho g \frac{u^2}{C_b^2} \tag{A.13}$$

in which τ the average total shear stress, ρ the water density, g the gravitational constant, R the hydraulic radius, I_e the energy slope, u the depth average flow velocity, C the total Chézy value, f the Darcy-Weisbach friction coefficient, ν the viscosity of the water, Re the Reynolds number, f_{wall} the wall friction factor, f_b the friction coefficient related to the bed, R_b the hydraulic radius related to the bed, h the water depth, B the width of the flume, τ_b the bed shear stress.

Appendix B

Bulk Sediment distribution

Table B.1: Sediment parameters and distribution of data set BS-I

	f_{gravel}	D_{50}	D_{90}	D_m	$D_i(mm)$					
					0.5	**0.7**	**1.0**	**1.4**	**5.0**	**8.0**
1	1.00	6.36	7.67	7.75	0.00	0.00	0.00	0.00	0.08	0.92
2	0.98	6.33	7.67	7.63	0.00	0.00	0.01	0.00	0.08	0.90
3	0.98	6.32	7.66	7.59	0.00	0.00	0.01	0.00	0.08	0.90
4	0.93	6.25	7.65	7.30	0.00	0.01	0.04	0.01	0.08	0.86
5	0.88	6.13	7.63	6.91	0.01	0.02	0.07	0.02	0.07	0.80
6	0.72	5.73	7.55	5.86	0.01	0.06	0.17	0.04	0.06	0.66
7	0.60	5.27	7.45	5.04	0.02	0.08	0.24	0.06	0.05	0.55
8	0.55	5.04	7.41	4.72	0.02	0.09	0.27	0.07	0.05	0.51
9	0.47	1.27	7.31	4.19	0.03	0.11	0.32	0.08	0.04	0.43
10	0.39	0.99	7.17	3.63	0.03	0.12	0.36	0.09	0.03	0.36
11	0.37	0.97	7.11	3.46	0.03	0.13	0.38	0.09	0.03	0.34
12	0.28	0.93	6.85	2.90	0.04	0.14	0.43	0.11	0.02	0.26
	f_{gravel}	D_{50}	D_{90}	D_m	$D_i(mm)$					
					0.5	**0.7**	**1.0**	**1.4**	**11.2**	**16.0**
13	1.00	10.37	14.94	13.38	0.00	0.00	0.00	0.00	0.55	0.45
14	1.00	10.37	14.94	13.38	0.00	0.00	0.00	0.00	0.55	0.45
15	1.00	10.37	14.94	13.38	0.00	0.00	0.00	0.00	0.55	0.45
16	1.00	10.34	14.94	13.33	0.00	0.00	0.00	0.00	0.54	0.45
17	0.97	10.12	14.91	13.05	0.00	0.01	0.02	0.00	0.53	0.44
18	0.95	9.88	14.88	12.74	0.00	0.01	0.03	0.01	0.52	0.43
19	0.88	9.18	14.80	11.93	0.01	0.02	0.07	0.02	0.48	0.40
20	0.83	8.49	14.72	11.23	0.01	0.03	0.10	0.03	0.45	0.37
21	0.62	4.90	14.30	8.68	0.02	0.08	0.23	0.06	0.34	0.28
22	0.53	2.39	14.00	7.54	0.02	0.09	0.28	0.07	0.29	0.24
23	0.47	1.23	13.72	6.74	0.03	0.11	0.32	0.08	0.25	0.21
24	0.41	1.00	13.42	6.06	0.03	0.12	0.35	0.09	0.22	0.19
25	0.36	0.97	13.04	5.40	0.03	0.13	0.39	0.10	0.20	0.16
26	0.30	0.94	12.53	4.76	0.03	0.14	0.42	0.10	0.17	0.14

Table B.2: Sediment parameters and distribution of data set BS-II

	f_{gravel}	D_{50}	D_{90}	D_m	$D_i(mm)$						
					0.5	**0.7**	**1.0**	**1.4**	**8.0**	**11.2**	**16.0**
1-1	1.00	10.55	14.81	12.77	0.00	0.00	0.00	0.00	0.11	0.48	0.40
1-2	0.85	9.97	14.59	10.99	0.01	0.03	0.09	0.02	0.10	0.41	0.34
1-3	0.85	9.97	14.59	10.99	0.01	0.03	0.09	0.02	0.10	0.41	0.34
1-4	0.56	7.29	13.85	7.54	0.02	0.09	0.27	0.07	0.06	0.27	0.22
1-5	0.53	4.20	13.73	7.17	0.02	0.09	0.28	0.07	0.06	0.25	0.21
1-6	0.36	0.97	12.71	5.26	0.03	0.13	0.38	0.10	0.04	0.18	0.15
1-7	0.20	0.89	10.56	3.34	0.04	0.16	0.48	0.12	0.02	0.10	0.08
1-8	0.13	0.87	8.67	2.48	0.04	0.17	0.52	0.13	0.01	0.06	0.05
1-9	0.09	0.86	1.38	2.06	0.05	0.18	0.55	0.14	0.01	0.04	0.04
1-10(a)	0.06	0.85	1.28	1.64	0.05	0.19	0.57	0.14	0.01	0.03	0.02
2-1	1.00	10.55	14.81	12.77	0.00	0.00	0.00	0.00	0.11	0.48	0.40
2-2	0.85	9.97	14.59	10.99	0.01	0.03	0.09	0.02	0.10	0.41	0.34
2-3	0.56	7.29	13.85	7.54	0.02	0.09	0.27	0.07	0.06	0.27	0.22
2-4	0.38	0.98	12.84	5.43	0.03	0.12	0.37	0.09	0.04	0.18	0.15
2-5	0.21	0.89	10.70	3.45	0.04	0.16	0.47	0.12	0.02	0.10	0.08
2-6	0.13	0.87	8.74	2.50	0.04	0.17	0.52	0.13	0.01	0.06	0.05
2-7	0.09	0.86	1.38	2.08	0.05	0.18	0.54	0.14	0.01	0.05	0.04
3-1	0.81	9.77	14.52	10.51	0.01	0.04	0.11	0.03	0.09	0.39	0.33
3-2	0.56	7.29	13.85	7.54	0.02	0.09	0.27	0.07	0.06	0.27	0.22
3-3	0.35	0.96	12.59	5.10	0.03	0.13	0.39	0.10	0.04	0.17	0.14
3-4	0.22	0.90	10.84	3.56	0.04	0.16	0.47	0.12	0.02	0.11	0.09
3-5	0.13	0.87	8.74	2.50	0.04	0.17	0.52	0.13	0.01	0.06	0.05
3-6(a)	0.06	0.85	1.28	1.65	0.05	0.19	0.57	0.14	0.01	0.03	0.02
4-1	0.81	9.77	14.52	10.51	0.01	0.04	0.11	0.03	0.09	0.39	0.33
4-2	0.53	4.20	13.73	7.17	0.02	0.09	0.28	0.07	0.06	0.25	0.21
4-3	0.35	0.96	12.59	5.10	0.03	0.13	0.39	0.10	0.04	0.17	0.14
4-4	0.21	0.89	10.70	3.45	0.04	0.16	0.47	0.12	0.02	0.10	0.08
5-1	0.85	9.97	14.59	10.99	0.01	0.03	0.09	0.02	0.10	0.41	0.34
5-2	0.81	9.77	14.52	10.51	0.01	0.04	0.11	0.03	0.09	0.39	0.33
5-3	0.63	8.62	14.11	8.42	0.02	0.07	0.22	0.06	0.07	0.31	0.25
5-4	0.38	0.98	12.84	5.43	0.03	0.12	0.37	0.09	0.04	0.18	0.15
5-5	0.21	0.90	10.77	3.50	0.04	0.16	0.47	0.12	0.02	0.10	0.09
5-6	0.13	0.87	8.88	2.54	0.04	0.17	0.52	0.13	0.02	0.06	0.05
5-7(a)	0.06	0.85	1.28	1.65	0.05	0.19	0.57	0.14	0.01	0.03	0.02
6-1(a)	0.06	0.85	1.28	1.65	0.05	0.19	0.57	0.14	0.01	0.03	0.02
6-2(a)	0.06	0.85	1.28	1.65	0.05	0.19	0.57	0.14	0.01	0.03	0.02

Table B.3: Sediment parameters and distribution of data set BS-III

	f_{gravel}	D_{50}	D_{90}	D_m	$D_i(mm)$ **0.5**	**0.7**	**1.0**	**1.4**	**4.0**	**5.0**	**8.0**	**11.2**	**16.0**	**22.4**
1	0.00	0.83	1.13	0.98	0.05	0.20	0.60	0.15	0.00	0.00	0.00	0.00	0.00	0.00
2	0.12	0.86	8.32	2.41	0.04	0.18	0.53	0.13	0.00	0.00	0.01	0.06	0.05	0.00
3	0.20	0.89	10.58	3.36	0.04	0.16	0.48	0.12	0.00	0.00	0.02	0.09	0.08	0.00
4	0.30	0.93	12.14	4.55	0.03	0.14	0.42	0.11	0.00	0.00	0.03	0.14	0.12	0.01

Table B.4: Sediment parameters and distribution of data set BS-IV

	f_{gravel}	D_{50}	D_{90}	D_m	$D_i(mm)$ **0.5**	**0.7**	**1.0**	**1.4**	**4.0**	**5.0**	**8.0**	**11.2**	**16.0**	**22.4**
1	0.05	0.84	1.26	1.57	0.05	0.19	0.57	0.14	0.00	0.00	0.01	0.02	0.02	0.00
2	0.10	0.86	1.40	2.16	0.05	0.18	0.54	0.14	0.00	0.00	0.01	0.05	0.04	0.00
3	0.15	0.87	9.45	2.75	0.04	0.17	0.51	0.13	0.00	0.00	0.02	0.07	0.06	0.00
4	0.15	0.87	9.45	2.75	0.04	0.17	0.51	0.13	0.00	0.00	0.02	0.07	0.06	0.00
5	0.15	0.87	9.45	2.75	0.04	0.17	0.51	0.13	0.00	0.00	0.02	0.07	0.06	0.00
6	0.20	0.89	10.58	3.34	0.04	0.16	0.48	0.12	0.00	0.00	0.02	0.09	0.08	0.00

Table B.5: Sediment parameters and distribution of data set Blom

	D_{50}	D_{90}	D_m	$D_i(mm)$ **0.5**	**0.7**	**2.1**
1	1.39	4.63	2.82	0.33	0.33	0.33
2	1.39	4.63	2.82	0.33	0.33	0.33
3	1.39	4.63	2.82	0.33	0.33	0.33
4	0.68	2.10	1.32	0.80	0.10	0.10

Table B.6: Sediment parameters and distribution of data set BK

	D_{50}	D_{90}	D_m	D_m **0.1**	$D_i(mm)$ **0.3**	**0.34**	**0.42**	**0.47**	**0.58**	**0.80**	**1.4**	**2.3**	**3.8**	**6.0**	**7.5**	**9.3**	**11.3**	
1	1.40	9.30	3.54	0.00	0.02	0.03	0.05	0.05	0.05	0.10	0.10	0.10	0.10	0.10	0.10	0.05	0.05	0.10
2	1.40	9.30	3.54	0.00	0.02	0.03	0.05	0.05	0.05	0.10	0.10	0.10	0.10	0.10	0.10	0.05	0.05	0.10
3	1.40	9.30	3.54	0.00	0.02	0.03	0.05	0.05	0.05	0.10	0.10	0.10	0.10	0.10	0.10	0.05	0.05	0.10
4	1.40	9.30	3.54	0.00	0.02	0.03	0.05	0.05	0.05	0.10	0.10	0.10	0.10	0.10	0.10	0.05	0.05	0.10

Appendix C

Performance of the transport models, scoring method

Comparing the performance of the three transport models is done with a scoring method used by van der Scheer et al. (2002). A score is calculated for the uniform and graded approach of each transport model using:

$$Score = \frac{1}{n} \sum_{j=1}^{n} factor(j) \tag{C.1}$$

in which:

$$factor(j) = min \left\{ ratio(j), \frac{1}{ratio(j)} \right\} \tag{C.2}$$

$$ratio(j) = \frac{q_{b,predicted}}{q_{b,measured}} = \frac{\sum q_{b,predicted}}{q_{b,i,measured}} \tag{C.3}$$

where $q_{b,i,predicted}$ is the predicted fractional transport rate, $q_{b,predicted}$ is the predicted total transport rate, $q_{b,measured}$ is the measured total transport rate, n is the number of experimental runs, j is a specific run. A score of one represents a perfect prediction, the lower the score the worse the prediction.

Appendix D

Photograph conversion

In Figure D.1,Figure D.2 and Figure D.3 photographs of the final bed state of data set BS-II are depicted alongside converted images in which white represents gravel and black represents sand. From the relative black and white areas the relative amount of gravel was calculated.

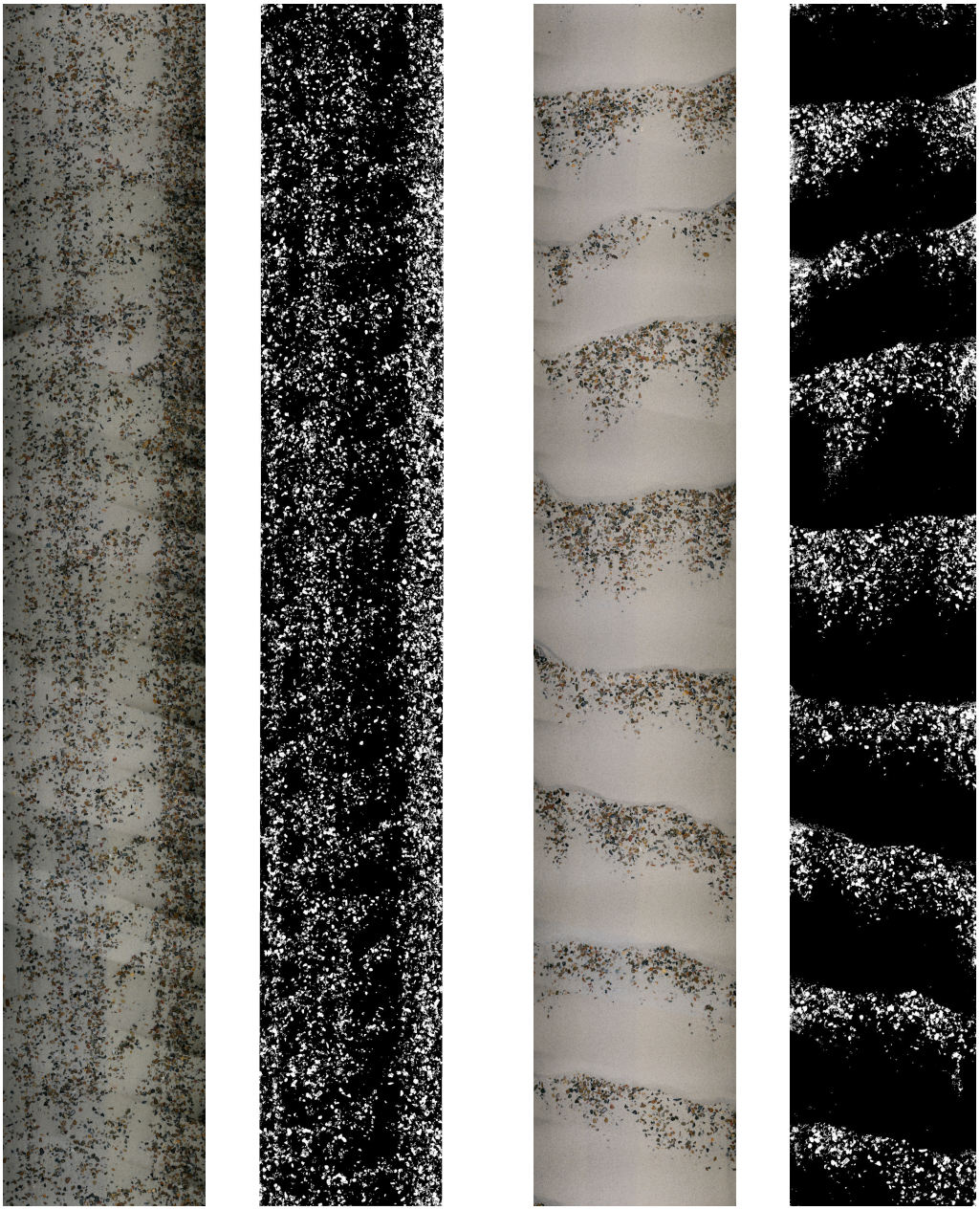

Figure D.1

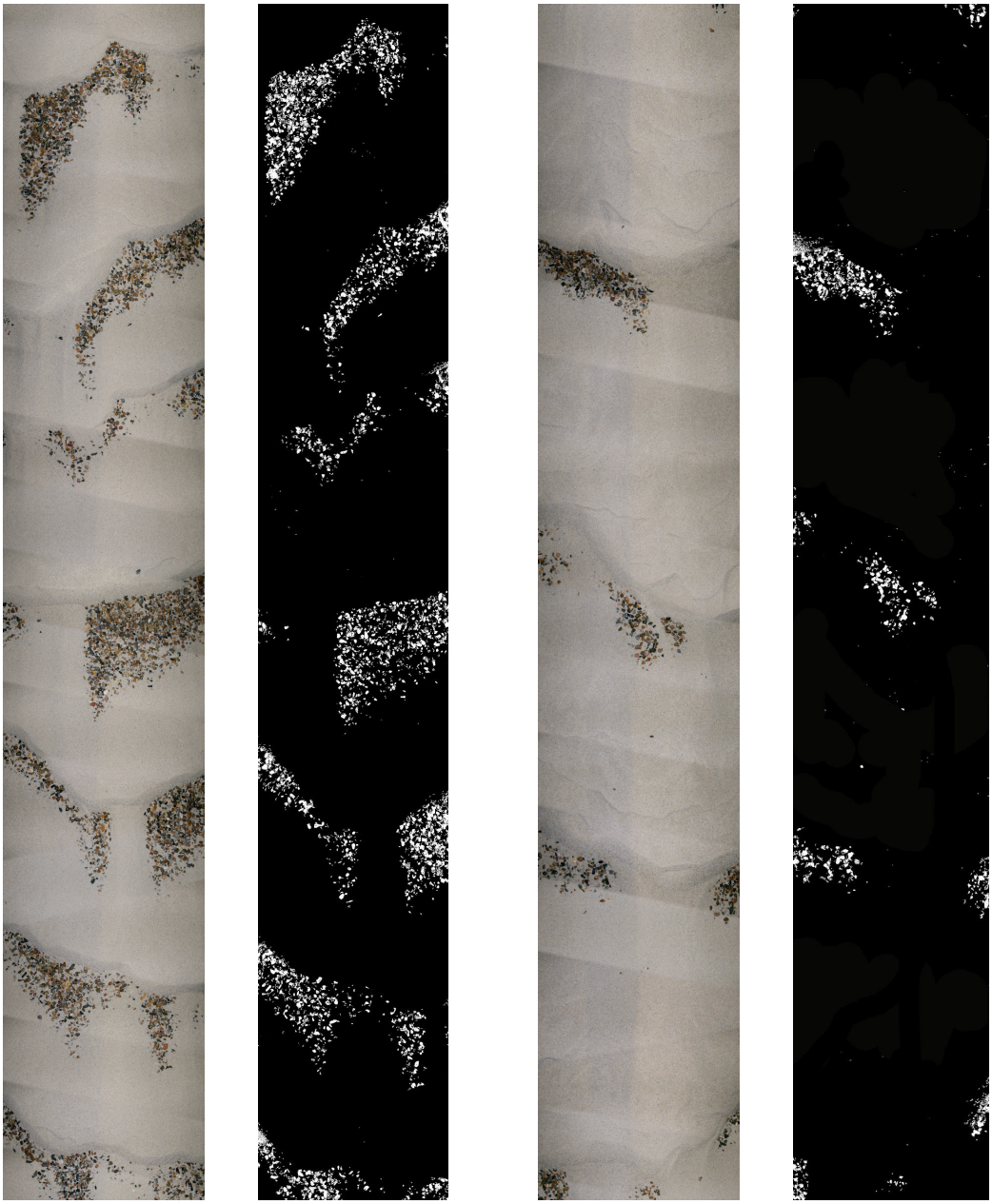

Figure D.2

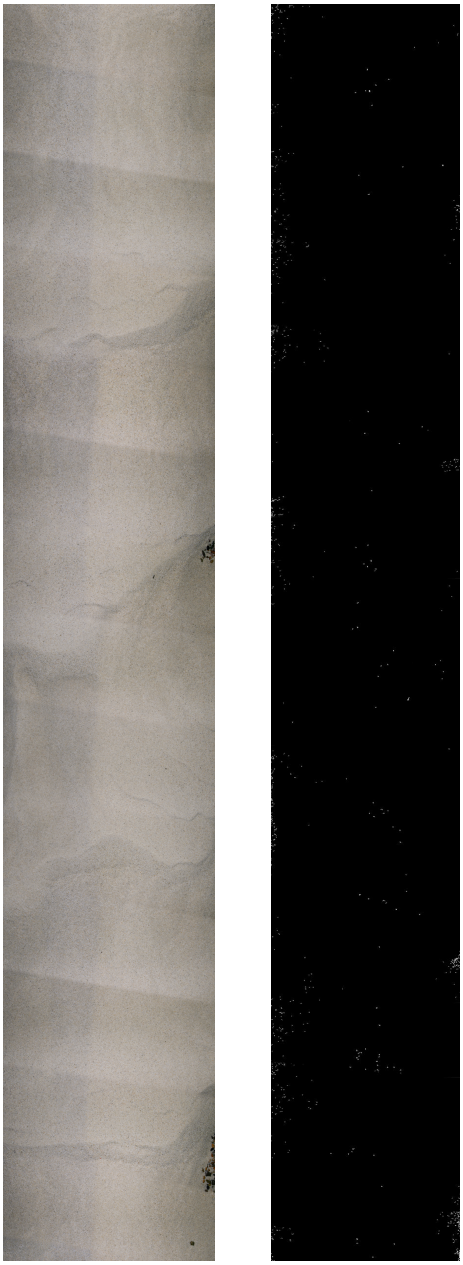

Figure D.3

Appendix E

Surface sediment distribution

Table E.1: Sediment parameters and distribution of data set BS-II

	f_{gravel}	D_{50}	D_{90}	D_m	$D_i(mm)$						
					0.5	**0.7**	**1.0**	**1.4**	**8.0**	**11.2**	**16.0**
1-1	1.00	10.55	14.81	12.77	0.00	0.00	0.00	0.00	0.11	0.48	0.40
1-2	0.83	9.90	14.57	10.82	0.01	0.03	0.10	0.02	0.09	0.40	0.34
1-3	0.83	9.90	14.57	10.82	0.01	0.03	0.10	0.02	0.09	0.40	0.34
1-4	0.16	0.88	9.83	2.91	0.04	0.17	0.50	0.13	0.02	0.08	0.07
1-5	0.15	0.88	9.59	2.80	0.04	0.17	0.51	0.13	0.02	0.08	0.06
1-6	0.10	0.86	1.39	2.13	0.05	0.18	0.54	0.14	0.01	0.05	0.04
1-7	0.03	0.84	1.21	1.32	0.05	0.19	0.58	0.15	0.00	0.01	0.01
1-8	0.01	0.83	1.15	1.05	0.05	0.20	0.60	0.15	0.00	0.00	0.00
1-9	0.00	0.83	1.14	0.99	0.05	0.20	0.60	0.15	0.00	0.00	0.00
1-10(a)	0.00	0.83	1.13	0.98	0.05	0.20	0.60	0.15	0.00	0.00	0.00
2-1	1.00	10.55	14.81	12.77	0.00	0.00	0.00	0.00	0.11	0.48	0.40
2-2	0.83	9.90	14.57	10.82	0.01	0.03	0.10	0.02	0.09	0.40	0.34
2-3	0.16	0.88	9.83	2.91	0.04	0.17	0.50	0.13	0.02	0.08	0.07
2-4	0.10	0.86	3.47	2.20	0.04	0.18	0.54	0.13	0.01	0.05	0.04
2-5	0.03	0.84	1.22	1.37	0.05	0.19	0.58	0.15	0.00	0.02	0.01
2-6	0.01	0.83	1.15	1.06	0.05	0.20	0.60	0.15	0.00	0.00	0.00
2-7	0.00	0.83	1.14	0.99	0.05	0.20	0.60	0.15	0.00	0.00	0.00
3-1	0.68	8.99	14.24	8.98	0.02	0.06	0.19	0.05	0.08	0.33	0.27
3-2	0.16	0.88	9.83	2.91	0.04	0.17	0.50	0.13	0.02	0.08	0.07
3-3	0.09	0.86	1.38	2.07	0.05	0.18	0.54	0.14	0.01	0.04	0.04
3-4	0.04	0.84	1.23	1.41	0.05	0.19	0.58	0.14	0.00	0.02	0.01
3-5	0.01	0.83	1.15	1.06	0.05	0.20	0.60	0.15	0.00	0.00	0.00
3-6(a)	0.00	0.83	1.13	0.98	0.05	0.20	0.60	0.15	0.00	0.00	0.00
4-1	0.68	8.99	14.24	8.98	0.02	0.06	0.19	0.05	0.08	0.33	0.27
4-2	0.15	0.88	9.59	2.80	0.04	0.17	0.51	0.13	0.02	0.08	0.06
4-3	0.09	0.86	1.38	2.07	0.05	0.18	0.54	0.14	0.01	0.04	0.04
4-4	0.03	0.84	1.22	1.37	0.05	0.19	0.58	0.15	0.00	0.02	0.01
5-1	0.83	9.90	14.57	10.82	0.01	0.03	0.10	0.02	0.09	0.40	0.34
5-2	0.68	8.99	14.24	8.98	0.02	0.06	0.19	0.05	0.08	0.33	0.27
5-3	0.18	0.89	10.26	3.15	0.04	0.16	0.49	0.12	0.02	0.09	0.07
5-4	0.10	0.86	3.47	2.20	0.04	0.18	0.54	0.13	0.01	0.05	0.04
5-5	0.03	0.84	1.22	1.39	0.05	0.19	0.58	0.14	0.00	0.02	0.01
5-6	0.01	0.83	1.15	1.06	0.05	0.20	0.60	0.15	0.00	0.00	0.00
5-7(a)	0.00	0.83	1.13	0.98	0.05	0.20	0.60	0.15	0.00	0.00	0.00
6-1(a)	0.00	0.83	1.13	0.98	0.05	0.20	0.60	0.15	0.00	0.00	0.00
6-2(a)	0.00	0.83	1.13	0.98	0.05	0.20	0.60	0.15	0.00	0.00	0.00

Table E.2: Sediment parameters and distribution of data set Blom

	D_{50}	D_{90}	D_m	D_i		
				0.5	**0.7**	**2.1**
1	0.71	2.00	1.66	0.49	0.44	0.07
2	1.20	4.32	2.52	0.36	0.38	0.26
3	0.68	2.06	1.69	0.52	0.39	0.09
4	0.68	0.92	1.02	0.89	0.06	0.05

Appendix F

Data set BS-II parameters (extended)

Exp	h	u	I_e	R_b	$k_{s,b}$	τ_b	C_b	f_{gravel}	d	Δ_0	f_h	p	$q_{b,meas}$
-	m	m/s	10^{-3}	cm	mm	Nm^{-2}	$m^{1/2}s^{-1}$	cm	-	cm	cm	(-)	g/s
1-1	0.2	0.37	0.7	18.06	32.19	1.25	32.91	1	0	8	14.8	0.92	0
1-2	0.2	0.52	0.8	17.11	6.61	1.33	44.87	0.78	0.3	8	14.6	0.77	4.3
1-3	0.2	0.52	0.8	17.16	7.04	1.38	44.39	0.78	0.3	8	14.6	0.71	3.8
1-4	0.2	0.52	0.8	17.16	7.04	1.35	44.39	0.49	1.1	8	9.8	0.28	11.6
1-5	0.2	0.53	0.8	17.07	6.2	1.41	45.35	0.47	1.2	8	9.6	0.27	7.9
1-6	0.2	0.52	1.2	17.93	22.1	2.06	35.79	0.35	2	8	1.4	0.21	15
1-7	0.2	0.52	1.6	18.39	45.63	2.87	30.32	0.21	4.1	8	1.2	0.06	21.2
1-8	0.2	0.52	1.8	18.53	58.26	3.37	28.47	0.13	6.8	8	1.1	0.02	26.6
1-9	0.2	0.52	1.9	18.59	64.81	3.32	27.67	0.1	9.7	8	1.1	0	25.5
1-10(a)	0.2	0.52	2.2	18.73	82.25	3.97	25.86	0.06	16.1	8	1.1	0	31.8
2-1	0.3	0.5	0.8	25.93	35.62	2.17	34.95	1	0	9.1	14.8	0.96	0
2-2	0.3	0.52	0.6	24.58	12.33	1.36	42.82	0.78	0.3	9.1	14.6	0.78	3.9
2-3	0.3	0.52	0.4	22.3	2.24	0.9	55.41	0.49	1.1	9.1	9.8	0.31	6
2-4	0.3	0.52	0.7	25.23	20.3	1.66	39.12	0.36	1.9	9.1	3.5	0.27	9.9
2-5	0.3	0.51	0.8	25.85	33.23	2.06	35.46	0.21	3.9	9.1	1.2	0.12	13.6
2-6	0.29	0.54	1.2	25.86	60.91	3.18	30.73	0.14	6.7	9.1	1.1	0.03	20.1
2-7	0.3	0.52	0.9	26.09	39.66	2.24	34.15	0.1	9.5	9.1	1.1	0.01	16.5
3-1	0.15	0.53	1.3	13.54	10.13	1.74	39.7	0.73	0.4	6.7	14.2	0.58	4.6
3-2	0.15	0.53	1.2	13.44	8.01	1.56	41.47	0.49	1.1	6.7	9.8	0.24	10.8
3-3	0.15	0.51	1.4	13.68	14.26	1.94	37.1	0.34	2.1	6.7	1.4	0.14	15.1
3-4	0.16	0.49	1.4	14.69	22.77	1.95	34	0.22	3.7	6.7	1.2	0.04	18.1
3-5	0.15	0.53	2	13.97	29.78	2.88	31.51	0.14	6.7	6.7	1.1	0.01	15.2
3-6(a)	0.15	0.53	2.6	14.15	48.45	3.7	27.8	0.06	16	6.7	1.1	0	32.1
4-1	0.2	0.68	1.2	17	4.83	2.07	47.26	0.73	0.4	8.1	14.2	0.65	17.9
4-2	0.2	0.68	1.7	17.76	14.79	3.01	38.85	0.47	1.2	8.1	9.6	0.31	35
4-3	0.2	0.58	1.6	18.11	27.81	2.82	34.07	0.34	2.1	8.1	1.4	0.21	26.2
4-4	0.2	0.58	2.1	18.49	51.35	3.91	29.44	0.21	3.9	8.1	1.2	0.08	38.2
5-1	0.2	0.46	0.6	16.94	5.57	1.05	46.12	0.78	0.3	8.1	14.6	0.69	2.1
5-2	0.2	0.46	0.7	17.31	9.34	1.12	42.25	0.73	0.4	6.9	14.2	0.62	1.5
5-3	0.2	0.46	0.6	16.99	6	0.92	45.56	0.54	0.9	6.9	10.3	0.24	3.2
5-4	0.2	0.46	0.6	16.94	5.57	1.05	46.12	0.36	1.9	6.9	3.5	0.15	6
5-5	0.2	0.46	0.8	17.58	14	1.43	39.21	0.22	3.8	6.9	1.2	0.06	10
5-6	0.2	0.46	1.2	18.26	39.42	2.24	31.41	0.14	6.5	6.9	1.2	0.01	11.1
5-7	0.2	0.47	1.5	18.53	60.35	2.84	28.19	0.06	16	6.9	1.1	0	14.5
6-1(a)	0.25	0.52	1.7	23.08	96.36	3.87	26.25	0.06	16	8.3	1.1	0	25.2
6-2(a)	0.26	0.58	2.2	24.12	117.51	5.21	25.05	0.06	16	9.5	1.1	0	45.2